ASPECTS OF WOOD ADHESION: APPLICATIONS OF ^{13}C CP/MAS NMR AND FRACTURE TESTING

by

Robert G. Schmidt

A Dissertation submitted to the Faculty of

Virginia Polytechnic Institute and State University

in partial fulfillment of the requirements for the degree of

DOCTOR OF PHILOSOPHY

in

Wood Science and Forest Products

Approved by:

Charles E. Frazier, Chairman

Wolfgang G. Glasser

Frederick A. Kamke

Thomas C. Ward

James P. Wightman

January 30, 1998
Blacksburg, Virginia

ASPECTS OF WOOD ADHESION:
APPLICATION OF ^{13}C CP/MAS NMR
AND FRACTURE TESTING

by

Robert G. Schmidt

C.E. Frazier, Chairman

Wood Science and Forest Products

ABSTRACT

Phenol Formaldehyde (PF) and polymeric isocyanate (pMDI) are the two main types of adhesives used in the production of structural wood-based composites. Much is unknown about various aspects of adhesion between these two types of resins and wood. The present research describes the development of techniques which will permit an enhanced understanding of 1.) the extent of cure of PF within a wood based composite, 2.) the scale of molecular level interactions between PF and pMDI and wood, 3.) mechanical performance and durability of wood-adhesive bonds.

Correlations were established between conventional methods of characterization of neat PF (thermomechanical analysis, swelling studies) and measurements made using ^{13}C CP/MAS NMR. These correlations were then utilized to characterize PF cured in the presence of wood. The use of ^{13}C labeled PF allowed estimates of relative degrees of resin conversion to be made. The use of ^{13}C and deuterium labeled PF allowed qualitative estimates of resin molecular rigidity to be made.

The scale of molecular level interactions between PF and pMDI and wood was probed using NMR relaxation experiments. Evidence was shown to suggest the formation of an interpenetrating polymer network (IPN) morphology existing at both types of wood-resin interphases. The formation of the IPN morphology was strongly influenced by resin molecular weight, cure temperature and the presence of solvent.

A new test geometry for the evaluation of the fracture toughness of wood-adhesive bonds was developed. Consistent and reliable results were obtained. It was found that low molecular weight PF possessed enhanced durability over high molecular weight PF.

ACKNOWLEDGEMENTS

An effort such as this is never solely the result of a single individual's efforts. I would like to take the time here to thank those who made it possible.

I would like to express my sincere gratitude to my advisor and committee chair, Dr. Chip Frazier. One could not have asked for a better teacher or mentor. At few times in our lives, does someone so deeply and positively affect the course of our professional development. I can say with confidence that he is one of those people.

I wish to also extend my appreciation to the members of my committee: Dr. Wolfgang Glasser, Dr. Fred Kamke, Dr. Tom Ward and Dr. Jim Wightman. They have served as my teachers and guides through my graduate career.

Many thanks go to the staff, students and faculty at the Department of Wood Science and Forest Products and the Center for Adhesive and Sealant Science. Special thanks go to "Uncle" Geza Ifju, Debbie Garnand, Jody Jervis, Carl Price, Katy Hatfield, Linda Haney and Kim Mills and the members of the Wood Adhesion Group, past and present. Tom Glass and Bill Bebout also deserve special recognition for their technical assistance with the NMR portion of this work.

I would like to thank my mother, Wendy, father, Robert Sr., Clea, Jason, and Alyson for their love, support and encouragement during the course of my studies. It has often been difficult to be separated from them, but I want them to know that they were always in my thoughts.

Last, but by no means least, I would like to thank Eva Park. Words can not adequately describe the love and gratitude I feel for the one who shares my life. She is my love, my confidante, my best friend and so much more. The love and support that she has unselfishly given has shared my greatest moments and sustained me through my darkest hours. I am forever indebted to her.

Table of Contents

List of Figures

List of Tables

Chapter 1

Introduction

As a result of changing societal attitudes towards the use of forested lands, the amount of land available for the production of wood-based products has declined significantly. The forest industry itself has had to radically change its policies and practices as a result. While the availability of solid sawn timber for structural applications has steadily declined, the demand for structural materials has continued to rise. This fact has given rise to the increased role of wood-based composite materials for structural applications. Wood-based composites offer several advantages over solid-sawn wood members, including uniformity, versatility and superior mechanical properties. In addition, they are more environmentally sound than alternate materials such as steel, concrete and synthetic polymers, originating from a renewable resource, requiring less energy and emitting fewer pollutants during production.

In order to be successful, wood-based composites must have the capability to fulfill the requirements of existing end-uses, expand into non-traditional markets and successfully compete against non-wood materials. In order to accomplish these objectives, new products must be developed and the properties of existing products must be improved upon. A necessary starting point is an improved understanding of the fundamental nature of adhesion between adherend and adhesive. When dealing with any type of composite material, the state of the cured adhesive and its interactions with the adherends plays a crucial role in determining mechanical performance and durability of the composite. These aspects of adhesion are investigated in this dissertation. The emphasis is on wood, bonded with the two major types of adhesives used in the production of structural wood-based composite materials, namely phenol formaldehyde (PF) and polymeric isocyanate (pMDI) resins.

The main analytical tool used in this work is ^{13}C cross polarization (CP), magic angle spinning (MAS) nuclear magnetic resonance (NMR) spectroscopy. This technique is recognized as one of the most powerful tools in polymer chemistry for the elucidation of solid-state chemical structure and molecular dynamics. While its use has been widespread in the characterization of synthetic composite systems, very little work has been done in the area of wood-based composites. This dissertation shows the suitability and valuable information, which can be gained from using ^{13}C CP/MAS NMR to characterize aspects of adhesion in wood-based composite systems.

Fracture toughness testing has been recognized as one of the most informative tools in the evaluation of adhesive performance and durability. This dissertation evaluates a new fracture toughness test geometry and attempts uses it to relate macroscopic performance to molecular level information obtained from ^{13}C CP/MAS NMR.

This dissertation is written in manuscript format. Aside from Chapters 2 and 9, each chapter is written with its own Materials/Methods, Results and Discussion sections. While these chapters represent individual studies, the reader will find that the results from each complement one another. Chapters 3, 4 and 6 describe a technique, which has been developed to monitor the degree of cure of phenol formaldehyde resin within a wood-based composite panel. Chapter 5 describes a technique for the synthesis of isotopically labeled paraformaldehyde, an essential starting material in the synthesis of thermosetting wood adhesives. Chapter 7 evaluates molecular interactions between wood and phenol formaldehyde and polymeric isocyanate. Chapter 8 describes an improved test geometry for the evaluation of wood-adhesive bond

performance and durability. Finally, Chapter 9 provides a summary of the conclusions obtained from this research.

Chapter 2

Literature Review

2.1 Phenol Formaldehyde

2.1.1 History

Phenol formaldehyde resin was first discovered in 1872 by A. von Bayer while experimenting with phenolic dyes (1). A reddish-brown resinous mass was the product of the reaction of bitter almond oil and pyrogallic acid. Shortly after this discovery, a large number of researchers began work in this area. Early experiments were performed mainly under acid-catalyzed conditions, which produced soluble resins. The first work which produced a curable phenolic resin from the reaction of resorcinol, formaldehyde and ammonia was done by Speier (2). This was later expanded upon by the work of Smith (3), Luft (4) and Henschke (5), who reacted phenol with excess formaldehyde in the presence of alkali. It remained little more than a laboratory curiosity however, until 1907, when Leo H. Baekeland developed a commercial manufacturing process (6). In 1910, the first commercial phenolic resin plant was opened in Germany (1). Their product was sold under the trade name Bakelite. This was in fact, the first commercially available synthetic resin. Due to the importance of the modern polymer industry, the significance of this event is quite profound.

The first products made with phenolic resins were mainly molded and impregnated products and insulation materials. They became widely used in the wood products industry for the manufacture of particleboard and plywood in the mid 1930's (7). They became the dominant adhesive system used for the manufacture of oriented strand board (OSB), since its introduction in the mid 1970's. These resins possess highly desirable performance properties such as high glass transition temperature, high modulus and tensile strength, good dimensional stability and solvent resistance as well as being relatively low cost (1). For these reasons they remain the dominant adhesive system for the production of wood-based composites for exterior applications.

2.1.2 Synthesis and Cure Chemistry

Phenol formaldehyde (PF) resins are produced industrially by the reaction of phenol with formaldehyde in the presence of a catalyst. They are grouped into two general classes, novolaks (novolacs) and resoles (resols), based upon the molar ratios of reactants as well as the type of catalyst used. These two types of resins differ significantly in terms of both properties and applications. Resoles are the major type of resin used in the wood-based composite industry.

Novolaks are produced by the reaction of formaldehyde with excess phenol under acidic conditions (pH 1 – 6) (1). Typical phenol:formaldehyde ratios are approximately 1 : 0.70 – 0.85 (1). The most common industrial catalysts are oxalic, hydrochloric, sulfuric, phosphoric and toulene sulfonic acids (1). An overview of the reactions under these conditions is shown in Figure 2.1.

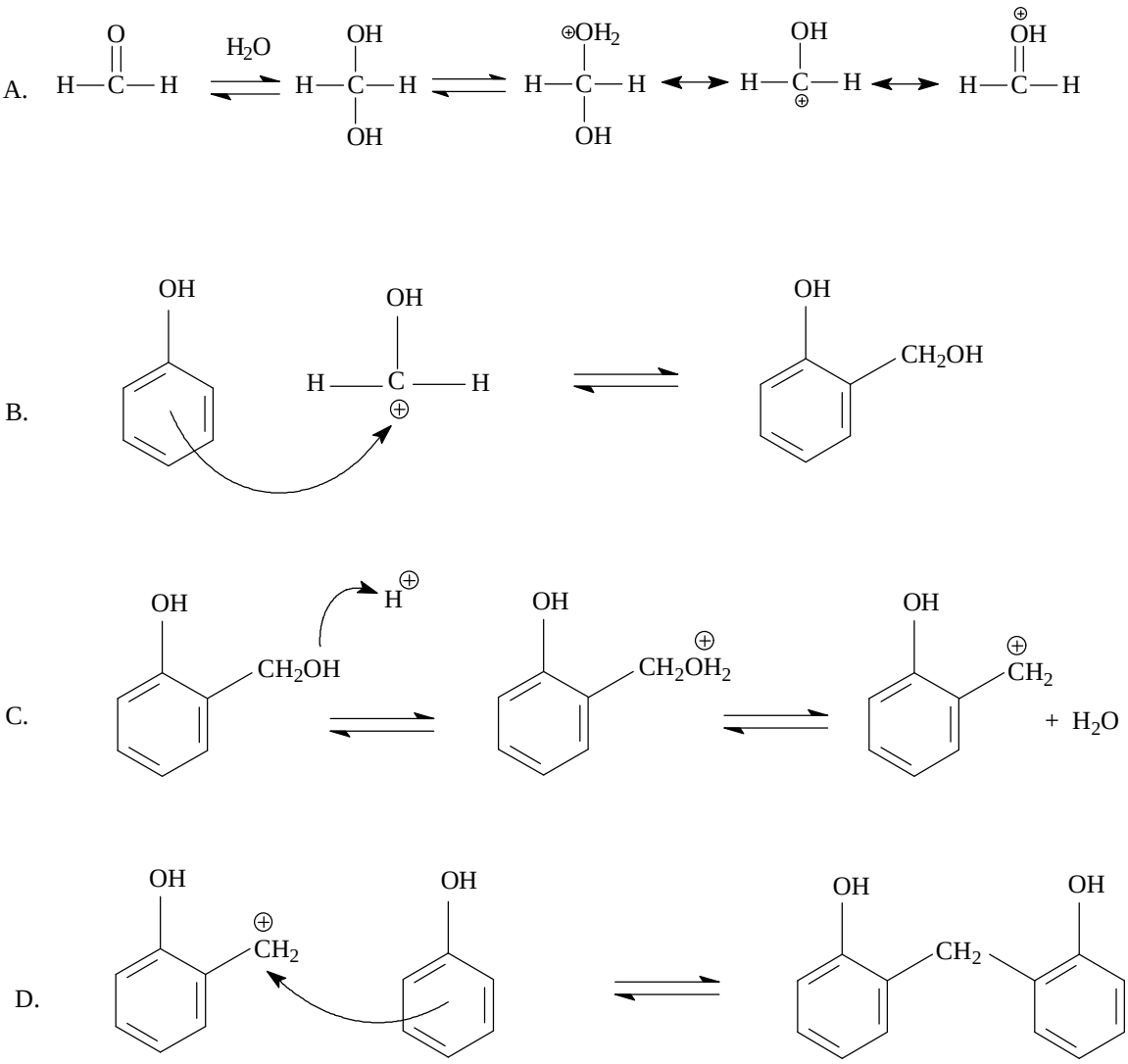

Figure 2.1: Reactions of Phenol and Formaldehyde Under Acidic Conditions

For novolaks, the initial reaction proceeds by protonation of methylene glycol by the acidic media to form a resonance stabilized carbocation (Figure 2.1, Scheme A). This is followed by an electrophilic substitution mainly at the para positions of the phenolic ring to form a mono-substituted hydroxymethyl phenol (HMP) (Figure 2.1, Scheme B). The amount of ortho substitution can be increased by performing the reaction under mildly acidic conditions (pH 4-7) and the use of divalent metal salts as catalysts (1). PF resins produced in this manner are referred to as highly ortho (or high o-o') novolaks. The reason for the selectivity of the reaction is due to the coordinating effects of the metal compounds, with chelate complexes as intermediates.

The mono-substituted HMP's produced in the initial reaction are short-lived under acidic conditions. Protonation of the methylol oxygen results in the conversion to benzylic carbocations with the release of water (Figure 2.1, Scheme C). These species then react with phenol to form diphenylmethane species (Figure 2.1, Scheme D). Additional polymerization occurs resulting in the formation of a linear or slightly branched thermoplastic material (1). Cure

(i.e. crosslinking) of novolaks can be accomplished through the use of a crosslinking agent such as hexamethylenetetramine (HMTA – 8-12 %) or ammonia (1).

Resoles are produced by the reaction of excess formaldehyde with phenol under alkaline conditions (pH 8 – 13). The solvent used is water. Typical phenol : formaldehyde ratios range from 1 : 1 – 1 : 3. The most common industrial catalyst for this reaction is sodium hydroxide, however, ammonia, HMTA, or a variety of metallic hydroxides can also be used. Formaldehyde is usually in 37% solution (formalin) or can be used in its polymeric form, paraformaldehyde (8). An overview of the reaction mechanisms under alkaline conditions is given in Figure 2.2.

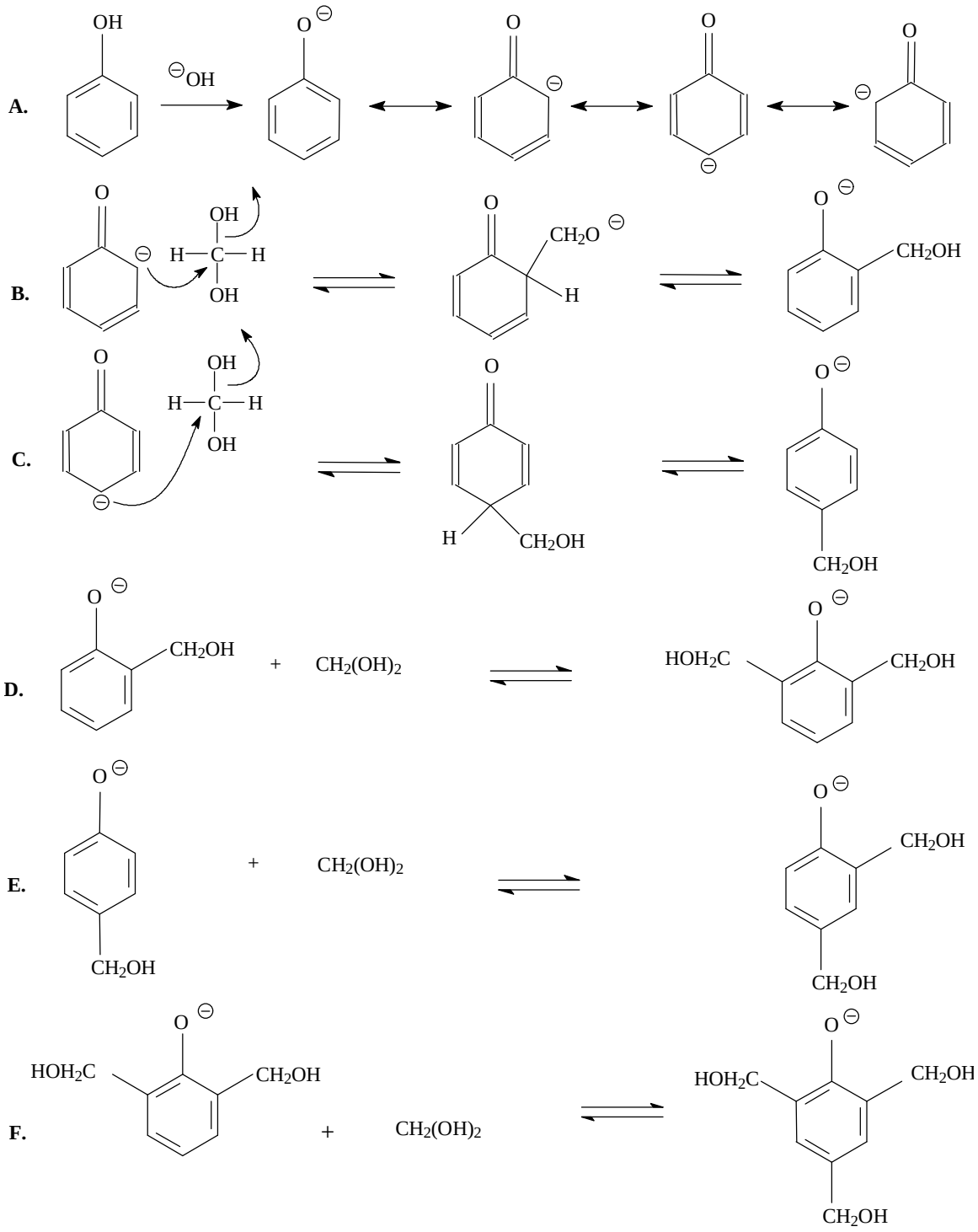

Figure 2.2: Addition Reactions in the Synthesis of Resoles

In alkaline media, the phenolic hydroxyl, being a weak acid, will react readily to form a phenoxide ion (Figure 2.2, Scheme A). The resonance stabilized forms of this ion will result in a nucleophilic substitution of the methylene glycol at either the ortho or para positions on the ring, forming a mono-substituted HMP (Figure 2.2, Schemes B and C). These mono-substituted species then react further with the excess methylene glycol present through a similar mechanism

to form di and tri-substituted hydroxymethyl phenols (Figure 2.2, Scheme D-F). A study of the reaction kinetics of prepolymer formation for NaOH catalyzed PF was performed by Freeman and Lewis (9). They found that phenol is more reactive towards para substitution than ortho. This is compensated for however, by the fact that there are two ortho positions available for substitution. They also found that the reaction proceeds to high levels of tri-substitution prior to the formation of higher order oligomers which eventually gel to form an infinite molecular weight network. Solution NMR characterization of PF has shown that hemiformal species may also be present (10). These structures would result from the reaction of methylene glycol with hydroxymethyl moieties.

A complete understanding of the reactions which take place during the cure of PF resoles is not available at present. It is generally accepted that the polymerization of PF under alkaline conditions proceeds by condensation of the mono-, di- and tri-substituted HMPs. An overview of these reactions is shown in Figure 2.3. Typically this is accomplished thorough the application of pressure and heat (industrially between 110 – 200 ^{o}C), the sodium hydroxide present acting as catalyst for this reaction. It is thought that the bulk of the polymerization proceeds via a quinone methide intermediate. The ring electrons of adjacent HMP attack the electrophillic methide carbon resulting in the

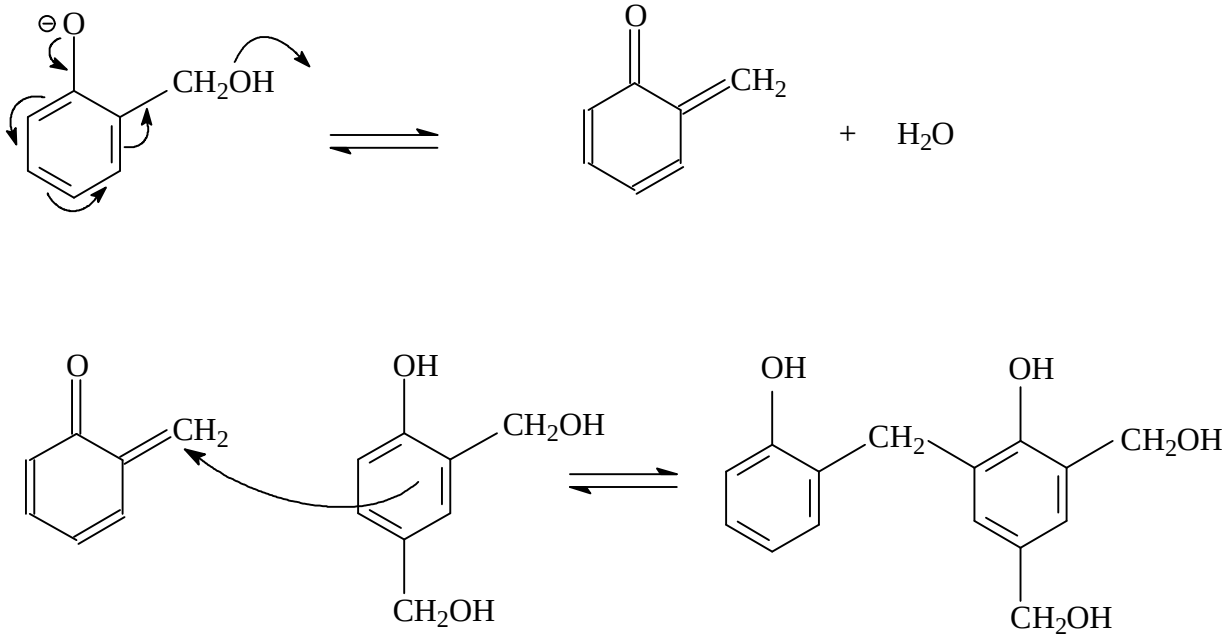

Figure 2.3: Condensation of PF Prepolymers

formation of methylene bridge units. Lilley and Osmond (11) postulate two distinct methods of quinone methide formation, occurring at different stages in the reaction. These are shown in Figure 2.4.

In the early stages of reaction when abundant water is present, the formation of the quinone methide intermediate is solvent assisted (Figure 2.4, Scheme A). In the later stages of the reaction, when most of the water has been evaporated, formation of the quinone methide is promoted by hydrogen bond formation between the hydroxymethyl group and the phenolic hydroxyl (Figure 2.4, Scheme B).

A.

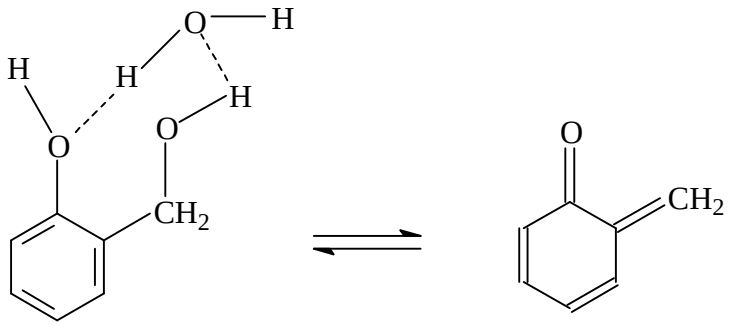

B.

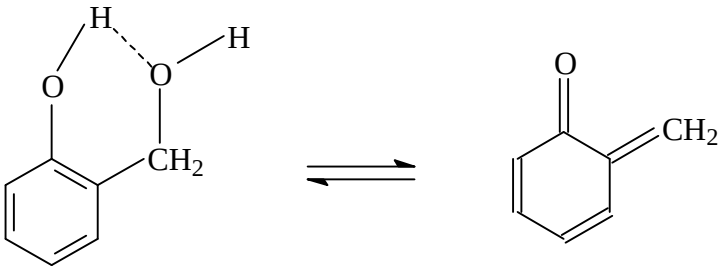

Figure 2.4: Quinone Methide Formation

There are a number of other reaction mechanisms that have been proposed to take place during the cure of PF resoles. It is thought that hydroxymethyl groups may react with one another to form dimethylene ether linkages. This structure however is unlikely to be prevalent under alkaline conditions (pH > 10), as confirmed by an infrared study of cured resoles (12). It may however, participate under alkaline conditions (pH > 10) as a very short lived intermediate which rapidly collapses to a methylene bridge, although it has not been isolated. Methylene ether formation can be substantial at neutral or slightly acidic pHs at low temperatures. However, these are uncommon commercial reaction conditions. A recent study of the structure of cured PF by ^{13}C solid-state NMR (13) has found evidence of additional mechanisms which may play a role during cure (Figure 2.5 Schemes A-C). This study postulates the direct involvement of the phenolic hydroxyl in the crosslinking reaction. In addition, it suggests that free formaldehyde may react with methylene bridges, a mechanism originally proposed by Zinke (14).

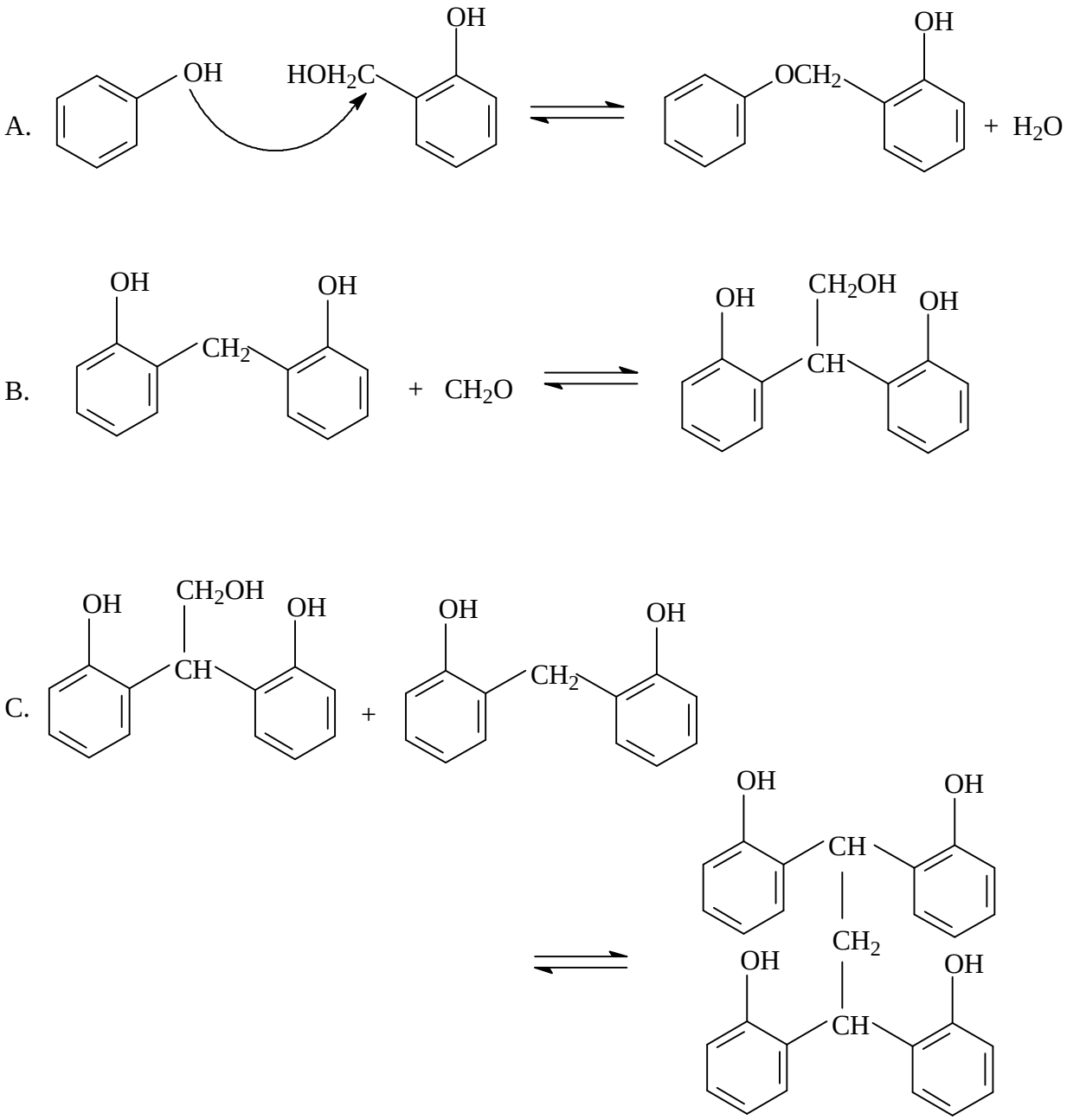

Figure 2.5: Additional Crosslinking Reactions in the Cure of Resoles

The influence of solvent (i.e. water) plays a critical role in the initial formation of prepolymers as well as their subsequent cure. The reactions involved in the network formation of PF resoles consists of multiple sequential and simultaneous condensation equilibria. The effects of water vapor pressure during the cure of neat resole PF was studied by Ballerini (15). He found that increasing the amount of water vapor during cure led to a decrease in the gel time. The effects on the physical properties of the cured resin however, remain unclear.

2.1.3 Cure Characterization

A thermosetting material such as PF, is one which undergoes irreversible chemical changes during polymerization (i.e. curing) to form an infusible three-dimensional network. For most thermosetting resins, this process is thought to occur in three stages (7). In the first stage (or A-stage), the resin is a soluble, fusible liquid consisting of monomers and low molecular weight oligomers. As cure advances, the molecular weight of the resin material increases, but it is still in liquid form (B-stage). The third stage (or C-stage) is the cured state of the resin, solid and infusible. It has undergone gelation (the formation of an infinite molecular weight material) and vitrification ($T_g = T_{cure}$). These processes have been described theoretically and empirically by the works of Flory (16) and Gillham (17).

The ability to characterize the cure of a thermoset is of great benefit from an application standpoint, since the degree of cure will significantly influence the properties of the cured resin (i.e. modulus, durability).

The curing of resole PF has been successfully studied by a number of techniques (18-23). Kim et al. (18) used dynamic mechanical thermal analysis (DMTA) to determine gelation and vitrification events of PF as a function of cure temperature and resin composition. Infrared (IR) spectroscopy has been used to monitor cure (19). Ballerini (15) and Rials (20) used microdielectric spectroscopy (DEA) to determine cure events within PF cured at a variety of water vapor pressures. Mizumachi and Morita (21) used differential scanning calorimetry (DSC) to determine the activation energies for the cure of PF in the presence of wood powder. Steiner and Warren (22) used DSC coupled with torsional braid analysis to monitor cure. Tchir (23) was able to study the cure of PF using ^{13}C CP/MAS NMR by monitoring the relative intensities of the methylene bridge and hydroxymethyl groups as a function of cure time and temperature. It must be pointed out that while these techniques have been useful for investigating the cure of neat PF, there has been no technique, which allows for the characterization of resin within a composite material.

2.2 Polymeric Diphenylmethane Diisocyanate Adhesive

2.2.1 History

Polymeric diphenylmethane diisocyanate (pMDI) adhesives were developed during World War II in a search to bond tire cords and rubber (7). Their high reactivity towards materials with available hydroxyl functional groups prompted exploration of the possibility of their use in bonding lignocellulosics. Relatively speaking, they are new to the wood products industry. Their primary industrial application is use in the manufacture of polyurethane and polyurea materials. Their use for the manufacture of wood-based composites came in the late 1960's, when they were used to bond particleboard (7). Their widespread use began in the early 1980's with the introduction of waferboard/oriented strand board (OSB). They offer numerous advantages for these applications, including higher moisture tolerances, lower press times and improved composite mechanical properties over phenol formaldehyde resins (24-27). They possess several drawbacks including toxicity and high cost. In addition, isocyanate bonded wood composites have been known to adhere to the metal caul plates during production (28).

2.2.2 Synthesis and Cure Chemistry

Polymeric diphenylmethane diisocyanate (pMDI) is produced commercially by a two-stage reaction process. In the first stage, aniline is condensed with formaldehyde under acidic conditions to form a polyamine. In the second stage, the amine groups of the polyamine are phosgenated to form a polyisocyanate. This mechanism has been summarized by Frisch et al. (29). An overview of these reactions is shown in Figure 2.6.

The condensation begins with protonation of the methylene glycol by the HCl to form a resonance stabilized carbocation. The aniline nitrogen then attacks the carbocation to form a resonance stabilized iminium ion with the liberation of water (Figure 2.6 Scheme A). The iminium ion then reacts with excess aniline to form either ortho or para substituted aminobenzyl aniline (Figure 2.6 Scheme B). These secondary amines are readily protonated by HCl (Figure 2.6 Scheme C). Additional aniline then attacks the electrophillic methylene group of the protonated aminobenzyl aniline to form methylene dianiline, a diamine (Figure 2.6 Scheme C). A number of structural isomers of methylene dianiline may be formed (Figure 2.6 Scheme C). Methylene dianiline can also react with additional aniline to form a triamine (Figure 2.6 Scheme D). The type (i.e. isomers) and molecular weight of the polyamines formed during the condensation have been shown to be controlled by aniline : formaldehyde and aniline: HCl ratios, as well as reaction time.

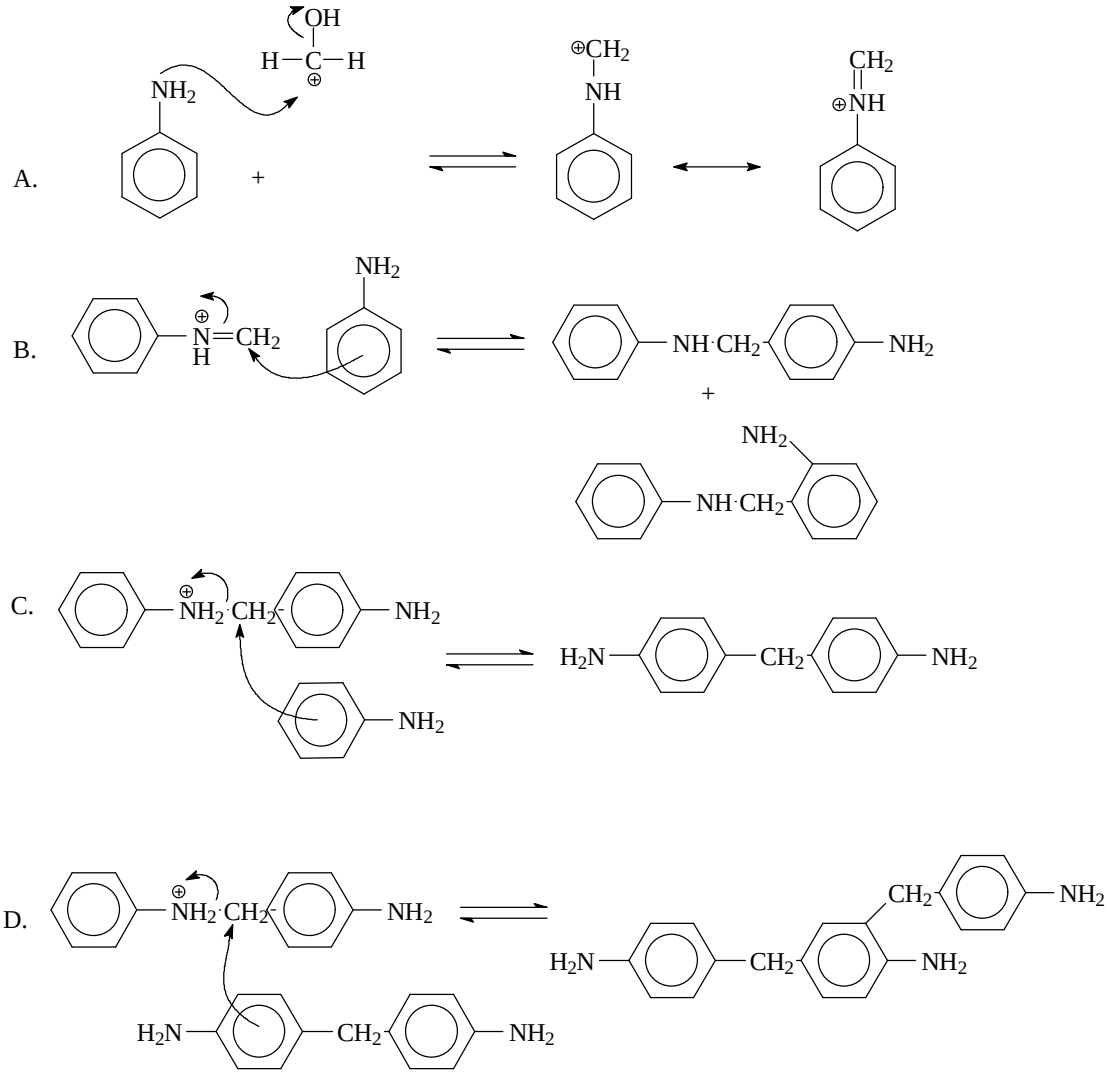

Figure 2.6 : Condensation Reactions Involved in the Synthesis of pMDI

The second stage of production (phosgenation) is accomplished by reacting the polyamine with an excess of phosgene in a dry environment with an inert solvent such as chlorobenzene or dichlorobenzene.

The primary amine groups of the polyamine react with phosgene to produce carbamoyl chloride (Figure 2.7, Scheme A). This species is unstable and will readily decompose to form isocyanate groups with the liberation of HCl (Figure 2.7, Scheme B).

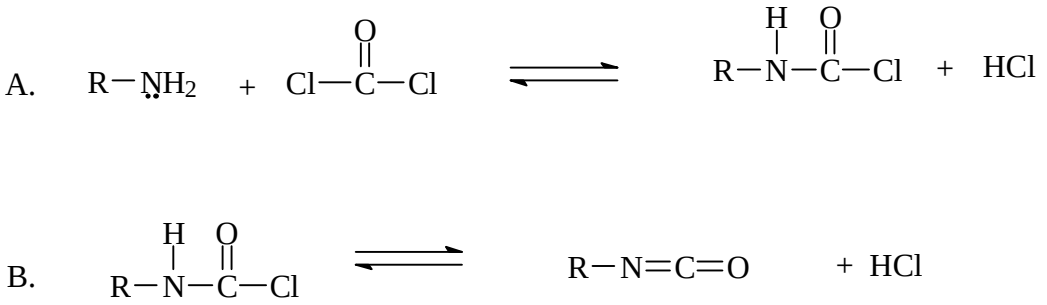

Figure 2.7: Reactions Involved in the Phosgenation of Amines

A number of side reaction can occur during the phosgenation. Linear ureas can be formed by the reaction of isocyanate with excess amine present as an impurity. This can be avoided by complete distillation of residual aniline from the first stage and maintenance of a dry atmosphere during the phosgenation reaction. Ureas can react to form polyurea or biuret structures (Figure 2.8, Scheme A and B). They can also react with phosgene to produce N-carbonyl chlorides (Figure 2.8, Scheme C). Aniline can also react with phosgene to form secondary carbamoyl chlorides (Figure 2.8, Scheme D). Dimerization of isocyanates can occur to form uretediones (Figure 2.8, Scheme E). This reaction is reversible at high temperatures (above 200^{o}C), so the amount of uretediones can be controlled by high temperature treatment.

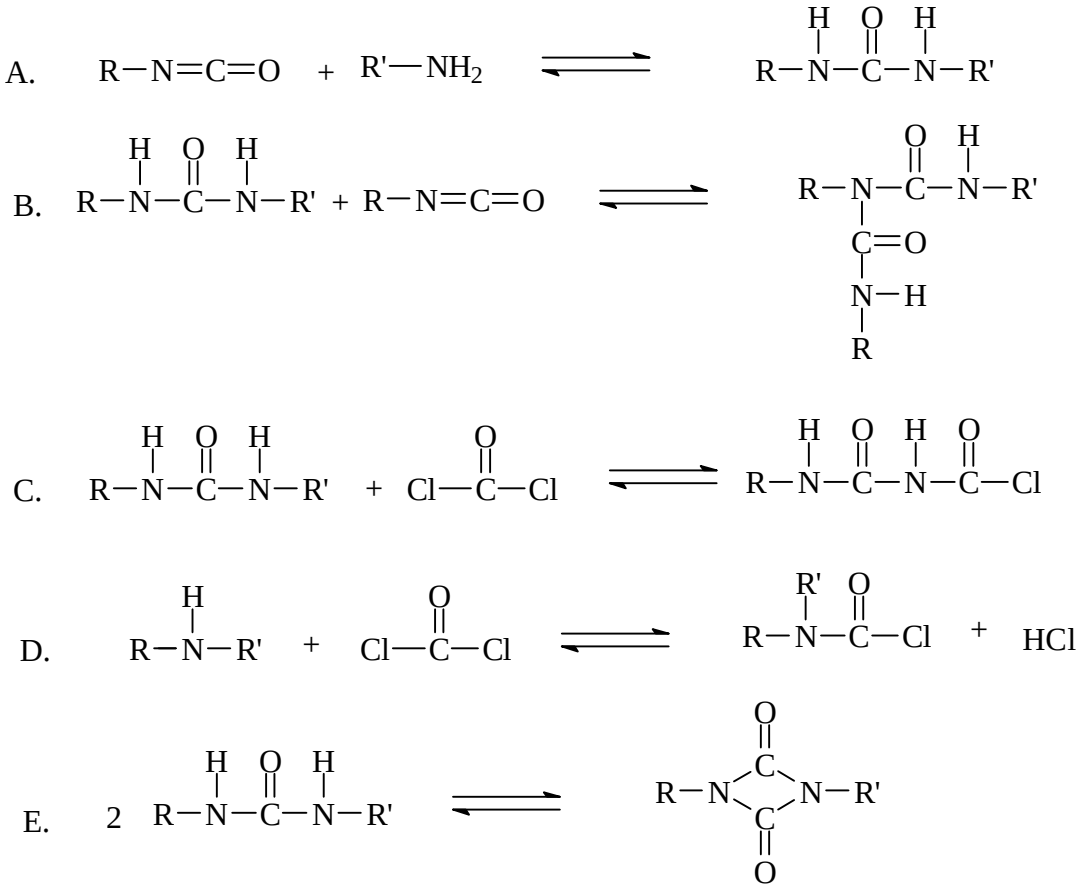

Figure 2.8: Phosgenation Side Reactions

The network formation (cure) of pMDI occurs as a result of the reaction of the available isocyanate functional groups. For polymerization to occur, a second component is normally required. Depending on the chemical nature of this second component, a number of reaction mechanisms can take place.

Reaction of pMDI with available hydroxyl groups is important for a number of industrial applications. An overview of this reaction is shown in Figure 2.9. Urethane formation is the result of the reaction with a primary alcohol (Figure 2.9, Scheme A). Urethanes can then react with isocyanate to form allophanate structures (Figure 2.9, Scheme B). Isocyanate will react readily with water to form carbamic acid, which decomposes to an amine with the liberation of carbon dioxide (Figure 2.9, Scheme C). Isocyanates can react with amines to form urea linkages (Figure 2.9, Scheme D). As mentioned previously, ureas formed can subsequently react with additional isocyanate to form biuret structures. Biurets can further react to form polyuret networks (Figure 2.9, Scheme E). Isocyanates can also self-polymerize, as already mentioned, forming dimers and trimers.

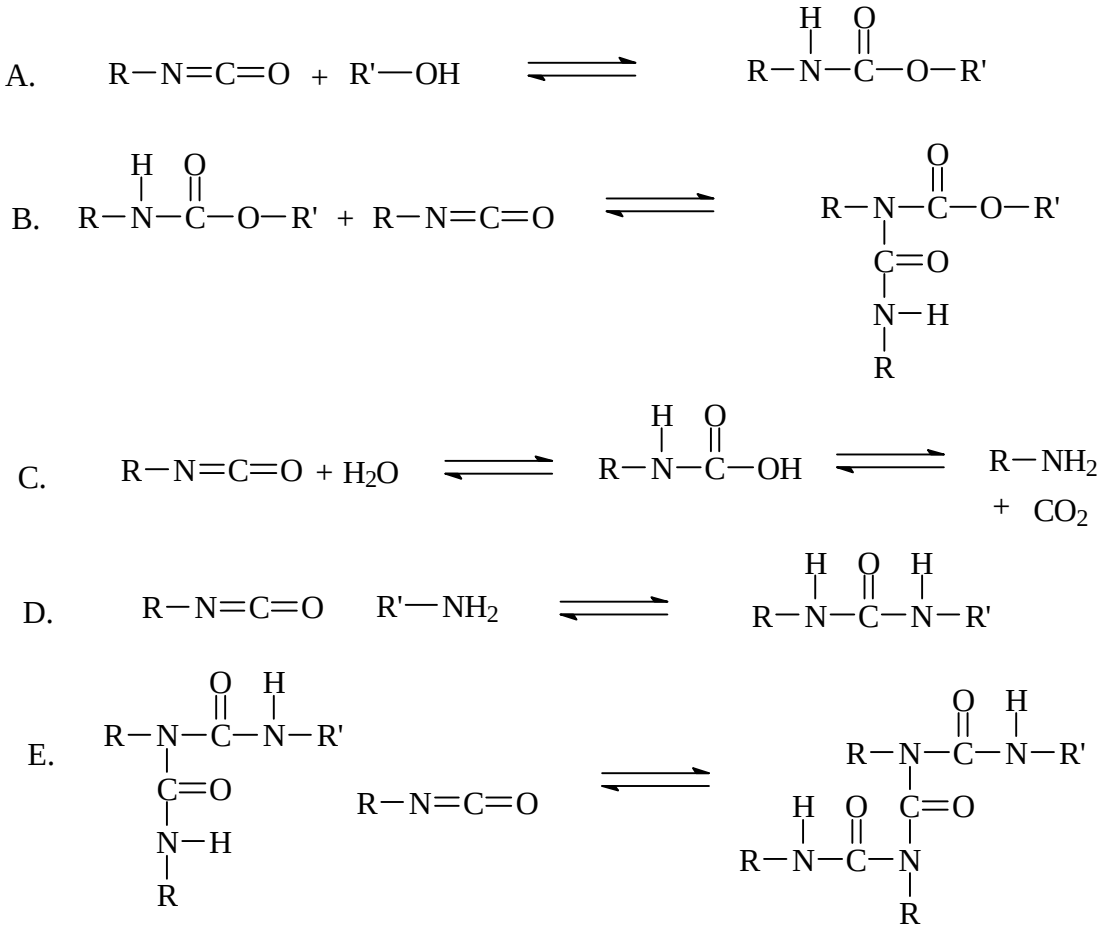

Figure 2.9: Reactions of Isocyanates

2.2.3 Cure Characterization

A large amount of work has gone into studying the reaction (i.e. cure) of isocyanates with various materials (29). For the purposes of this research, studies done on pMDI cured in the presence of wood are most pertinent. Galbraith and Newman (30) used DSC and FTIR to study the reaction of pMDI with wood. They found evidence of urethane formation. McLaughlin (31) also used FTIR but found no evidence of urethane formation. Several studies have used ^{15}N CP/MAS NMR to characterize the structure of pMDI cured in the presence of wood (32-34). Wendler and Frazier (35,36) also used ^{15}N CP/MAS NMR to study the effects of time, temperature and wood moisture content on the structure of pMDI cured in the presence of wood. Evidence of urethane formation was found only under severe conditions (high temperatures, long times). They found that the isocyanate-water reaction (i.e urea/polyuret formation) predominates the cure chemistry. This work was later expanded upon by Ni and Frazier (37) to develop an overall scheme for the reactions take place. These results are shown in Figure 2.10.

2.3 Wood Adhesion

2.3.1 Introduction to Adhesion

The phenomenon of adhesion has been commonly defined from two perspectives (38). From a physical chemistry standpoint, the atomic or molecular attraction between a solid and a liquid phase is called adhesion (39). From a technological standpoint, the term adhesion (also referred to as “practical adhesion” (40) is used to characterize the mechanical resistance to separation of a system of joined materials (38).

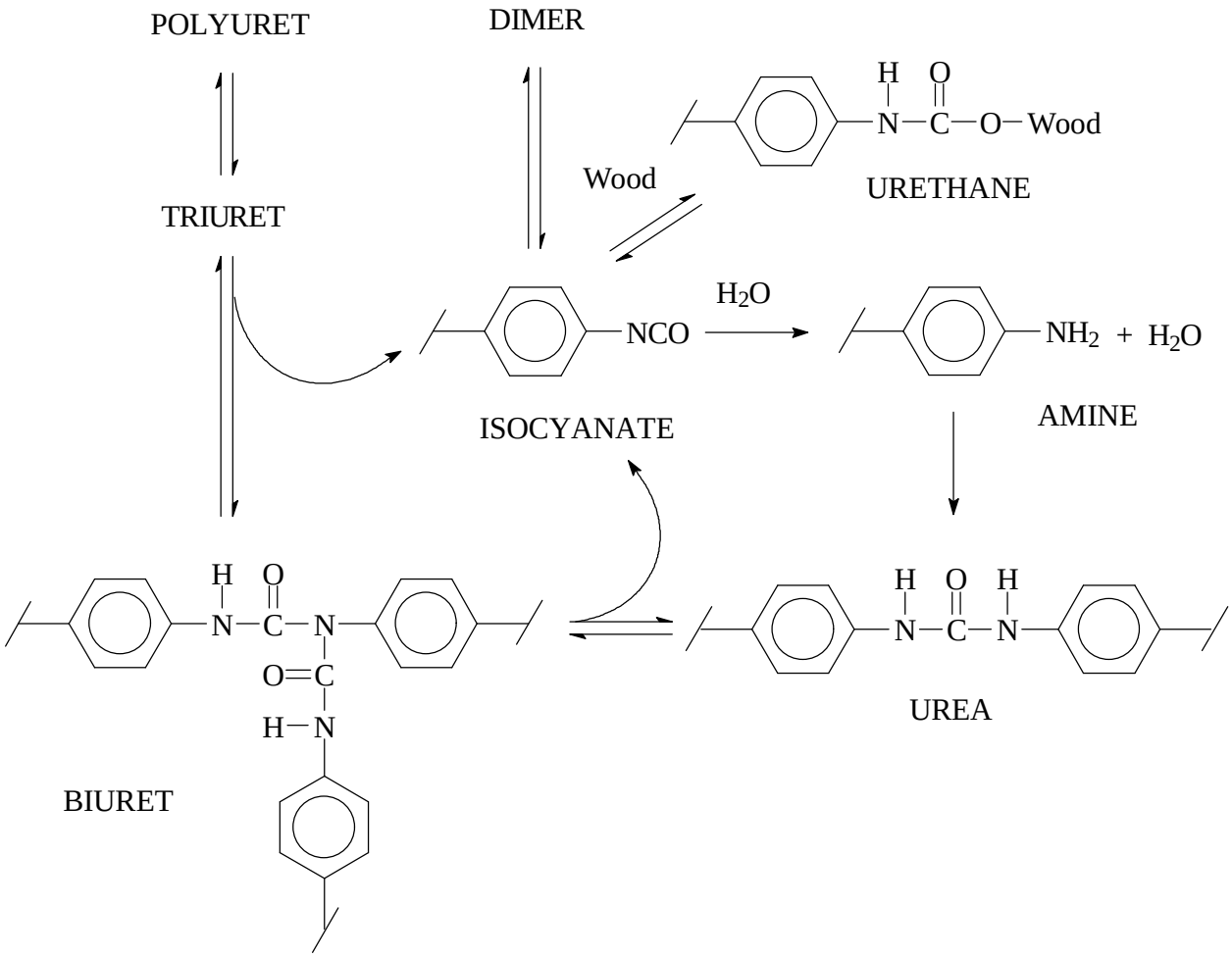

Figure 2.10: Reactions of pMDI in the presence of wood (37)

When two materials (i.e. a liquid and solid) are brought into contact, their surfaces are replaced by an interfacial region. From the above definitions, the ability to which the two materials resist separation is referred to as adhesion and it is the result of interactions between the two materials. Quantification of this interaction was first introduced by Young (41). In a thermodynamic approach, surface tensions (or surface free energies) of the bulk materials were related to that of the interface by Young's equation:

$$g_{sv} = g_{sl} + g_{lv}\cos\Theta \tag{2.1}$$

where γ_{sv} is the surface free energy of the solid in equilibrium with the vapor, γ_{sl} is the surface free energy of the solid-liquid interface, γ_{lv} is the surface free energy of the liquid in equilibrium with its vapor and θ is the contact angle formed between the liquid and the solid. A diagram illustrating the concept of the contact angle for a liquid on a solid wood surface is shown in Figure 2.11.

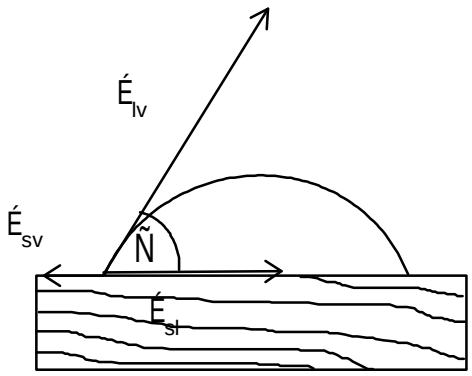

Figure 2.11: Contact Angle a Liquid Forms on the surface of wood.

Surface free energies of solids are related to the type and strength of secondary chemical interactions, which exist in the bulk. This work was later expanded upon by Dupre (42) to introduce a quantity referred to as the work of adhesion, or the amount of energy which must be expended to re-form the two original surfaces (Dupre equation):

$$W_a = g_{sv} + g_{lv} - g_{sl} \tag{2.2}$$

where W_a is the work of adhesion.
These equations can be simplified to the Young-Dupre equation:

$$W_a = g_{lv}(1 + \cos\Theta) \tag{2.3}$$

The Young-Dupre equation relates the work of adhesion to two easily accessible quantities, namely the surface tension of the liquid in question and the contact angle (Θ) that the liquid forms on contact with the surface.

A problem with the above treatments is that the interfacial region being characterized is assumed to be a two-dimensional plane. This has prompted a revision in the way this region is defined. As opposed to a two-dimensional plane, a three-dimensional region termed the "interphase" has been introduced (38). An "interphase" is defined as: "A region intermediate to two (usually solid) phases in contact, the composition and/or structure and/or properties of which may be variable across the region and which also may differ from the composition and/or structure and/or properties of either of the two connecting phases" (38).

It has been accepted that as requirements for good adhesion between materials, they must be in intimate contact on a molecular level. This is thought to occur through the phenomena of wetting and spreading. A liquid is said to spontaneously wet a solid surface if the contact angle is zero. In general, liquids will spontaneously wet solid surfaces if the surface free energy of the solid is greater that that of the liquid (43). In addition to wetting, spreading of a liquid is necessary to create sufficient surface area to provide a strong adhesive bond. To describe spreading, a term known as the spreading coefficient has been introduced (43):

$$S = g_{sv} - g_{lv} + g_{sl} \tag{2.4}$$

A liquid will spread on a solid surface if the spreading coefficient (S) ≥ 0.

2.3.2 Adhesion Theory

There have been five main theories put forward to explain the mechanism by which materials adhere to one another (44). They are electrostatic, diffusion, adsorption/specific adhesion, mechanical entanglement/interlocking, and covalent bonding.

The electrostatic theory was first put forward by Deryaguin (48). It is thought that in some instances, electron transfer between adhesive and adherend leads to the formation of an electrical double-layer. Adhesion therefore is a result of electrostatic attractive forces operating at the double-layer. There has been no literature which has used this theory to describe wood adhesion.

The diffusion theory of adhesion is attributed to Voyutskii (47), which postulates that interdiffusion of polymeric materials at the interphase is the primary contributing factor to adhesion. This requires mutual diffusion of both adhesive and adherend molecules. There has been no literature which discusses diffusion of constituent wood polymers into the adhesive phase.

Since two surfaces must be in very close proximity to adhere to one another, the adsorption/specific adhesion (or secondary interaction) theory explains adhesion on the basis of secondary chemical interactions occurring across the interphase. This has long been thought of as the dominant mechanism by which adhesive bonding to wood occurs due to the polar and polyhydroxylic nature of its constituent polymers (45).

The mechanical entanglement/interlocking (or hooking) theory proposes that the mechanical, physical interlocking of a hardened adhesive into the macro- and micro-irregularities of a substrate's surface is the major contribution to adhesion (46). Wood has a porous cellular structure. Most adhesives, which are used to bond wood, have been shown to penetrate into the cell lumens (7). It is likely therefore that contributions from mechanical interlocking play a role in the strength of wood adhesives bonds. Wood surfaces are always damaged to some degree by machining prior to bonding. This can result in what is termed a weak boundary layer. Penetration of adhesive into the damaged surface may act to reinforce it, thereby enhancing the strength of the adhesive bond.

Covalent interaction theory attributes good adhesion to the formation of covalent bonds between the adhesive and adherend. While it is theoretically possible for covalent linkages to be formed between wood and all of the adhesive pre-polymers which are used to bond wood, little conclusive evidence has been put forward to support this claim. Chow (49) has postulated that PF-wood covalent linkages act as intermediates in the cure of PF. Much early work done with

pMDI-wood systems attributed the superior performance of pMDI bonded wood was attributed to the formation of covalent urethane linkages. Recent studies of the wood-pMDI bondline using ^{15}N CP/MAS NMR indicate that urethane formation may be minimal under common processing conditions for the manufacture of wood-based composites (35,36).

It is important to note that adhesion is an extremely complex process. It has been recognized that no single theory can, as yet, fully describe the phenomenon of adhesion. The quest for a unified theory remains ongoing.

2.3.3 Wood-Adhesive Bond Formation

Early research in the field of adhesion science identified four criteria which must be met in order for the formation of a strong adhesive bond. These are: 1) removal of the weak boundary layer; 2) good wetting by the adhesive liquid; 3) solidification of the adhesive liquid and 4) sufficient deformability to reduce the effect of elastic stresses in the formation of the joint (44). To demonstrate bond durability, the solidification of the adhesive must involve chemical crosslinking.

2.3.4 Investigations of Wood Adhesion

2.3.4.1 Adherend Effects

The use of contact angle to describe wettability and adhesion phenomena in lignocellulosic materials was first described by Orchon (50). This work was primarily concerned with adhesion of coatings to paper, fabrics and vulcanized coatings. Gray (51) first used this technique to determine the critical surface free energy of wood as a function of species. This work was expanded upon by Herczeg (52), who showed that earlywood had a higher surface free energy than latewood. This indicated that both chemical composition and anatomical characteristics within species were important factors in wood adhesion.

A number of early studies showed that sanding of the wood surface immediately prior to bonding improved its wettability and that with aging, the wettability of wood surfaces decreased (51-54). Stumbo (53) investigated this effect and correlated a decrease in the tensile strength of casein and phenol formaldehyde bonded wood with decreased wettability. The conclusions of these studies were that the primary factor contributing to the decrease in wood surface free energy was migration and oxidation of extractives to the wood surface. Extraction of wood surfaces and/or storage in a dark environment were found to diminish the effects of ageing on the surface free energy (53).

It has been found that exposing wood to elevated temperatures reduces the surface free energy and bonding strength of wood-adhesive joints. This is thought to be the result of a number of factors: accelerated migration and oxidation of extractible materials, reorientation of wood polymers at the surface and oxidation and pyrolysis of wood polymers (54).

The influence of wood surface texture (i.e. roughness) on the surface free energy has also been examined (55-58). It has been determined that mechanical treatment of wood results in changes in both morphology (through fiber tearing and deformation), and chemistry (through thermal effects) of the wood surface (55). It was found that milling of beech wood surfaces resulted in a cell wall plastification and compression and resulted in a decrease in the surface free energy (56). Grinding of the same surfaces on the other hand, was found to tear fibers from the

surface and increase the surface free energy (56). Marian et al. (58) showed a compression shear strength maximum as a function of surface roughness. They attributed the decline in performance to decreased strength and increased porosity of the wood surface from mechanical treatment. A study by Triboulet et al. (57) showed that the fracture toughness of bonded assemblies of planed MDF positively correlated with surface roughness and recommend a maximum attainable roughness of the surfaces be achieved prior to bonding.

The influence of the wood substrate itself on the reaction mechanisms involved in the curing of wood adhesives has received some attention. Chow (49) studied the kinetics of PF polymerization in the presence of wood and found that reaction activation energy decreases as the number of accessible hydroxyl groups increases. Pizzi has also advanced the theory of wood-induced catalytic activation. He suggests that wood is able to reduce the energy of activation for the polymerization of phenol formaldehyde (59), melamine-urea formaldehyde (60) and isocyanate (61) adhesives.

2.3.4.2 Adhesive Considerations

It is well known that adhesives, which are used to bond wood, often penetrate into the porous cellular structure. For this reason, mechanical interlocking has always thought to play a role in wood adhesion. The extent of the penetration has been found to be a function of both wood density (62) and adhesive variables such as viscosity (7). It has been well documented that in order for superior mechanical performance, the viscosity of resins must be controlled to allow a degree of penetration, but not so much that overpenetration occurs, leaving insufficient adhesive to span the gap between adherends at the glue-line (7).

A recent study by Marcinko et al. used dynamic mechanical analysis to show that wood treated with liquid pMDI becomes plasticized (63). This effect was further investigated by Ni and Frazier, using both dynamic mechanical analysis and solid-state NMR (37) to evaluate the effects of liquid pMDI on Yellow poplar (*Liriodendron tulipifera*). In this case, no clear evidence was found to indicate that liquid pMDI plasticizes wood. For a material to act as a plasticizer, it must be molecularly miscible with the material it is plasticizing (64). If pMDI does in fact plasticize wood, this would suggest that penetration of the adhesive does not only occur macroscopically into the cell lumens, but also molecularly, into the cell wall substance. Wood is known to be capable of swelling in a variety of liquids, including water and a host of organic solvents. This fact has been exploited for a variety of uses such as pulping, preservative treatment and chemical modification. It has been shown that the degree and rate of swelling is strongly related to the size of the solvent molecule (65). The main difference between pMDI and other thermosetting adhesives used to bond wood is its molecular weight at application. Commercial pMDI used as a wood binder has a weight average molecular weight (Mw) below 500 g/mol, approximately 50% of which is in the form of monomeric diphenylmethane diisocyante (66). Commercial PF, on the other hand, has a Mw in the range of 1500-2000 g/mol (1). It is possible that this low molecular weight material can diffuse into the wood cell wall to form a molecular interphase between the adhesive and wood. If the adhesive pre-polymers are capable of interdiffusing with the wood cell wall polymers, it is possible that subsequent polymerization could lead to the formation of an interpenetrating polymer network (IPN) morphology (71), creating a molecular interphase between the bulk wood and adhesive. If this were the case, an additional theory to explain the phenomenon of adhesion could be added to the aforementioned list. Recent work by Vick et al., lends credence to this hypothesis (67-70).

Hydroxymethyl resorcinol (HMR) was found to promote adhesion between wood and several adhesives (66-70). The authors attribute this phenomenon primarily to secondary interactions and possibly covalent attachments.

2.4 Solid State Nuclear Magnetic Resonance Spectroscopy

2.4.1 Introduction

Since the discovery of the phenomenon of nuclear magnetic resonance, this technique has emerged as one of the most powerful approaches for the elucidation of structure and dynamics in pure and applied chemistry (72). The phenomenon arises as the result of the interactions which take place when nuclei which possess a magnetic moment (i.e. which have both electric charge and mechanical spin) are placed in a strong external magnetic field.

For years, the application of high-resolution NMR was restricted to the study of solutions. High resolution could not be obtained in the study of solid systems due to severe line broadening as a result of the chemical shift anisotropy and the dipolar coupling between protons and the nuclei of interest (72). These problems were addressed by the development of signal enhancement such as cross polarization (73), and line narrowing techniques such as magic angle spinning (74) and high-powered proton decoupling (75). Schaefer and Stejskal (74) were the first to combine these techniques to obtain solution-like resolution in solid-state spectra of polymeric materials. Since then, the growth of ^{13}C CP/MAS NMR as an analytical tool, has been explosive (72). While several excellent references (76-78) are available which discuss the detailed theory behind nuclear magnetic resonance and the CP/MAS experiment, it is useful to introduce some of the basic concepts.

2.4.2 The NMR Experiment

When spin ½ nuclei (i.e. ^{13}C) are placed in an external magnetic field, B_o, the nuclei will precess at a frequency ν. The precessional (or Lamor) frequency of the nuclei is represented by:

$$\nu = gB_o \tag{2.5}$$

where γ is the magnetogyric ratio, and B_o is strength of the external magnetic field. The spin populations will be distributed between two orientations with respect to the magnetic field (opposed and aligned) according to a Boltzmann distribution:

$$\frac{N_{high}}{N_{low}} = e^{\frac{-\Delta E}{kT}} \tag{2.6}$$

where N_{high} is the population of nuclei in the high energy state (i.e. opposing B_o), N_{low} is the population of nuclei in the low energy state (i.e. aligned with B_o), ΔE is the difference in energy

between the two levels, k is the Boltzmann constant and T is the absolute temperature. The population of nuclei initially in the low energy state is in excess. Therefore, when nuclei are irradiated with a radiofrequency (RF) source at the same frequency as the precessional frequency, spins in the low energy state are transferred to the high energy state. The absorption of energy is recorded as the NMR signal.

2.4.3 Resolution and Signal Enhancement Techniques – The Solid-State ^{13}C CP/MAS Experiment

Magic angle spinning (MAS) was first reported by Schaefer and Stejskal (74) and is accomplished by spinning the entire sample at an angle of 54^o 44' with respect to B_o. Sample spinning rates are rapid, on the order of kHz. This has the effect of averaging out the line broadening effects of the chemical shift anisotropy (76).

Cross polarization is a method of signal enhancement, whereby energy is transferred from abundant spins (^1H) to the rare spins (^{13}C). This phenomenon was first described by Hartmann and Hahn (73) and is accomplished by a double resonance experiment. RF pulses are applied to both ^1H and ^{13}C nuclei, so that:

$$\gamma_H H_H = \gamma_C H_C \tag{2.7}$$

where γ is the magnetogyric ratio and H_1 is the RF field strength. This is referred to as the Hartmann-Hahn condition. Under this condition, static transfer of magnetization occurs from the ^1H reservoir to the ^{13}C reservoir, resulting in an enhancement of the ^{13}C signal. Additional requirements for efficient cross polarization are: sufficient molecular rigidity and close proximity (less than 10 angstroms) (77).

A typical pulse sequence used to obtain ^{13}C CP/MAS NMR spectra is shown in Figure 2.12.

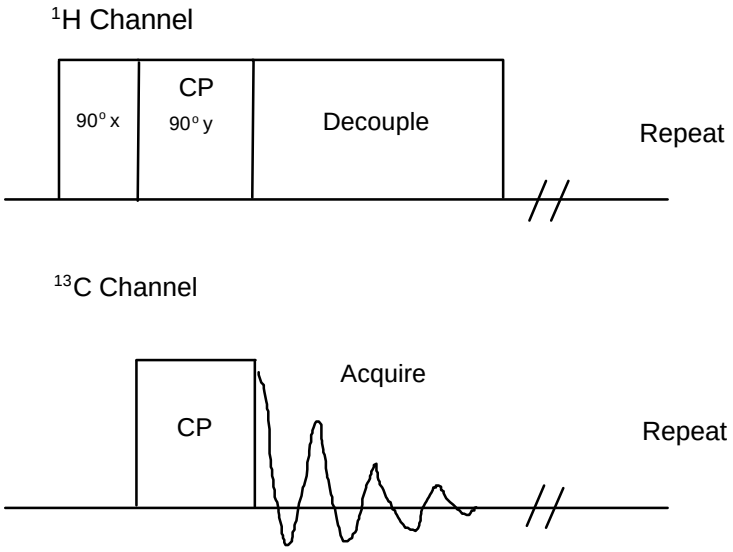

Figure 2.12: A Typical ^{13}C CP/MAS Pulse Sequence

A radiofrequency pulse is applied to the proton channel along its x-axis (with respect to B_o), flipping the spin orientation 90^o. This is referred to as the spin-locking pulse. Radiofrequency pulses are then applied to both the proton and carbon reservoirs which phase shifts the protons 90^o along their y-axis and allows the Hartmann-Hahn match to be established. Cross polarization is allowed to occur during a contact time T. During this time the ^{13}C signal builds. The CP pulse is then turned off. The ^{13}C signal is obtained while the protons are subjected to a decoupling pulse, removing their dipolar coupling effects. The experiment is then repeated, the signal accumulated to give the required sensitivity.

2.4.4 Relaxation Measurements

The nature of the CP/MAS experiment allows for the measurement of a set of relaxation parameters, which can provide information on time dependant phenomena (i.e. molecular motions) within polymeric materials (72). These relaxation parameters allow the measurement of a wide range of molecular motions present in solid materials, from near static to MHz frequencies (77).

When the RF field applied at the Lamor frequency is turned off, the nuclei which had been excited to their high energy state will transfer energy to their surroundings in order to "relax" back to the original Boltzmann distribution of spins. The mechanism by which this energy transfer occurs can be divided into two general categories: spin-lattice and spin-spin. Spin-lattice (or T_1) relaxations, also referred to as longitudinal relaxations, are the result of coupling of the observed nuclei with local dipolar fields created by molecular motion (76). Spin-spin (or T_2) relaxations, also referred to as transverse relaxations, are the result of static transfer of energy between adjacent nuclei. These relaxation parameters can be measured through any nuclei observable in the NMR.

Several types of spin-lattice relaxations have been used to study molecular motions within solid polymeric materials. The main difference is the frequency of motions which they probe (77). ^{13}C spin-lattice relaxations (T_1) have been used to measure MHz frequency motions in highly mobile systems such as the soft segment of polyurethanes (79).

^{13}C spin-lattice relaxations in the rotating frame ($T_{1\rho}$), have been used to distinguish mid-kHz frequency main and side-chain motions in a wide range of glassy polymers (80-84). Motions in this frequency range are of particular interest, since they modulate bulk properties such as impact toughness (77). Interpretation of proton spin-lattice rotating frame relaxations (H $T_{1\rho}$) are more complex, since they not only arise from coupling of local dipolar fields, but from static transfer of energy between protons, due to their high natural abundance and close proximity (76). This type of interaction is rare for ^{13}C nuclei, due to their low natural abundance however, it has been shown to be a contribution to $T_{1\rho}$ in highly ordered, crystalline systems (81). Proton $T_{1\rho}$ experiments have been used primarily to probe the morphology of multi-phasic systems, such as polyurethanes (85). It has been found that individual phases relax independently of one another, each with its own characteristic proton $T_{1\rho}$ (85). From these measurements, estimates of domain size have been made (86). The use of variable temperature T_1 and $T_{1\rho}$ measurements of both protons and ^{13}C has allowed the determination of activation energies and correlation times for a variety of molecular motions (87-91). The measurement of cross polarization times (T_{CH}) probes very low frequency, near static motions (83). As previously mentioned, the efficiency of the cross polarization phenomenon is dependent on two factors: rigidity of the nuclei and their spatial proximity. Correlations between average T_{CH}, and dynamic storage modulus have been made for a variety of synthetic polymers (92,93), as well as for wood (94). Interphase morphology has also been investigated by measuring cross polarization behavior between protonated and per-deuterated polymers (95, 96). Measurement of CP from protonated polymer chains to per-deuterated polymer chains can yield information regarding molecular miscibility of polymer chains.

2.4.5 Applications of CP/MAS NMR to the Study of Wood Adhesives

CP/MAS NMR has been used extensively to study a variety of neat adhesives commonly used to bond wood (97-103). In particular, ^{13}C CP/MAS NMR has been useful in studying the chemical structure of urea formaldehyde (UF) (97), fufuryl alcohol (98), melamine formaldehyde (99) and phenol formaldehyde resins (100-102). ^{15}N CP/MAS NMR has been used to characterize the structure of UF (103) and polymeric isocyanate resins (32-34). The use of relaxation measurements to determine molecular motions within these materials has not been widespread.

Recent work has shown that CP/MAS NMR is ideally suited for the characterization of intact wood-isocyanate bondlines. Wendler and Frazier (35,36) used ^{15}N CP/MAS NMR to probe cure chemistry and molecular dynamics of ^{15}N labelled polymeric isocyanate adhesive cured in the presence of wood as a function of cure time, temperature and moisture content. From these results, the application of CP/MAS NMR for the study of other intact wood-adhesive bondlines holds great promise.

2.5 Fracture Toughness Testing of Bonded Wood Assemblies

2.5.1 Introduction

The strength and durability of a bonded joint in service is critical to its acceptance for a particular end use (104). In order to estimate these properties for the purposes of design, the mechanical performance and durability of adhesive bonds can be evaluated in a number of ways. In the field of wood adhesion, common ASTM tests are: compression shear block (D 905 - for glued lumber products) and tensile plywood shear (D 805-72 -for veneer products). There are several limitations to these tests, which hinder their capability in accurately evaluating adhesive performance.

The ASTM standards for both tensile and compression shear tests use amount of wood failure as a measure of adhesive performance. A recognized problem with this approach is that the amount of wood failure for one type of adhesive will vary significantly with the density of the adherends. It is known that wood density varies between species, within the same species (grown under different conditions) and as a function of position in the stem (heartwood vs. sapwood, juvenile wood vs. mature wood) (105). Therefore, the selection of the adherend will play a critical role in the test results.

Traditional shear testing of wood-adhesive bonds has been shown to introduce complex stress states to the bond under evaluation (7). In compression shear testing, grain angle plays a critical role in the applied stress-state. Tensile and compressive stresses perpendicular to the applied stress can arise depending on the grain angle of the adherends. Compression failure (crushing) of the adherends can also occur at points of loading. Okkonen and River (106) studied some of the factors affecting the strength of compression shear block specimens and have identified several sources of variability including radial vs. tangential plane of cut, species, shear tool, nature of notching and specimen size. Tensile shear specimens also have stresses perpendicular to the applied load, resulting in peel stresses being created. In addition to the complex loading involved, shear testing measures an average stress level, not a critical value at which failure occurs (106). Critical values are what design limits are based upon. Despite the aforementioned limitations of these tests, their use is still widespread.

Cleavage mode testing has been recognized as providing a more informative approach to evaluating the mechanical performance of adhesive bonds (107). This is because the stress state applied to the bondline is more consistent and controllable than with other test geometries (107). In addition, the type of failure, which the adhesive bonds undergo, is a more realistic estimate of failure of in situ composite or laminated members (108).

Cleavage testing, or fracture testing is based on concepts of fracture mechanics which originated with the work of Griffith (109). Historically, fracture mechanics developed around various criteria for crack initiation and propagation (110). The underlying assumption of this approach is that the materials under evaluation behave in a linear elastic fashion (i.e. no permanent deformation). The most important parameter, determined from fracture testing is the strain energy release rate (G_c). This is a measure of the energy required to create two new surfaces through fracture of the adhesive bond (110).

When a crack extends through the adhesive layer between two adhesively bonded beams, it is assumed that no change in total energy of the system occurs (assumption of linear elasticity). The total energy of the system is represented by (110):

$$dE = dD + dS = 0 \tag{2.8}$$

where E is the total energy of the system, D is the potential energy of deformation and S is the surface energy. The strain energy release rate (G), or rate of change in potential energy with crack length is defined as (110):

$$G = \frac{-dD}{bda} \tag{2.9}$$

where b is the width of the specimen and da is the crack extension. The potential energy of deformation (D) is represented by (110):

$$D = U - P\Delta \tag{2.10}$$

where U is the strain energy, P is the applied load and Δ is the displacement. For a linear elastic material (110):

$$U = 1/2P\Delta \tag{2.11}$$

and the strain energy release rate becomes (110):

$$G = \frac{P_c^{\,2}}{2b}\frac{dC}{da} \tag{2.12}$$

where G_{Ic} is the crack initiation energy, P_c is the critical load at crack initiation, b is the width of the specimen and dC/da is the change in compliance of the beam with crack length. The subscript I denotes opening mode fracture. This approach to the calculation of G is often referred to as the direct compliance method (111). This approach is most often taken when using a contoured double cantilevered beam (CDCB) geometry. The reason for this is that the contours can be designed so that dC/da is constant. This removes the need to monitor crack length during testing.

Strain energy release rates can also be calculated using the simple beam theory approach which models the adherends as beams on elastic foundations. In this approach, G is represented by (111):

$$G = \frac{12P^2a^2}{b^2h^3E} \tag{2.13}$$

where h is the height of the specimen and E is the modulus. The modulus may be calculated by (111):

$$E = \frac{8Pa^3}{bh^3d} \tag{2.14}$$

where d is the beam displacement.

It has been found that in cases where the adherends possess low ratios of plane shear to axial modulus, application of simple beam theory is not appropriate. In these cases, flexure of the adherends causes shear forces to develop at small crack lengths. This effect causes the measured value of crack length to be underestimated. In order to correct for the effects of shear, Williams (112) has derived a shear correction factor χ, which allows the correction of measured crack lengths. The shear correction factor can be calculated from the experimental relationship between compliance and crack length (111):

$$C^{1/3} = \left(\frac{8}{Bh^3 E} \right) (a + ch) \tag{2.15}$$

Since crack length is used in simple beam theory for the calculation of both modulus and strain energy release rate, both must be corrected. Corrected modulus is represented by (111):

$$E_c = \frac{8P(a + ch)^3}{bh^3 d} \tag{2.16}$$

and corrected strain energy release rate is represented by (111):

$$G = \frac{12P^2(a + ch)^2}{b^2 h^3 E_c} \tag{2.17}$$

Calculation of G by this approach is referred to as the shear corrected beam theory approach. Use of the beam theory approach (corrected or uncorrected) to the calculation of G is most often used when a simple cantilevered beam (DCB) geometry is used.

In an opening mode fracture test, an adhesively bonded assembly with a pre-crack is simply pulled apart. Critical loads (P_c) are measured and used to calculate G_c.

Arrest loads (P_a), which are the loads maintained by the specimen after the crack arrests, can be used to calculate G_a, which is the amount of energy stored in a specimen upon fracture. Both G_a and G_c can be used to calculate I, the brittleness index (113):

$$I = \frac{G_c - G_a}{G_c} \tag{2.18}$$

2.5.2 Applications of Fracture Testing to the Study of Wood-Adhesive Bonds

Early work in this area concentrated on the use of contoured specimens to evaluate G_c (113). As mentioned, the prime reason for this is it removes the need to monitor crack growth during testing. Contoured double cantilever beams (CDCB) were either made from solid wood pieces (113) or from flat beams with contoured aluminum bonded to the backs (115). Later, the use of contoured OSB backing was introduced (106).

It was recognized that in order to prevent crack propagation into the adherends, the grain angle of the wood adherends should converge at the bondline (113). The effect of grain angle was studied by Ebewele et al. (115). They found that G_c was highly dependent on grain angle, reaching a maximum at a grain angle of 90^o.

Numerous studies used the CDCB approach for opening mode fracture to study various aspects of wood adhesion. Ebewele et al. (118) studied the effects of filler on the fracture energy of PRF adhesives bonded to hard maple (*Acer* sp.). River et al. (119) used this technique to evaluate the effects of ageing on UF-yellow birch (*Betula* sp.) bonds. Ebewele et al. (118) studied the effects of cure time on PRF – hard maple (*Acer* sp.) bonds.

While the CDCB approach has yielded valuable information, the procedure for specimen preparation and calibration has been found to be time consuming. For this reason, a number of studies have used cantilevered beam (DCB) specimens and application of simple beam theory for the evaluation of wood-adhesive assemblies (120-122). Lim et al. (120) evaluated Japanese birch (*Betula maximowiczana* Regel) bonded to a variety of adhesives in Modes I, II and III failure. Lim and Mizumachi (121) studied Japanese birch-polyurethane bonds. Wood-epoxy bonds have also been the subjects of several studies (122) using DCB geometry. It should be noted however, that no use of shear correction was used in the aforementioned DCB studies.

2.6 References

1. Knop, A. and W. Scheib. 1979. Chemistry and Application of Phenolic Resins. New York: Springer-Verlag

2. Speier A. 1897. Danish Patent 99570.

3. Smith, A. 1899. Danish Patent 112685.

4. Luft, A. 1902. Danish Patent 140552.

5. Henschke, F. 1903. Danish Patent 157553.

6. Baekeland, L.H. 1907. U.S. Patent 942699.

7. Marra, A.A. 1992. Technology of Wood Bonding: Principles In Practice. New York: Van Nostrand Reinhold.

8. Broline, Bruce. Personal communication.

9. Freeman, J.H. and C.W. Lewis. 1954. J. Amer. Chem. Soc., 76, 2080.

10. Werstler, D.D. 1986. Polymer 27, 750-756.

11. Lilley, H.S. and D.W. Osmond. 1947. Proceedings of the XIth International Chemistry Congress, London.

12. Fyfe, C.A., A. Rudin and W. Tchit. 1980. Macromolecules, 13, 1322-1324.

13. Maciel, G.E., I-S Chuang and L. Gollob. 1984. Macromolecules 17, 1081-1087.

14. Zinke, A. 1951. J. Appl. Chem, 1, 257.

15. Ballerini, A.A. 1994. Ph.D. Dissertation. Virginia Polytechnic and State University. Blacksburg, Virginia.

16. Flory, P. 1953. Principles of Polymer Chemistry. Cornall University Press. New York.

17. Gan, S., J.K. Gillham and R.B. Prime. 1989. Journal of Appl. Poly. Sci., 37, 803-816.

18. Kim, M.G., W. Nieh and R.H. Meacham. 1990. Ind. Eng. Chem. Res., 30 (4).

19. Chow, S. 1977. Holzforschung, 31 (6)

20. Rials, T.G. 1992. ACS Symposium Series 489, 282-294.

21. Mizumachi, M. and H. Morita. 1975. Wood Science, 7 (3), 256-260.

22. Steiner, P.R. and S.R. Warren. 1981. Holzforschung, 35, 273-278.

23. Tchir, W. 1981. Ph.D. Dissertation. University of Waterloo. Waterloo, Canada.

24. Hawke, R.N., B. Sun and M.R. Gale. 1993. Forest Products Journal, 43 (1), 15-20.

25. Sun, B., R.N. Hawke and M.R. Gale. 1994. Forest Products Journal, 44 (3), 34-40.

26. Hawke, R.N., B. Sun and M.R. Gale. 1992. Forest Products Journal, 42 (11/12), 61-68.

27. Sun, B., R.N. Hawke and M.R. Gale. 1994. Forest Products Journal, 44 (4), 53-58.

28. Adams, A.D. 1980. Proceedings of the 14th International Particleboard/Composite Materials Symposium. T.M. Maloney ed., Pullman Washington. 195-205.

29. Frisch, K.C. and H.C. Voight. 1964. Chemical Reactions of Polymers. E.m. Fettes ed. Interscience Publishers. 927-1008.

30. Galbraith, C.J. and W.H. Newman. 1992. Pacific-Rim Bio-Based Composite Symposium. Rotorua, New Zealand. 130-142.

31. McLaughlin, A.W., W.J. Farrissey, L.M. Alberino and D.P. Waszecick. 1981. Proceedings of the 15th International Particleboard/Composite Materials Symposium. T.M. Maloney ed. Pullman, Washington. 255-264.

32. Duff, D.W. and G.E. Maciel. 1990. Macromolecules, 23, 3069-3079.

33. Duff, D.W. and G.E. Maciel. 1991. Macromolecules 24, 651-658.

34. Duff, D.W. and G.E. Maciel. 1991. Macomolecules 24, 387-397.

35. Wendler, S.L. and C.E. Frazier. 1994. Journal of Adhesion**,** 50, 135-153.

36. Wendler, S.L. and C.E. Frazier. 1996. International Journal of Adhesion and Adhesives, 16, 179-186.

37. Ni, Jianwen. 1996. Ph.D. Dissertation. Virginia Polytechnic and State University. Blacksburg, Virginia.

38. Sharpe, L.H. 1992. In The Interfacial Interactions in Polymeric Composites. Gunerli Akovali ed. NATO ASI Series E: 320, 1-20.

39. Adamson, A.W. 1976. Physical Chemistry of Surfaces, 3rd ed. Interscience Publishers. New York.

40. Sharpe L.H. and H. Schonhorn 1964. Surface Energetics, Adhesion and Adhesive Joints, Advances in Chemisty 43, 189.

41. Young, T. 1805. Phil. Trans. 95, 65.

42. Dupre, A. 1869. Theorie mechanique de la Chaleur. Gauthier-Villars. Paris, France.

43. Shaw, D.J. 1989. Introduction to Colloid and Surface Chemistry 4th ed. Butterworth-Heineman. Oxford.

44. DeLollis, Nicolas J. 1985. Adhesives, Adherends, Adhesion. Robert E. Kreiger Publishing Co. Malabar, Florida.

45. McLaren, D. 1948. Tappi, Tech. Assoc. Papers Series 31, 214-216.

46. Pizzi, A. 1994. Advanced Wood Adhesives Technology. Marcel Dekker Inc. New York.

47. Voyutski, S.S. and V.L. Vakula. 1963. Journal of Appl. Poly. Sci., 7, 475-491.

48. Krotova, N.A., L. Kirillova and B.V. Deryagin. 1954. Zhur. Fiz. Khim, 30 (9) 1921-1931.

49. Chow, S.Z. 1969. Wood Science**,** 1(4), 215-221.

50. Orchon, S. 1958. Technical Association of the Pulp and Paper Industry (TAPPI**),** 41(1), 33-37.

51. Gray, V.R. 1962. Forest Products Journal**,** . 12 (9), 452-461.

52. Herczeg, A. 1965. Forest Products Journal**,** 15(11), 499-505.

53. Stumbo, D.A. 1964. Forest Products Journal**,** 14(12), 582-589.

54. Gunnells, D.W., D.J. Gardner and M.P. Wolcott. 1994. Wood and Fiber Science, 26(4), 447-455.

55. Liptakova, E. and J. Kudela. 1994. Holzforschung, 48(2), 139-144.

56. Liptakova, E., J. Kudela, Z. Basti and I. Spirovova. 1995. Holzforschung, 49(4), 369-375.

57. Triboulot, P., C. Sales, A. Zerizer and P. Martin. 1995. Holzforschung, 49(5), 465-470

58. Marian, J.E., D.A. Stumbo and C.W. Maxey. 1958. Forest Products Journal**,** . 8(12), 345-351.

59. Pizzi, A., B. Mtsweni and W. Parsons. 1994. Journal of Appl. Poly. Sci. 52, 1847-1856.

60. Pizzi, A. and L.A. Panagama. 1995. Journal of Appl. Poly. Sci. 58, 109-115.

61. Pizzi A. and N.A. Owens. 1995. Holzforschung. 49, 269-272.

62. Freeman, H.A. 1959. Forest Products Journal**,** 9 **(**12), 451-458.

63. Marcinko, J.J. 1996. Proceedings of the Third Pacific Rim Bio-Based Composite Symposium. Hiromu Kajita and Kunio Tsunoda eds. Kyoto, Japan.

64. Cowie, J.M.G. 1991. Polymers: Chemistry and Physics of Modern Materials 2nd ed. Blackie Academic and Professional. London.

65. Mantanis, G.I. R.A. Young and R.M. Rowell. 1994. Holzforschung, 48 (6)

66. Twitchett, H.J. 1974. Chem Soc. Rev. 3 (2), 209.

67. Vick, C.B., K. Richter, B.H. River and A.R. Fried. 1995. Wood and Fiber Science, 27 (2), 2-12.

68. Vick, C.B. 1995. Forest Products Journal, 45 (3), 78-84

69. Vick, C.B. In Proceedings of Wood Adhesives 1995. Proc. No. 7296. 47-55 Forest Products Society. Mdison, Wisconsin.

70. Vick, C.B., K.H. Richter and B.H. River. U.S. Patent 5543487

71. Frazier, C.E., R. G. Schmidt and J. Ni. 1996. Proceedings of the Third Pacific Rim Bio-Based Composites Symposium. Hiromu Kajita and Kunio Tsunoda eds. Kyoto, Japan.

72. Maciel, G.E. 1984. Science, 226, 282-288.

73. Hartmann, S.R. and E.L. Hahn. 1962. Phys. Rev. 128, 2042.

74. Schaefer, J. and E.O. Stejskal. 1975. J. Amer. Cehm. Soc. 98 (4), 1031-1032.

75. Andrew, E.R. 1971. Prog. Nucl. Magn. Reson. Spectrosc., 8, 1

76. Mehring, M. 1983. Principles of High Resolution NMR in Solids. 2nd ed. Springer-Verlag, Berlin.

77. Fyfe, C.A. 1980. Solid State NMR for Chemists. Guelph University Press. Guelph, Canada.

78. Komoroski, R.A. High Resolution NMR Spectroscopy of Synthetic Polymers in Bulk. VCH Publishers. Deerfield Beach, Florida.

79. Marcinko, J.J., A.A. Parker, Y.T. Shieh and W.M. Ritchey. 1990. Journal of Polymer Science: Part C: Polymer Letters, 28, 301-306.

80. Schaefer, J., E.O. Stejskal and R. Buchdahl. 1977. Macromolecules, 10(2), 384-405.

81. Schaefer, J., M.D. Sefcik, E.O. Stejskal and R.A. McKay. 1984. Macromolecules, 17, 1118-1124.

82. Vanderhart, D.L. and A.N. Garroway. 1979. J. Chem. Phys, 71(7), 2773-2787.

83. Stejskal, E.O., J. Schaeffer and T.R. Steger. 1978. Faraday Symposium of the Chemical Society, 13, 56-62.

84. Garroway, A.N., W.B. Moniz and H.A. Resing. 1978. Faraday Symposium of the Royal Chemical Society, 13, 56-62.

85. Moreland, J.C., G.L. Wilkes, C.G. Moreland, S.S. Sankar, E.O Stejskal and R.B. Turner. 1994. Journal of Applied Polymer Science, 52, 1175-1180.

86. McBriety, V.G. and D.C. Douglass. 1981. Journal of Polymer Science: Macromolecular Review, 16, 295.

87. Chen, Q., T. Yamada, H. Kurosu, I. Ando, T. Shiono and Y. Doi. 1992. Journal of Polymer Science: Part B: Polymer Physics, 30, 591-601.

88. Laupretre, F., J. Virlet and J.P. Bayle. 1985. Macromolecules, 18, 1846-50.

89. Fleming, W.W., C.A. Fyfe, R.D. Kendrick, J.R. Lyerla, H. Vanni and C.S. Yannoni. 1980. Journal of the American Chemical Society, 193-217.

90. Fleming, W.W., J.R. Lyerla and C.S. Yannoni. Journal of the American Chemical Society 92-95.

91. Fleming, W.W., J.R. Lyerla and C.S. Yannoni. 1984. Journal of the American Chemical Society, 83-94.

92. Marcinko, J.J., A.A. Parker, P.L. Rinaldi and W.M. Ritchey. 1994. Journal of Applied Polymer Science, 51, 1777-1780.

93. Parker, A.A., J.J. Marcinko, P.Rinaldi, D.P. Hedrick and W.M. Ritchey. 1993. Journal of Applied Polymer Science, 48, 677-681.

94. Ni, J. and C.E. Frazier. 1996. Holzforschung, 50, 327-334.

95. Takegoshi, K. 1995. Annual Reports on NMR Spectroscopy, 30. Academic Press Limited. 98-130.

96. Parmer, J.F., L.C. Dickinson, J.C.W. Chien and R.S. Porter. 1987. Macromolecules 20, 2308-2310.

97. Maciel, G.E., N.M. Szeverenyi, T.A. Early, and G.E. Myers. 1983. Macromolecules, 16 (4), 598-604.

98. Maciel, G.E., I. Chuang and G.E. Myers. 1982. Macomolecules, 15 (4), 1218-1220.

99. Chuang, I., G.E. Maciel and G.E. Myers. 1984. Macromolecules 17 (5), 1087-1090.

100. Bryson, R.L., G.R. Hatfield, T.A. Early, A.R. Palmer and G.E. Maciel. 1983. Macromolecules, 16 (10), 1669-1672.

101. Maciel, G.E., I. Chuang and L. Gollob. 1984. Macromolecules, 17 (5), 1081-1087.

102. So, S. and A. Rudin. 1985. J. Poly. Sci. – Poly. Letts. Ed., 23, 403-407.

103. Chuang, I., B.L. Hawkins, G.E. Maciel and G.E. Myers. 1985. Macromolecules, 18 (7), 1482-1485.

104. Ebewele, R., B. River and J. Koutsky. 1979. Wood and Fiber, 11(3), 197-213.

105. Panshin, A.J. and C. de Zeeuw. 1980. Textbook of Wood Technology. McGraw-Hill Publishing Co. New York.

106. River, B.H. and E.A. Okkonen. 1993. Journal of Testing and Evaluation, 21(1), 21-28.

107. Dillard, D.A. and D. Lefebvre. 1990. Engineered Materials Handbook – Adhesives and Sealants – Section 5 – Testing and Analysis. H. Brinson, technical chairman. ASM International.

108. Hasmemi, S., A.J. Kinloch and J.G. Williams. 1990. Proc. Royal. Soc. Lond. A**.**, 427, 173-199.

109. Griffith, A.A. 1920. Phil. Trans. Roy. Soc. Lond., 221. 163

110. Liechti, K. Fracture Testing and Failure Analysis. 1990. Engineered Materials Handbook – Adhesives and Sealants – Section 5 – Testing and Analysis. H. Brinson, technical chairman. ASM International.

111. Blackman, B., J.P. Dear, A.J. Kinloch and S. Osiyemi. 1991. Journal of Materials Science Letters, 10. 253-256.

112. Williams, J.G. 1989. Composites Science and Technology, 21, 367-376.

113. River, B.H. 1994. In Pizzi, A. and K.L. Mittel, ed. Handbook of Adhesive Technology. New York: Marcel Dekker, Inc., 151-177.

114. Ripling, E.J., S. Mostovoy and H.T. Corten. 1971. Journal of Adhesion, 3, 107-123.

115. Ebewele, R., B. River and J. Koutsky. 1979. Wood and Fiber, 11(3), 197-213.

116. Scott, C.T., B.H. River and J.A. Koutsky. 1992. Journal of Testing and Evaluation, 20(4), 259-264.

117. Ebewele, R., B. River and J. Koutsky. 1986. Journal of Applied Polymer Science, 31, 2275-2302.

118. Ebewele, R., B. River and J. Koutsky. 1982. Journal of Adhesion, 14, 189-217.

119. River, B.H., R.O. Ebewele and G.E. Myers. 1994. Holz als Roh- und Werkstoff, 52, 179-184.

120. Lim, W.W., Y. Hatano and H. Mizumachi. 1994. Journal of Applied Polymer Science, 52, 967-973.

121. Lim, W.W. and H. Mizumachi. 1997. Journal of Applied Polymer Science, 63, 835-841.

122. Takatani, M. and H. Sasaki. 1980. Wood Research, 66, 30-50.

Chapter 3

Network Characterization of Phenol-Formaldehyde Thermosetting Wood Adhesive

3.1 Introduction

Wood-based composite products consist of wood in some refined form (strands, wafers, particles) with a thermosetting adhesive as the binder. The most common type of adhesive is resole, phenol-formaldehyde (PF) applied in liquid form. The strength and durability of wood-based composites is strongly related to the cured state of the binder. Curing variables such as time, temperature and water vapor pressure will all have significant influences on the properties of the cured composite. Unfortunately, the adhesive within a cured wood-based composite is not amenable to characterization by conventional methods (i.e. thermomechanical analysis and swelling studies). Therefore, there is no direct way of determining the glass transition temperature or crosslink density of the adhesive within the composite.

Solid-state NMR employing cross polarization and magic angle spinning (CP/MAS) is ideally suited for the characterization of intact wood-adhesive bondlines (1,2). Isotopic labeling of the adhesive with a nucleus active in the NMR will provide information about chemical structure as well as molecular dynamics in the bondline. In order to use CP/MAS NMR for analysis of the wood-PF bondline, it is first necessary to characterize the neat resin structure and molecular dynamics as a function of cure conditions. The purpose of this work is to correlate conventional methods of analysis, (thermomechanical analysis and swelling studies) with the CP/MAS NMR characterization of neat phenol-formaldehyde resin. Once this correlation has been established, CP/MAS NMR can be employed towards the greater objective of characterizing the wood-PF bondline.

3.2 Experimental

3.2.1 Materials

All materials were purchased from Aldrich Chemical Company and used as received. Resole, phenol-formaldehyde resin was synthesized using P : F : Na molar ratios of 1 : 2 : 0.2. Resin was prepared in 200 g batches. Appropriate amounts of phenol (99+%), paraformaldehyde (95%) and aqueous NaOH (50%) were added to the reaction vessel. Distilled water was added to attain a target resin solids content of 50%. The solution was brought to reflux and allowed to heat for 30 minutes in the open atmosphere. Subsequently, the reaction was quenched by immersing the reaction vessel in a cold water bath. Also, a deuterium enriched resin was synthesized with 85% deuterium labeling using the same procedure as above but substituting with the appropriate amounts of phenol-d_6 and paraformaldehyde-d_2.

3.2.2 Methods

Thermomechanical Analysis

Liquid resin (5 g) was placed in aluminum weighing boats and cured at 70 ^{o}C for 36 hrs in a closed vacuum oven at atmospheric pressure. This provided flat surfaces free of pitting.

The samples were subsequently post-cured at 110, 120, 130 or 140 ^{o}C for 15 minutes in the same oven.

Glass transition temperatures were determined for these samples using a Perkin-Elmer TMS-2 thermomechanical analyzer operating in expansion mode. Resin samples were approximately 10 mm^2 and had a thickness of approximately 0.5 mm. The temperature was scanned from -20 ^{o}C to 200 ^{o}C at a rate of 5 ^{o}C/min under air purge. The oven was cooled using liquid nitrogen. Each sample analysis was replicated twice for a total of three data points at each post-cure temperature. These samples were also subjected to solid-state NMR analysis; see below.

Swelling Studies

Two separate series of resin samples were prepared; both were cured using a two-stage thermal treatment. Each series of samples was cured in a different oven and under different conditions of relative humidity. One series of samples was cured in a low relative humidity environment and the other series was cured in a high relative humidity environment; the precise humidity was not measured. The noted difference in relative humidity occurred during the first stage of cure. The two series of samples will be referred to as the Low RH Series and the High RH Series. For the Low RH Series, liquid resin(5 g) was placed in aluminum weighing boats and cured at 70 ^{o}C for 36 hrs in an oven at atmospheric pressure. The samples were subsequently post-cured at 110, 120, 130 or 140 ^{o}C for 15 minutes in the same oven. The low humidity designation is assigned because water was allowed to freely escape the oven during the first stage of cure. For the High RH Series, liquid resin(5g) was placed in aluminum weighing boats which were inside 500 mL beakers that were covered with aluminum foil. The samples were cured at 70 ^{o}C for 36 hours in an oven. The samples were subsequently post-cured at 140, 150, 160 or 170 ^{o}C for 30 minutes in the same oven. The High Humidity designation is assigned because the use of closed beakers trapped water which was evolved from the reaction during the first stage of cure; liquid water condensed within the beakers that held the samples.

Swelling samples were first extracted in acetone for 48 hours in a soxhlet. Samples were approximately 20 mg in mass with a thickness of 0.5 mm. Removal of the sol fraction by extraction eliminates the effects that sol molecules may have on the swelling results. The samples were subsequently dried under vacuum (1-2 mmHg) at room temperature overnight. Density measurements were performed on extracted samples at room temperature using a pycnometer with water as the non-swelling medium. The mass of extracted samples prior to swelling was recorded. Thermogravimetric analysis showed that the samples contained approximately 6% inorganic ash, presumably in the form of NaOH. The samples were void free by visual inspection, however light microscopy revealed that the samples were porous, with pore sizes ranging from 2 to 10μm.

Swelling was performed in DMSO for 24 hrs. Samples were immersed in 5 mL of DMSO, within vials which were suspended in a silicone oil bath at the appropriate temperature. Temperature control was maintained by a Laboratory Devices Inc. Set-Temp temperature controller (± 3 ^{o}C) connected to a variable transformer. Swelling measurements were performed at a number of temperatures for each series of samples in order to determine polymer-solvent interaction parameters. The Low RH Series was swollen at temperatures of 110, 120, 130, 140 and 150 ^{o}C. The High RH Series was swollen at temperatures of 140, 150, 160, and 170 ^{o}C. After equilibrium swelling had been attained, the liquid solvent was removed by quickly patting

the samples dry using lint-free tissue paper, and the equilibrium mass was then recorded. Two swelling analysis replicates were performed, giving a total of three data points at each swelling temperature.

NMR Experiments

^{13}C CP/MAS NMR spectra were obtained on a Bruker MSL-300 MHZ spectrometer using a 7 mm Probenkopf MAS.07.D8 probe operating at 75.47 MHZ for ^{13}C nuclei. Resin samples from swelling studies (extracted) and thermomechanical analysis (unextracted) were pulverized with a mortar and pestle using liquid nitrogen. Pulverized samples were placed in a zirconium oxide rotor which was then sealed with a Kel-f cap. Elevated temperature experiments were performed at 40 ^{o}C using boron nitride caps. The Hartmann-Hahn condition was established using adamantane. Standard phase cycling was used during acquisition. Spinning frequency was 4 kHz (± 20 Hz) for all samples.

Proton spin-lattice rotating frame relaxation rates were obtained at room temperature using two different pulse sequences. Low RH Series samples, and samples used for thermomechanical studies, were analyzed with a pulse using a variable spin-lock prior to a fixed contact time. Contact time was 1.5 msec and spin-lock times ranged from 100 μsec to 12 msec. The High RH Series samples were analyzed with a standard cross-polarization pulse using a variable contact time. Contact times ranged from 25 msec to 12 msec. For each experiment, 600 scans per delay time were accumulated and the recycle delay was 3.75 sec. NMR analyses were replicated once for the High RH Series samples giving two data points for each post-cure temperature. Low RH Series samples were analyzed by NMR once for each post-cure temperature.

3.3 Results and Discussion

Thermomechanical Analysis

A typical thermomechanical spectrum obtained for the resin samples is shown in Figure 3.1.

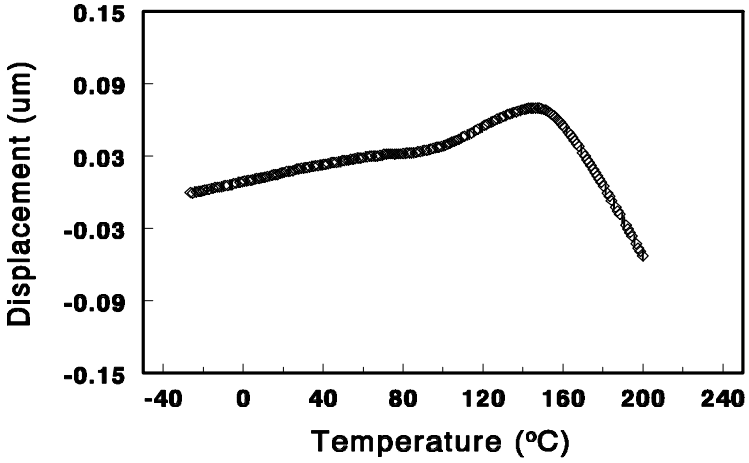

Figure 3.1: Typical Thermomechanical Spectrum of Cured PF

Glass transition temperatures (T_g's) were taken as the point of departure from the initial linearity of the trace, corresponding to the change from the coefficient of thermal expansion of the glassy state to the rubbery state. The results are shown in Table 3.1. The T_g's of the samples are shown to increase with post-cure temperature, as expected.

Table 3.1: Glass transition temperatures from thermomechanical analysis of cured PF as a function of post-cure temperature (mean value for three analyses).

Post Cure Temperature (^{0}C), Cure time = 15 mins	T_g (std err) ^{0}C
110	108 (5)
120	115 (3)
130	132 (1)
140	137 (3)

Swelling Studies

A variety of solvents were tested for their suitability in swelling cured PF. Initial solvent selection was based upon solvent boiling point and published solubility parameters of commercially produced Bakelite (3). Preliminary swelling studies showed that dimethyl sulfoxide (DMSO) proved
to be the best candidate, as shown in Table 3.2. These findings are in general agreement with calculated solubility parameters (δ) using the group contribution method (4):

$$d = \frac{r\Sigma F_i}{M} \tag{3.1}$$

where ρ is the polymer density, F is the contribution to the cohesive energy density by chemical group i of the repeat unit, and M is the molecular weight of the total repeat unit. The results of these calculations are shown in Table 3.3. Soluble fractions and sample densities are reported in Table 3.4.

Table 3.2: **Solubility parameters of solvents tested for PF swelling and the corresponding percentage mass increases determined for the solvents.**

Solvent	δ (MPa$^{1/2}$)	PF Mass Increase (%)
a-methyl styrene	16.0	0
Dicyclohexyl	17.4	0
2-ethyl hexanol	19.4	0
1,2-dichloroethane	20.1	1
Dimethyl oxalate	22.7	0
2-methyl pyrrolidone	23.1	28
Dimethyl sulfoxide	24.6	63
Ethylene glycol	29.7	26
Ethylene carbonate	30.1	1

Extreme care was needed to produce samples suitable for swelling analysis. This required a two-stage cure schedule in which the samples were first vitrified at low temperatures and subsequently post-cured at higher temperatures. This two-stage cure was used to produce two separate series of samples which were used for swelling analysis. The two groupings are designated the Low RH Series, and High RH Series. This is in reference to the relative humidity that the samples experienced during the first stage of cure, during vitrification (See experimental.). It will be shown

Table 3.3: Solubility parameters calculated from group contribution theory for a number of repeat units thought to be present in cured PF.

Repeat Unit and Solubility Parameter ($MPa^{1/2}$)	
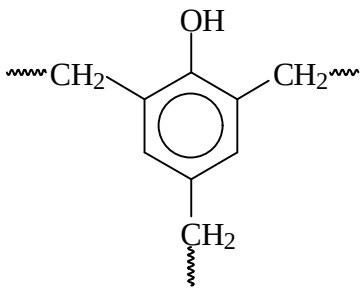	28.0
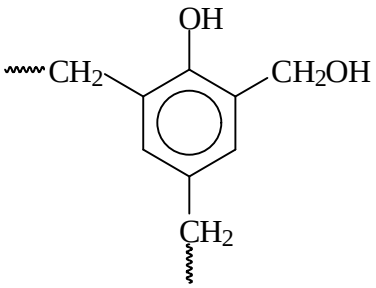	30.9
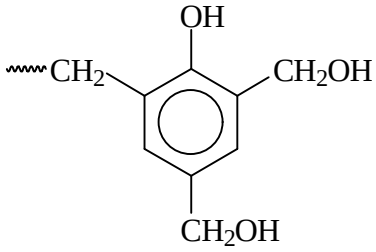	33.2
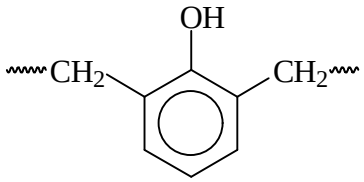	28.3
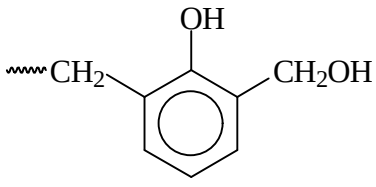	31.6

that this variable had a considerable effect on degree of cure. All samples were found to be extremely sensitive to both stages of cure. Samples which were not sufficiently cured fractured

within minutes of immersion in DMSO. Adequate control of both stages of cure resulted in smooth, monolithic samples which were homogeneous by visual inspection.

Table 3.4: Soluble fractions and densities of cured PF samples. Top: Low RH Series samples, Bottom: High RH Series samples (mean value for three analyses). Soluble fractions were determined from soxhlet extraction with acetone.

Post Cure Temperature(^{o}C), Post Cure Time = 15 mins	**density (std err) g/cm^3**	**Soluble fraction (%)**
110	1.3 (0.03)	1.0
120	1.3 (0.02)	1.1
130	1.4 (0.10)	1.7
140	1.3 (0.01)	1.6
Post Cure Temperature (^{o}C), Post Cure Time = 30 mins		
140	1.1 (0.10)	1.1
150	1.3 (0.10)	1.3
160	1.3 (0.04)	0.2
170	1.3 (0.10)	2.2

The number average molecular weight between crosslinks (M_c) can be determined by application of the Flory-Rehner swelling equation (4,5) given as:

$$M_c = \frac{V_s r_p \left(c^{1/3} - \frac{c}{2} \right)}{\ln c + c + cc^2} \tag{3.2}$$

where V_s is the molar volume of solvent, ρ_p is the polymer density, c is the polymer concentration at equilibrium and c is the polymer-solvent interaction parameter. The polymer concentration at equilibrium is given as:

$$c = \frac{m_o}{r_p V_\infty} \tag{3.3}$$

where:

$$V_\infty = \frac{m_o}{r_p} + \frac{(m_\infty - m_o)}{r_s} \tag{3.4}$$

m_o is the initial sample mass, m_∞ is the mass at equilibrium swelling and ρ_s is the solvent density. The polymer-solvent interaction parameter can be calculated from the temperature dependence of the equilibrium swelling by:

$$\frac{d\ln c}{d\ln T} = \frac{-3c(1-c)}{5(1-c)} \tag{3.5}$$

A plot of ln **c** as a function of ln T is used to calculate χ. An example of some of the swelling data from this study is shown in Figure 3.2.

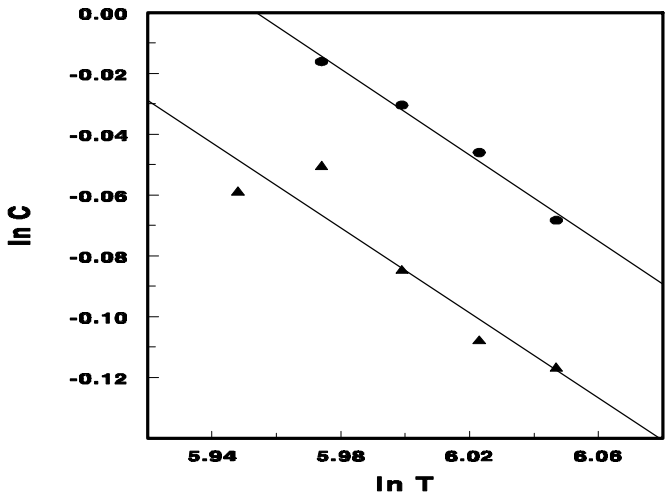

Figure 3.2: A plot of ln C vs. ln T used to calculate χ.

The molecular weight between crosslinks (M_c) for the different samples along with their corresponding **c** values are reported in Table 3.5.

Table 3.5: Molecular weight between crosslinks and polymer-solvent interaction parameters for cured PF obtained by swelling in DMSO. Top: Low RH Series samples, Bottom: High RH Series samples (mean value for three analyses).

Post Cure Temperature (^{o}C), Post Cure Time = 15 mins	M_c (std err) g/mol	χ parameter (std err)
110	55 (3.9)	0.98 (0.01)
120	--	--
130	28 (1.1)	0.99 (0.01)
140	19 (0.9)	0.97 (0.03)
Post Cure Temperature(^{o}C), Post Cure Time = 30 mins		
140	77 (6.3)	0.92 (0.02)
150	69 (6.3)	0.95 (0.02)
160	49 (9.8)	0.96 (0.01)
170	31 (2.7)[a]	--

[*] calculated using χ obtained at 160^{o}C.

No data is available for the samples post-cured at 120 ^{o}C because internal swelling stresses fractured those specimens. Also, it was not possible to calculate c for the sample post-cured at 170 ^{o}C, as significant swelling did not occur until the highest swelling temperature (170 ^{o}C). Therefore M_c for the samples post-cured at 170^{o}C were calculated using the **c** parameter of the sample post-cured at 160 ^{o}C. For the rest of the samples, M_c and c values were calculated at swelling temperatures equal to their post-cure temperatures, thus ensuring that the analysis was performed above the T_g. For each of the two series of samples, M_c is shown to decrease with increasing post-cure temperature. The values of M_c are shown to be unusually low, ranging from 77 - 19 g/mol, suggesting that the absolute values of M_c are questionable. It is well known that absolute values of M_c calculated using the Flory-Rehner approach have little practical significance due to some of the assumptions implicit to the theory (6). Also, NaOH trapped within the samples (see experimental) may be a confounding effect. However, relative comparisons of M_c obtained for similar systems, based on Flory-Rehner theory are valid, as demonstrated by the expected trends in Table 3.5. The reader should recall that while the samples were visually homogeneous, light microscopic examination revealed that the swelling samples where indeed microscopically porous. Pore sizes ranged from 2 to 10μm. Optical light micrographs of cured resin specimens are shown in Figure 3.4.

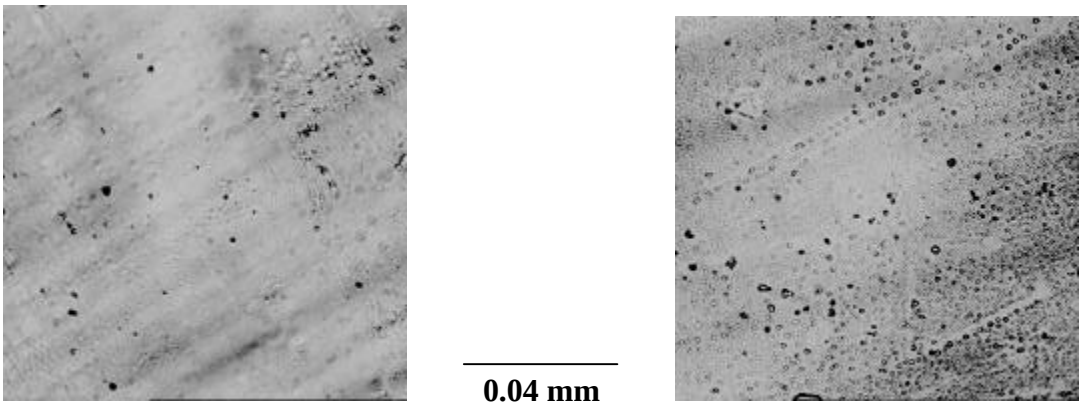

Figure 3.4: Optical Light Photomicrographs of Cured PF Resin. Post-Cure at 140°C (left), Post-Cure at 160°C (right). Magnification = 600 X.

The concern is that capillary uptake of solvent could affect the swelling results. One would expect sample capillarity to artificially inflate measured values of M_c. Since swelling decreased with increasing post-cure temperature, the low values for M_c suggest that capillary uptake of solvent is not a significant factor in this case.

Table 3.5 shows that crosslink density in these specimens is sensitive to the cure conditions. The Low RH Series is significantly more crosslinked than the High RH Series of specimens. This suggests that relative humidity has a significant effect on the degree of crosslinking. Recall that conditions of high and low humidity were imposed upon the respective series of samples during the first stage of cure, during vitrification. Notice that the Low RH Series is more heavily crosslinked than the High RH Series, even though the High RH Series was cured for longer times. This effect is anticipated given that PF resins cure via condensation equilibria. However, the sizable degree of this effect is surprising. It should be added that the two series of specimens were cured in different ovens. Consequently, the actual curing conditions may not be directly comparable, despite the nominal curing conditions indicated for the separate series. The apparent differences in cure conditions between these two series of samples become negligible, as will be shown later. The calculated χ parameters for PF (shown in Table 3.5) is 0.94 ($\pm$ 0.05). We believe that this is the first report of χ for this system.

^{13}C CP/MAS NMR

A typical ^{13}C CP/MAS spectrum for cured PF is shown in Figure 3.5. The peaks of interest are: the methylene bridge (35-40 ppm), unreacted hydroxymethyl (62 ppm), a composite signal of substituted and unsubstituted aromatic carbons not attached to the phenolic hydroxyl (Ar_2 - 135 ppm) and, the aromatic carbons directly attached to the phenolic hydroxyl (Ar_1 - 150 ppm). The remaining peaks in the spectrum are spinning side bands (labeled S) from the Ar_1 and Ar_2 peaks.

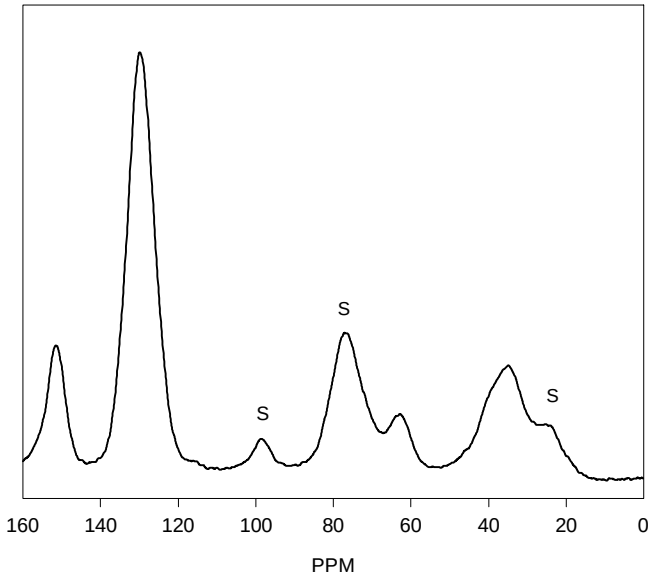

Figure 3.5: Typical ^{13}C CP/MAS NMR Spectrum of Cured PF

The polymerization of PF is known to occur via the condensation of hydroxymethyl groups to form methylene bridges. Partial spectra for the High RH Series of samples are shown in Figure 3.6. Subtle changes are apparent in these spectra.

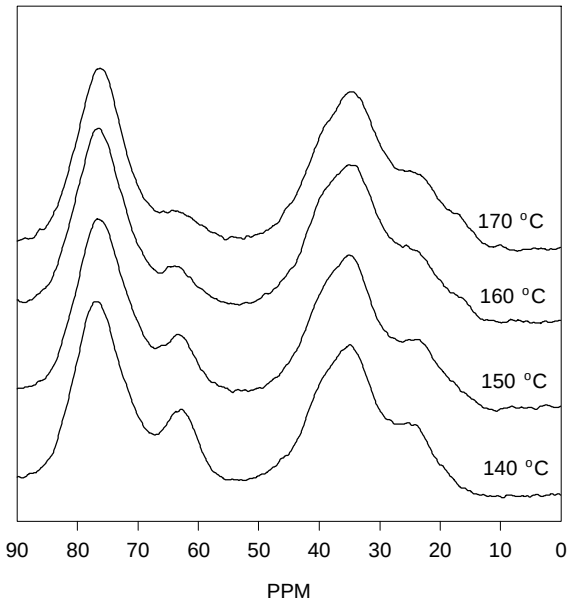

Figure 3.6: Partial ^{13}C CP/MAS NMR Spectra of Neat PF Specimens

As the post-cure temperature increases, the hydroxymethyl peak (62 ppm) diminishes and a slight broadening of the methylene bridge peak (35-40 ppm) occurs. However, the peak intensities shown in Figure 3.6 cannot be used to confidently estimate relative concentrations. This is due to the fact that different samples may display different cross polarization and spin-lattice relaxation rates. Consequently the peak intensities in Figure 3.6 must be corrected for this effect. The following relationship (7) provides a means to perform this correction:

$$I(t) = I^{*}\left(\frac{{}^{H}T_{1r}}{{}^{H}T_{1r} - T_{CH}}\right)\left(\exp^{-t/{}^{H}T_{1r}} - \exp^{-t/T_{CH}}\right) \tag{3.6}$$

where $I(\tau)$ is the intensity at contact time τ, I^{*} is the corrected intensity, $^{H}T_{1\rho}$ is the proton rotating frame spin-lattice relaxation time, and T_{CH} is the cross polarization time. The corrected signal intensity is that which would occur with instantaneous cross polarization and infinitely long $^{H}T_{1\rho}$. Figure 3.7 shows the ratio of the corrected intensities of the methylene to the hydroxymethyl, as a function of post cure temperature for the High RH Series of samples. This clearly shows increased conversion in the resin as a function of increasing post-cure temperature, as expected.

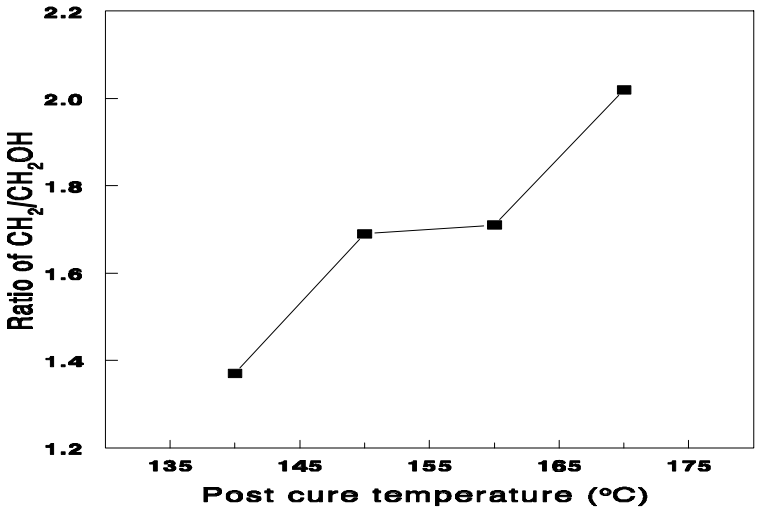

Figure 3.7: Corrected Ratios of Methylene : Hydroxymethyl as a Function of Post Cure Temperature

$^{H}T_{1\rho}$ is plotted as a function of post-cure temperature in Figure 3.8. These neat resins were found to relax homogeneously regardless of which carbon signal was used to measure $^{H}T_{1\rho}$. Consequently, relaxation rates were measured using the strongest signal (Ar_2,135 ppm). Both sets of samples show increases in $^{H}T_{1\rho}$ as a function of post-cure temperature. The disparity between the two series of samples is again evident. For example, Figure 3.8 shows that the High RH Series has lower values of $^{H}T_{1\rho}$, which corresponds to lower degrees of crosslinking.

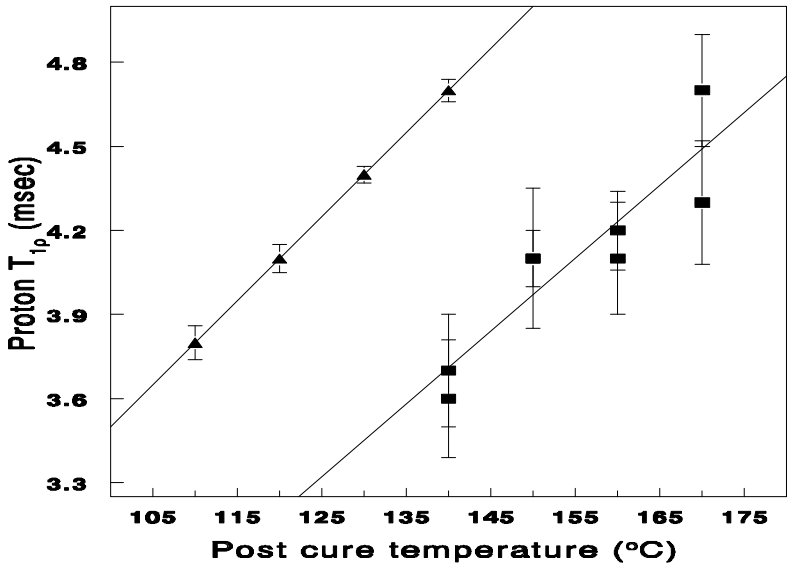

Figure 3.8: $^{H}T_{1\rho}$ as a function of post-cure temperature for the Low RH Series (▲) and the High RH Series (■) swelling specimens.

Variable temperature NMR experiments were performed on two samples from the High RH Series. $^{H}T_{1\rho}$'s are compared for NMR acquisition temperatures of 25 and 40 ^{o}C in Table 3.6.

Table 3.6: Proton $T^{H}_{1\rho}$ results obtained at NMR acquisition temperatures of 25 and 40^{o}C for two High RH Series specimens.

Post-Cure Temp (^{o}C)	$T^{H}_{1\rho}$ (std err) msec 25 ^{o}C	$T^{H}_{1\rho}$ (std err) msec 40 ^{o}C
140	3.7 (0.20)	3.6 (0.15)
	3.6 (0.21)	--
170	4.7 (0.20)	4.3 (0.11)
	4.3 (0.22)	--

For both samples, there was little or no significant difference in the value of $^{H}T_{1\rho}$. Relaxations such as $^{H}T_{1\rho}$ display minima as a function of the reciprocal of NMR acquisition temperature. A particular minimum value occurs at the nuclei's mean correlation time (t_c) (8) which is characteristic for a discrete motional process. On either side of the minimum are regions dominated by high frequency (high temperature) or low frequency (low temperature) molecular motions. A decrease in the value of $^{H}T_{1\rho}$ with increased acquisition temperature indicates the

protons are relaxing on the low frequency side of their t_c minima. An increase in the value of $^{H}T_{1\rho}$ with increased acquisition temperature indicates the protons are relaxing on the high frequency side of their t_c minima. No change in $^{H}T_{1\rho}$ means the protons are relaxing at or very near the minimum. Table 3.6 shows that the samples in this study are relaxing very close to, or at, the correlation time minimum. Consequently, increases in $^{H}T_{1\rho}$ with increased post-cure temperature indicate lower network mobility, as would be expected. With this knowledge we should predict that $^{H}T_{1\rho}$ could be correlated to network properties such as T_g. Figure 3.9 confirms this, showing that $^{H}T_{1\rho}$ is directly related to T_g in samples studied with thermomechanical analysis (R^2=0.96). The relaxations shown in Figure 3.8 were measured at room temperature, well below the lowest T_g shown in the figure. This suggests that $^{H}T_{1\rho}$ is revealing motional variations within the glassy states of these cured resins. These variations must arise from differences in network crosslink density. It follows that one could expect a correlation between $^{H}T_{1\rho}$ and crosslink density for the swelling samples. Indeed, Figure 3.10 shows that $^{H}T_{1\rho}$ and M_c are inversely related (R^2=0.79). The correlation shown in Figure 3.10 is independent of sample preparation. In other words, the noted dissimilarities between the Low RH Series and the High RH Series become unimportant. All samples are now described by a coherent relationship between $^{H}T_{1\rho}$ and M_c. This establishes a useful relationship between $^{H}T_{1\rho}$ and the degree of resin cure.

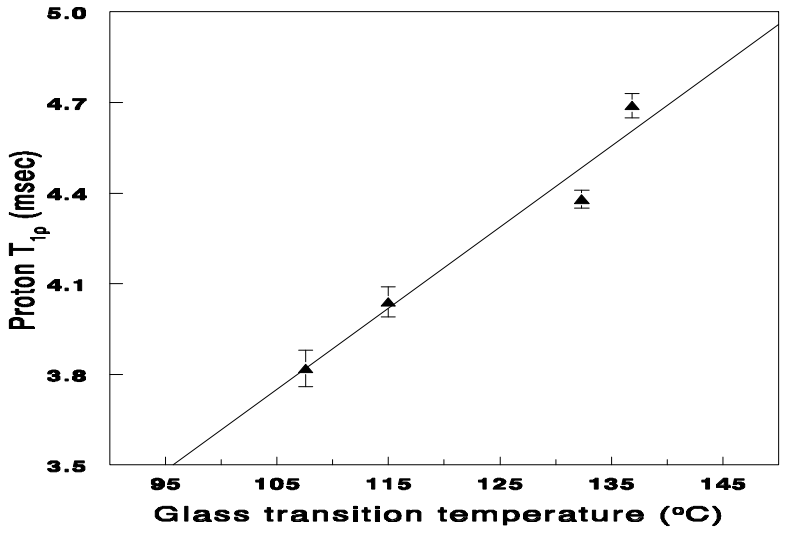

Figure 3.9: $^{H}T_{1\rho}$ as a function of glass transition temperature for samples tested with thermomechanical analysis

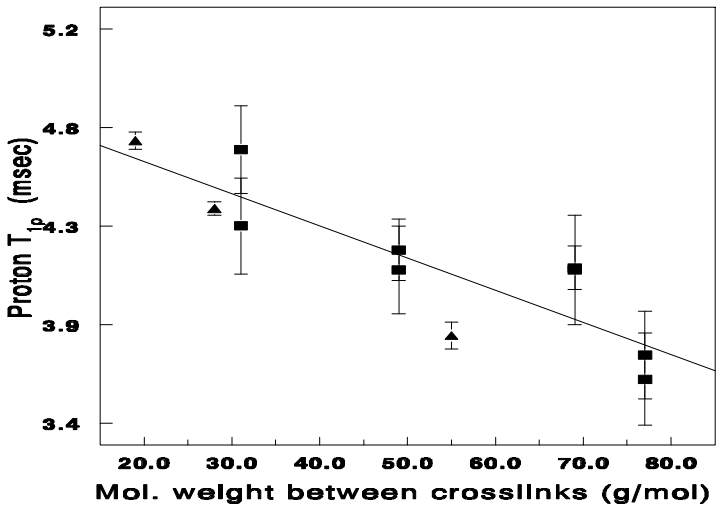

Figure 3.10: $^{H}T_{1\rho}$ as a function of molecular weight between crosslinks for Low RH Series (▲) and High RH Series (■).

The trends observed in Figures 3.9 and 3.10 do not display a great deal of sensitivity. While they are statistically significant, it is clear that the relationships are covering a narrow range of relaxation times. The probable reason for this is the contribution of spin diffusion to the observed values of $^{H}T_{1\rho}$. Spin diffusion is a spin-spin interaction and is therefore non-motional in origin. Spin diffusion occurs in organic solids due to the abundance and close proximity of protons. An equilibrium spin-temperature is established which allows magnetization transfer between static protons, effectively obscuring motional (spin-lattice) contributions to relaxation.

Two additional resins were made to evaluate the contribution of spin diffusion to the observed $^{H}T_{1\rho}$'s for this system. Samples from both resins were cured in a single stage process at different temperatures. One resin was synthesized as before; the other was enriched with 85% deuterium. Resin preparation and cure conditions were identical for both resins. The only difference between the two sets of samples was the presence of deuterium. $^{H}T_{1\rho}$ as a function of cure temperature for both samples is shown in Figure 3.11.

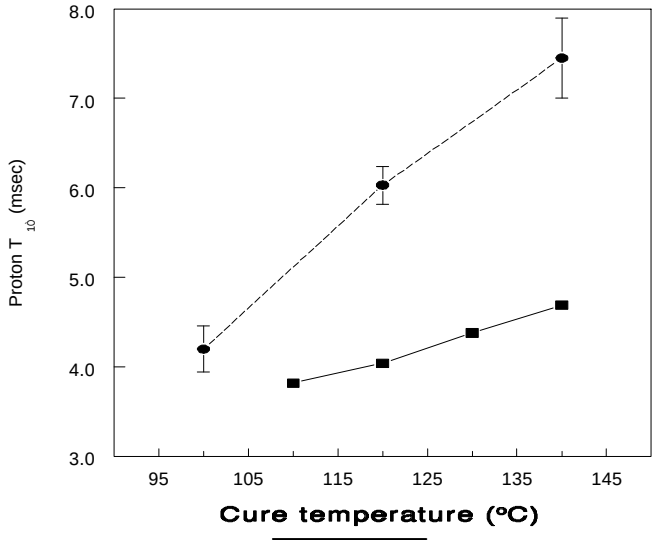

Figure 3.11: $^{H}T_{1\rho}$ as a function of cure temperature for ■ - fully protonated and ● - 85% deuterium enriched PF samples.

When compared to fully protonated samples, deuterium enriched samples display a greater sensitivity between $^{H}T_{1\rho}$ and resin cure temperature. Deuterium is inactive in this experiment and therefore dilutes the proton spin system, isolating protons and decreasing spin-spin interactions. This means that more of the motional characteristics of the resin are revealed by dilution of the spin system with deuterium. However it is important to note that spin-lattice contributions to $^{H}T_{1\rho}$ are amply evident in the fully protonated samples, as demonstrated by the trends in Figures 3.9 and 3.10.

3.4 Conclusions

The utility of ^{13}C CP/MAS NMR for the characterization of cured phenol-formaldehyde resin has been demonstrated. Relative degrees of conversion can be evaluated by monitoring the integrals of methylene and hydroxymethyl carbon signals. Proton longitudinal relaxation in the rotating frame ($^{H}T_{1\rho}$) probes molecular motions which correlate with cure temperature, glass transition temperature and crosslink density of neat cured phenol-formaldehyde. Although contributions from non-motional effects (i.e. spin diffusion) are present, they do not obscure this relationship. It was shown that the sensitivity of this technique can be increased by diluting the spin system with deuterium. This provides a method of determining relative degrees of network mobility within cured PF. With this technique established, the first steps toward the characterization of PF resin within a cured wood-based composite have been made.

3.5 References

1. Wendler, Steve L. and Charles E. Frazier. Int. J. Adhesion and Adhesives. 16, 179-186, 1996.

2. Wendler, Steve L. and Charles E. Frazier. J. Appl. Poly. Sci. 61, 775-782, 1996.

3. Shaefer, Jacob., E.O. Stejskal, T.R. Steger, M.D. Sefcik and R.A. McKay. Macromolecules. 13, 1121-1126. 1980.

4. Gundert, F. and B. A. Wolf. "Polymer Solvent Interaction Parameters" in Polymer Handbook, 3rd ed. J. Brandrup and E.H. Immergut eds. John Wiley and Sons, Inc. 1989.

5. Flory, Paul J. and John Rehner Jr. J. Chem. Phys. 11, 11, 1943.

6. Flory, Paul J. J. Chem Phys. 18, 1, 1950.

7. McKenna, G.B., K.H. Flynn and Y. Chen. Polymer Communications. 29, 1988.

8. Mehring, M. High Resolution NMR Spectroscopy in Solids, 2nd ed., Springer-Verlag, Berlin, 1983.

9. Fyfe, Colin A. Solid State NMR for Chemists**.** CFC Press. Guelph, Ontario Canada. 1983.

Chapter 4

^{13}C CP/MAS NMR as a Direct Probe of the Wood-Phenol Formaldehyde Bondline

4.1 Introduction

Large-scale solid wood members are gradually being replaced in structural applications by wood-based composite materials such as oriented strandboard, and laminated veneer lumber. These products consist of wood in a refined form (flakes, particles, veneer, strands) bonded with a thermosetting adhesive. The most common type of adhesive used is liquid resole phenol-formaldehyde.

The strength and durability of wood-based composite products is a function of the cured state of the adhesive. Processing variables during the cure of the adhesive, namely time, temperature and water vapor pressure, have significant influences on the physical and mechanical properties of the cured composite. Gradients in temperature and water vapor pressure can occur within a composite mat during production. PF is a thermosetting adhesive whose polymerization consists of condensation equilibria. Temperature and water vapor pressure gradients will therefore affect the cured properties of the adhesive. Unfortunately, cured adhesive within a wood-based composite is not amenable to characterization by conventional methods (i.e. thermomechanical analysis or swelling studies). Consequently, there is no direct way of analyzing the influence of curing variables on the properties of the cured adhesive. A direct probe of the cured adhesive within a wood-based composite would be valuable for the improvement of existing composite technologies.

Solid-state nuclear magnetic resonance spectroscopy (NMR) employing cross polarization and magic angle spinning (CP/MAS) has been demonstrated to be ideally suited for the characterization of intact wood-isocyanate bondlines (1,2). Information with regards to adhesive structure and molecular motions can be obtained. The results of Chapter 3 have shown that ^{13}C CP/MAS NMR is a powerful tool for the characterization of neat phenol-formaldehyde. It is possible to monitor resin conversion by assessing the ratios of chemical species present in the cured state. Additionally, molecular relaxation times have been correlated with both glass transition temperatures and crosslink densities for a series of neat resole phenol formaldehyde resins (see Chapter 3). This means that ^{13}C CP/MAS NMR can directly evaluate resin properties with the wood-resin bondline.

To demonstrate this technique, wood flake sandwich composites were manufactured and the bondlines were evaluated with ^{13}C CP/MAS NMR. To observe the adhesive in the presence of wood, it is necessary to use a PF resin enriched with ^{13}C. The purpose of this study is to employ ^{13}C CP/MAS NMR analysis to characterize phenol-formaldehyde cured in the presence of wood.

4.2 Experimental

4.2.1 Materials

Phenol (99+%) and 50% aqueous NaOH were purchased from Aldrich and used as received. 99% ^{13}C labelled paraformaldehyde was purchased from Cambridge Isotopes and used as received.

Flakes of yellow poplar (*Liriodendron tulipifera*) were hand turned from 2" x 2" x 8" blocks using a CAE Disk flaker. The blocks had previously been soaked in distilled water for 24 hours. Final dimensions of the flakes were 2" x 2" x 0.015". Flakes were oven-dried at 105 ^{o}C (± 3 ^{o}C) for 24 hrs and subsequently conditioned to a moisture content of approximately 5 %. This was accomplished by placing the flakes in a sealed dessicator over a saturated sodium sulfate solution for 24 hrs.

4.2.2 Methods

Resin Synthesis

Resole phenol formaldehyde resin was synthesized using a P : F : Na ratio of 1 : 2 : 0.2. Resin was synthesized in a 15 g batch by combining the appropriate amounts of phenol, ^{13}C labelled paraformaldehyde and 50% NaOH in a reaction vessel. Additional distilled water was added to attain a target resin solids content of 50%. The solution was brought to reflux and allowed to heat for 30 minutes in the open atmosphere. Subsequently, the reaction was quenched by immersing the reaction vessel in a cold water bath.

Composite Preparation

Flake composites were prepared by spraying resin onto a single flake, placing a second flake on top and then hot-pressing. Cure temperatures used were 110, 135 and 175 ^{o}C. At each temperature, three different cure times were employed: 1 min; 5 mins; and 10 mins. Replicates were made for the following cure conditions: 110^{o}C, 1 min; 135^{o}C, 5 mins; and 175^{o}C, 10 mins. Pressing was performed on a Micromet Instruments MP-2000 Minipress at a platen pressure of 40 psi. After each elapsed cured time, samples were weighed and stored at approximately 10 ^{o}C. Post-cure resin content was determined to be approximately 6 %.

NMR Experiments

Samples for NMR analysis were made by cutting small disks out of the flake composites using a paper hole puncher. These disks were randomly loaded into a zirconium oxide rotor and filled in and around with aluminum oxide powder. Kel-f caps were used to seal the rotors. Variable temperature experiments were performed using boron nitride caps.

NMR measurements were performed on a Bruker MSL-300 MHz spectrometer using a 7 mm Probenkopf MAS.07.D8 probe. The spectrometer operated at a frequency of 75.47 MHz for ^{13}C nuclei. The proton spin-lock field strength was approximately 56 kHz.

The Hartmann-Hahn match was established using adamantane. Standard phase cycling was used during acquisition.

Proton spin-lattice rotating frame relaxation times ($^{H}T_{1\rho}$) were obtained at room temperature by employing a standard cross polarization pulse with a variable contact time. Contact times ranged from 25 μsec to 9 msec. 600 scans were accumulated for each contact time. Recycle delay was 3.75 sec and all samples were spun at 4 kHz (± 20 Hz). Variable temperature experiments were performed at 0, 40, and 60°C.

4.3 Results and Discussion

A series of ^{13}C CP/MAS NMR spectra are shown in Figure 4.1. Yellow poplar flakes (top spectrum) are compared to two cured PF resins. The only difference between the two resins is that one is enriched with ^{13}C through the use of 99+% ^{13}C labelled paraformaldehyde during synthesis. The peaks of interest for the cured PF are: 150 ppm (carbons attached to the phenolic hydroxyl); 130 ppm (substituted and unsubstituted aromatic carbons); 63 ppm (unreacted hydroxymethyl carbons); and 35 ppm (methylene bridges). It is shown that the hydroxymethyl and methylene peaks of the labelled resin are enhanced. The signal enhancement is so pronounced that the other resin peaks are only slightly visible. It is shown that some signal overlap between the labelled resin and the wood flakes will occur when analyzing a flake composite. However, the intensities of the labelled peaks are so strong that overlap is not a significant problem.

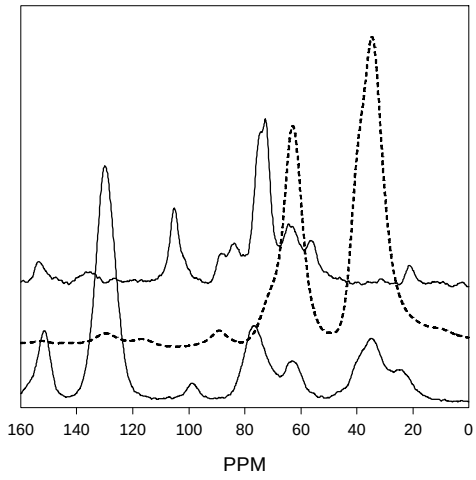

Figure 4.1: ^{13}C CP/MAS NMR Spectra for Neat Unlabeled PF (bottom), Neat ^{13}C labeled (100% ^{13}C on hydroxymethyl and methylene- bottom), and Yellow Poplar flakes (top)

^{13}C CP/MAS NMR spectra for composites at each cure temperature as a function of cure time are shown in Figures 4.2-4.4. The polymerization of PF proceeds by the condensation of substituted hydroxymethyl phenols to form methylene bridges as shown in

Figure 4.5. We can monitor the degree of conversion by observing the hydroxymethyl and methylene peaks in the spectra as a function of cure time or temperature. Figures 4.2-4.4 show that the reduction of the hydroxymethyl peak (63 ppm) and the increase of the methylene peak (35 ppm) may be followed as a function of cure time.

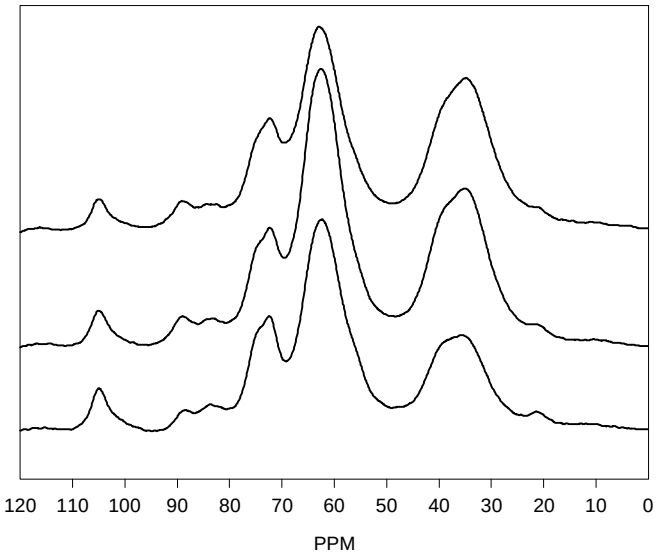

Figure 4.2: ^{13}C CP/MAS NMR Spectra for Yellow Poplar Composites made with ^{13}C labeled PF resin. Cure Temperature was 110 ^{o}C. Cure times were: 1 min (bottom), 5 mins (middle) and 10 mins (top)

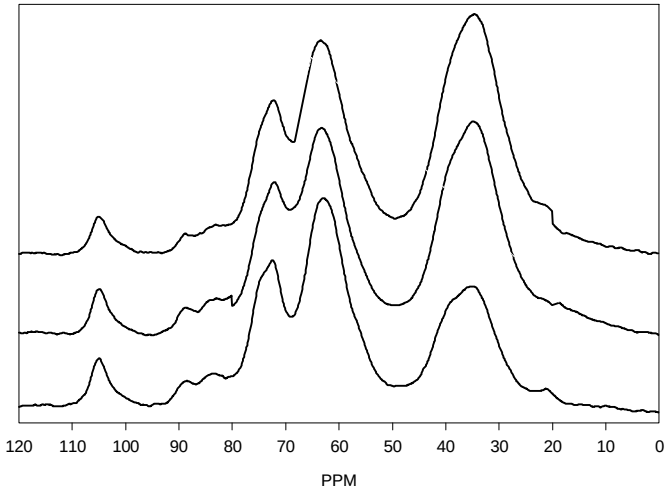

Figure 4.3: ^{13}C CP/MAS NMR Spectra for Yellow Poplar Composites made with ^{13}C labeled PF resin. Cure Temperature was 135 ^{o}C. Cure times were: 1 min (bottom), 5 mins (middle) and 10 mins (top)

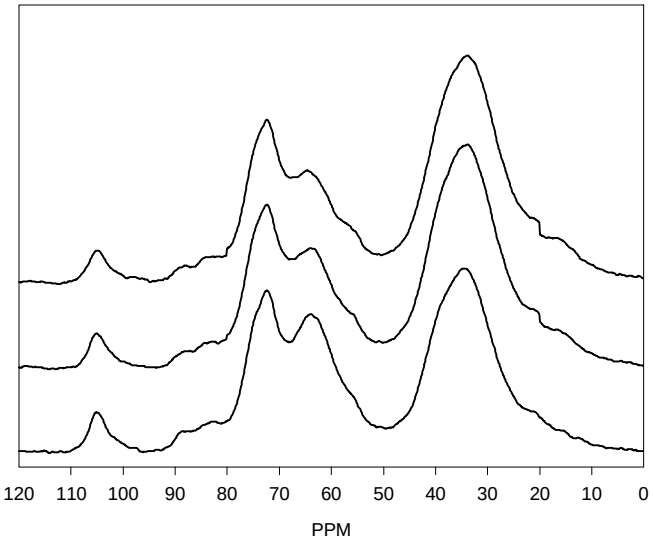

Figure 4.4: ^{13}C CP/MAS NMR Spectra for Yellow Poplar Composites made with ^{13}C labeled PF resin. Cure Temperature was 175 ^{o}C. Cure times were: 1 min (bottom), 5 mins (middle) and 10 mins (top)

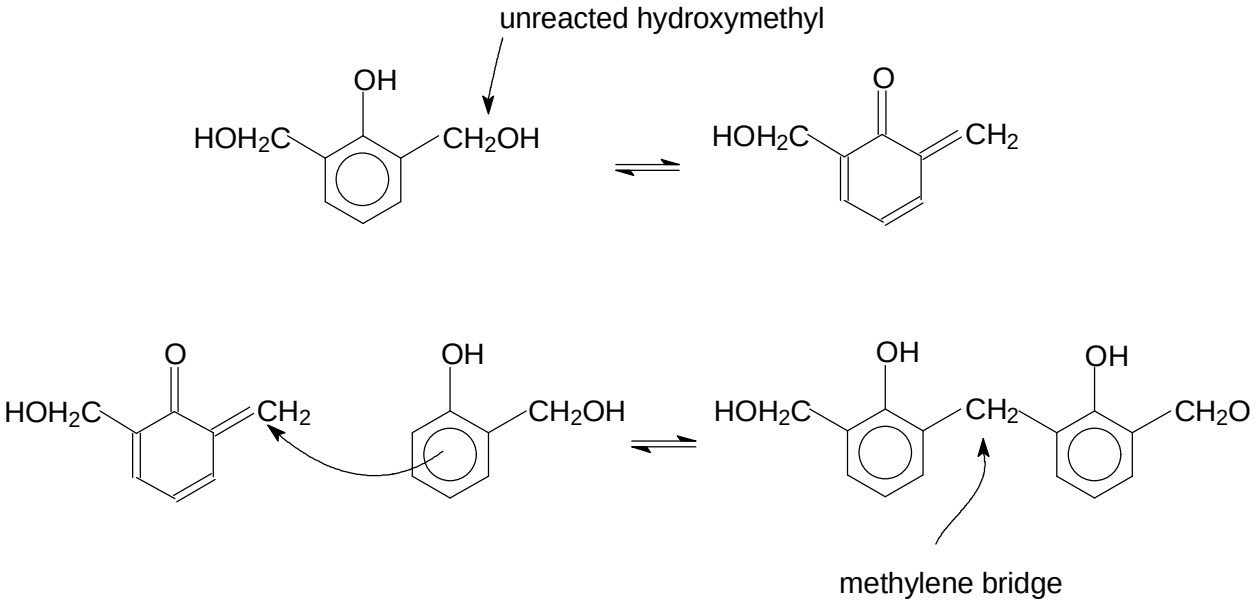

Figure 4.5: Polymerization of Phenol Formaldehyde

The changes shown in Figures 4.2-4.4 are more accurately followed by correcting the signal intensities for differential cross polarization and proton spin-lattice relaxation rates. For the variable contact time experiment, a relationship exists (3) which corrects spectral intensities:

$$I(t) = I^{*}\left(\frac{{}^{H}T_{1r}}{{}^{H}T_{1r} - T_{CH}}\right)\left(\exp^{-t/{}^{H}T_{1r}} - \exp^{-t/T_{CH}}\right) \qquad (4.1)$$

where $I(\tau)$ is the intensity at contact time τ, I^{*} is the corrected intensity, ${}^{H}T_{1\rho}$ is the proton rotating frame spin-lattice relaxation time, and T_{CH} is the cross polarization time. The correction gives a theoretical signal intensity at instantaneous cross polarization and infinitely long ${}^{H}T_{1\rho}$.

The ratio of corrected intensities of methylene to hydroxymethyl is shown in Figure 4.6. Increasing ratios indicate increasing resin conversion resulting from the effects of time and temperature, as expected. Figure 4.6 shows that the ratio of corrected signal intensities is highly sensitive to both cure time and temperature. However, note that the effects of cure temperature are more readily seen.

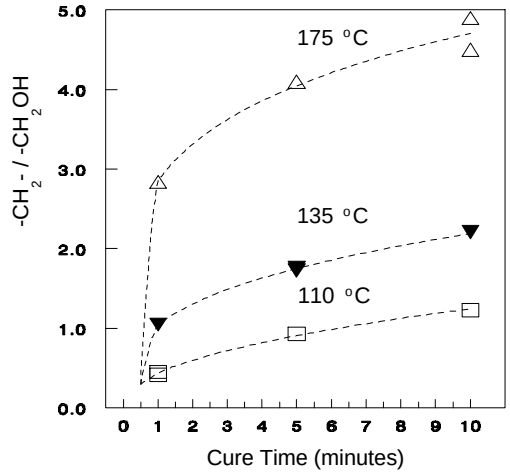

Figure 4.6: Corrected Ratios of Methylene: Hydroxymethyl Peak Areas for ^{13}C PF cured in the presence of wood. Cure temperatures: 110 °C (bottom), 135 °C (middle) and 175 °C (top)

It should be pointed out that signal overlap of the hydroxymethyl signal with that of the cellulose and hemicellulose C_6 may be causing an underestimation of methylene:hydroxymethyl at the cure temperature of 175 °C.

Values of $^{H}T_{1\rho}$ calculated from equation 4.1 are shown in Table 4.1 for the hydroxymethyl and methylene resonances. Rotating frame spin-lattice relaxation times such as $^{H}T_{1\rho}$, characterize molecular motions in the mid-kHz frequency range (4).

Table 4.1: Proton Spin-Lattice Relaxation Times for methylene (35 ppm) and hydroxymethyl (63 ppm) peak. Standard errors are shown in parenthesis

Peak	Cure Time = 1 min	Cure Time = 5 mins	Cure Time = 10 mins
Cure Temperature = 110°C			
62	4.1 (0.1) 4.1 (0.1)	4.3 (0.2)	4.7 (0.1)
35	4.3 (0.1) 4.3 (0.3)	4.4 (0.1)	4.4 (0.1)
Cure Temperature = 135°C			
62	4.6 (0.1)	4.9 (0.1) 4.5 (0.1)	5.1 (0.1)
35	4.2 (0.1)	4.4 (0.1) 4.3 (0.1)	4.4 (0.1)
Cure Temperature = 175°C			
62	5.4 (0.1)	6.1 (0.3)	5.9 (0.2) 5.7 (0.1)
35	4.7 (0.1)	5.2 (0.1)	5.4 (0.2) 5.1 (0.1)

$^{H}T_{1\rho}$ relaxation normally results from two processes: 1) the interaction of local dipolar fields and 2) static transfer of magnetization between spatially proximal protons, a process known as spin diffusion. Spin diffusion contributions are therefore non-motional in origin and can mask the motional contribution to the $^{H}T_{1\rho}$ relaxation. It has been shown that although spin diffusion is present in neat, cured PF, there is sufficient contribution from spin-lattice (i.e. motional) processes to allow qualitative evaluation of network mobility from $^{H}T_{1\rho}$ (see Chapter 3) Specifically, measurements of glass transition temperature and crosslink density have been found to correlate with $^{H}T_{1\rho}$. Increases in $^{H}T_{1\rho}$ follow increases in both T_g and crosslink density. Figures 4.7 and 4.8 show $^{H}T_{1\rho}$ as a function of both time and temperature.

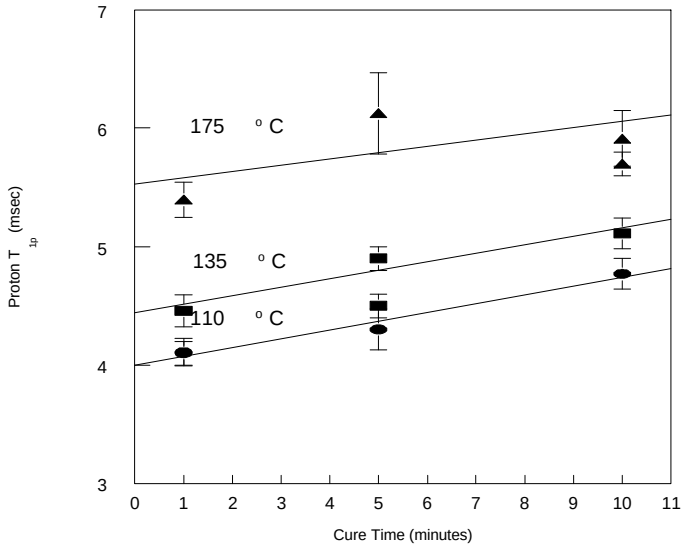

Figure 4.7: $^{H}T_{1\rho}$ as a function of cure time and temperature for the hydroxymethyl peak (63 ppm)

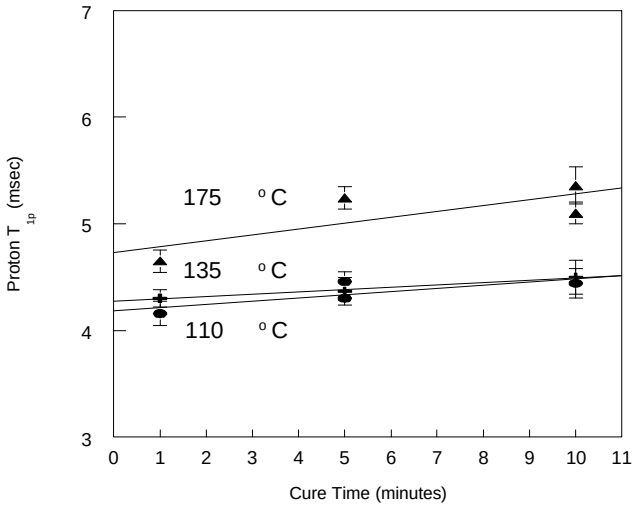

Figure 4.8: $^{H}T_{1\rho}$ as a function of cure time and temperature for the methylene peak (35 ppm)

At each temperature, little or no change in $^{H}T_{1\rho}$ occurs as a function of cure time. When comparing the $^{H}T_{1\rho}$ between cure temperatures, little or no difference is seen between 110 and 135°C. At each cure time however, cure at 175°C results in a significant increase in $^{H}T_{1\rho}$, indicating decreased network mobility. Figure 4.6 indicates that conversion increases as a function of both cure time and temperature. Increased conversion leads to reduced network mobility of the resin. These changes however, are not detectable in this case by $^{H}T_{1\rho}$. This lack of sensitivity to cure time and lower cure temperatures is most likely a result of contributions from spin diffusion (i.e. non-motional) processes. This complication has been encountered in work done on neat PF resin (see Chapter 3). It is possible to reduce the contribution of non-motional (spin diffusion) processes to the observed value of $^{H}T_{1\rho}$ by enriching the resin with deuterium (see Chapter 3). Deuterium is not active in a ^{13}C CP/MAS NMR experiment and acts to physically separate the remaining protons so that no static transfer of magnetization can occur (5).

It is interesting to compare the values of $^{H}T_{1\rho}$ obtained for the two adhesive resonances (63 and 35 ppm), as shown in Table 4.1 (p. 82). In previous experiments with neat resin, it has always been found that all protons within a sample shared a common $^{H}T_{1\rho}$ (see Chapter 3). This is indicative of a homogenous system in which all protons are in the same motional environment. In the case of PF cured in the presence of wood however, it appears that the $^{H}T_{1\rho}$ values of the protons of the hydroxymethyl carbons (63 ppm) are significantly different from those of the methylene carbons (35 ppm). This effect appears to be accentuated at longer cure times and higher cure temperatures. Effective spin-spin interactions (i.e. spin diffusion) are established when all protons are in the same motional environment. This results in an averaging of the proton relaxations resulting in a single value of $^{H}T_{1\rho}$ regardless of the carbons through which the relaxation is being probed. The results shown in Table 4.1 indicate that the protons of the hydroxymethyl groups are in a significantly different motional environment than those of the methylene groups. The effect of curing PF in the presence of wood then, is to significantly alter the motional processes which occur within the resin. These results could indicate that the hydroxymethyl groups are preferentially associated with the wood molecules.

The results from variable temperature CP/MAS NMR studies are shown in Figures 4.9 for both adhesive and wood resonances cured at 135°C for 1 min. and 175°C for 10 mins. $^{H}T_{1\rho}$ is plotted as a function of the inverse of acquisition temperature. Relaxation times such as $^{H}T_{1\rho}$ display minima in such plots when the precessional frequency of the observed nucleus becomes comparable to the inverse of the correlation time for a particular motion (6). This is expressed as:

$$w_o \sim \frac{1}{t_c} \qquad 4.2$$

where ω_0 = the precessional frequency (in this case ~ 56 kHz) and τ_c is the mean correlation time. Correlation time is defined as the mean time for a particular motion (i.e. side group rotation, backbone crankshaft motion) to occur. Slichter and Ailion (7) have postulated a relationship which relates $^{H}T_{1\rho}$ to τ_c:

$$^{H}T_{1r} = f(t_c) \qquad 4.3$$

Figures 4.9 and 4.10 show that for both adhesive resonances (methylene and hydroxymethyl respectively), significant differences in the motional character of the resin protons occur as a function of cure condition. In both cases, the values for $^{H}T_{1\rho}$ are larger for the samples cured at 175^{o}C for 10 minutes than the samples cured at 135^{o}C for 1 minute. This indicates that the correlation time for the particular motions being probed is increasing. Correlation time would be expected to increase as a result of lower mobility of the nuclei due to increased resin conversion.

Figure 4.9 shows that the methylene protons also show a decrease in the temperature sensitivity of $^{H}T_{1\rho}$ as a result of increased cure time and temperature. This phenomenon has been explained as a result of a broadening of correlation times for a particular motion (8). As resin conversion increases, it is expected that the distribution of molecular motions within the resin will also increase reflected by a broadening in the temperature response of the methylene $^{H}T_{1\rho}$'s. This effect is not seen for the hydroxymethyl protons (Figure 4.10). Motions probed via the methylene protons most likely represent backbone motions while the hydroxymethyl protons are more likely indicative of side group motions. Backbone motions would be much more sensitive to increased conversion as a result of increased crosslink density.

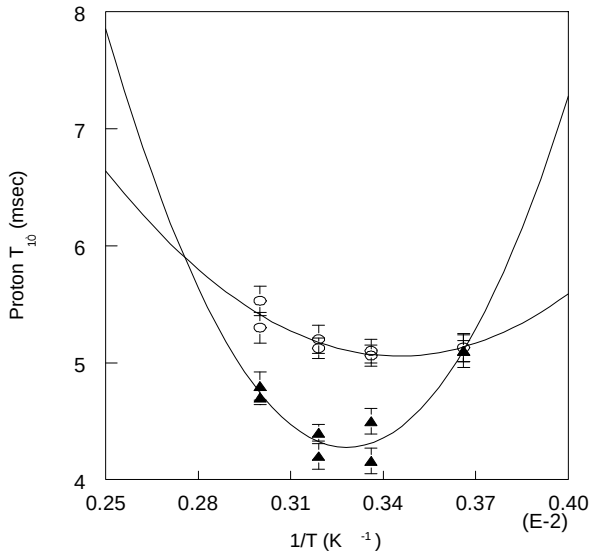

Figure 4.9: Variable Temperature $^{H}T_{1\rho}$ of the methylene protons (35 ppm). ▲ - cured at 135 ^{o}C for 1 minute ❍ - cured at 175 ^{o}C for 10 minutes.

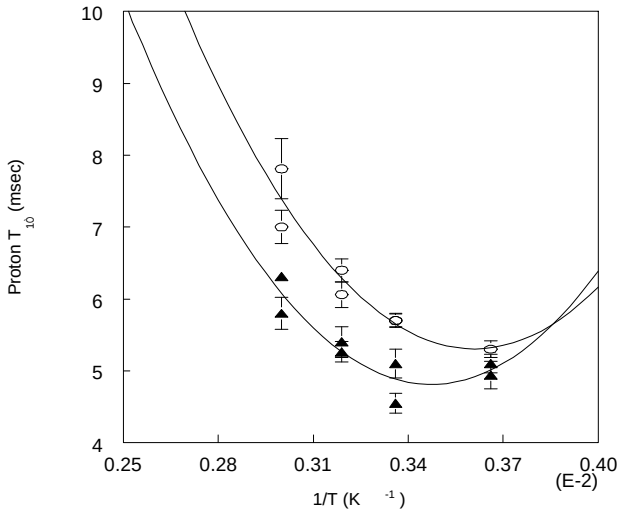

Figure 4.10: Variable Temperature $^{H}T_{1\rho}$ of the hydroxymethyl protons (63 ppm). ▲ - cured at 135 °C for 1 minute ❍ - cured at 175 °C for 10 minutes.

Figure 4.11, the temperature dependance of $^{H}T_{1\rho}$ for the 104 ppm wood resonance (C_1 of cellulose and hemicellulose), demonstrates little or no difference between the two cure conditions. This indicates that there is no significant difference in the motional character of the wood polymers between these two cure conditions.

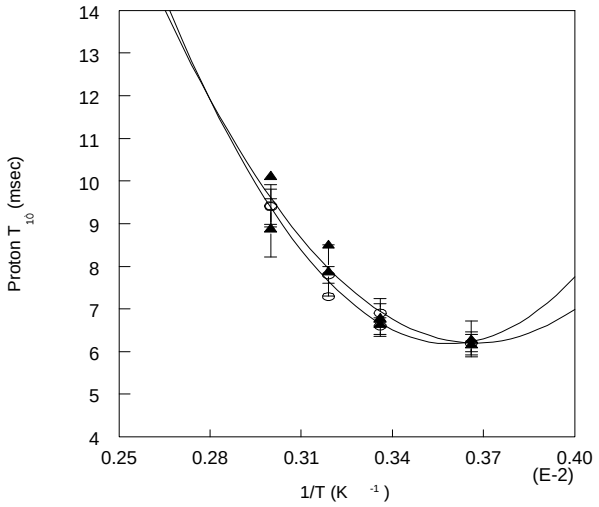

Figure 4.11: Variable Temperature $^{H}T_{1\rho}$ of the cellulose and hemicellulose C_1 protons (105 ppm).
▲ - cured at 135 °C for 1 minute ❍ - cured at 175 °C for 10 minutes.

4.4 Conclusions

The utility of ^{13}C CP/MAS NMR for elucidating molecular structure and dynamics of phenol-formaldehyde at the wood-adhesive bondline has been demonstrated. Corrected ratios of methylene to hydroxymethyl offer a qualitative estimate of relative degrees of resin conversion. Proton rotating frame spin lattice relaxation times ($^{H}T_{1\rho}$) can be used to assess relative degrees of adhesive network mobility, although the presence of spin diffusion can obscure motional contributions. Results from $^{H}T_{1\rho}$ measurements indicates that the protons of the hydroxymethyl carbons are in a significantly different motional environment than those of the methylene carbons. This may indicate preferential association of the hydroxymethyl groups with the wood substrate. Variable temperature $^{H}T_{1\rho}$ experiments can offer insight into changes in the distribution of molecular motions for both adhesive and wood components.

4.5 References

1. Wendler, Steve L. and Charles E. Frazier. Int. J. Adhesion and Adhesives. 16, 179-186, 1996.

2. Wendler, Steve L. and Charles E. Frazier. J. Appl. Poly. Sci. 61, 775-782, 1996.

3. Mehring, M. High Resultion NMR Spectroscopy in Solids, 2nd ed., Springer-Verlag, Berlin, 1983.

4. Shaefer, Jacob., E.O. Stejskal, T.R. Steger, M.D. Sefcik, R.A. McKay. Macromolecules. 13, 1121-1126. 1980.

5. Parmer, J.F., Charles Dickinson, James C.W. Chien and Roger S. Porter. Macromolecules 20, 2308-2310, 1987.

6. Fyfe, Colin A. Solid State NMR for Chemists**.** CFC Press. Guelph, Ontario Canada. 1983.

7. Slichter C.P. and D. Ailion. Phys. Rev**.** 135A, 1099. 1965.

8. McBrierty, Vincent J. and Dean C. Douglass. Journal of Polymer Science: Macromolecular Reviews, (16) 295-366 (1981)

Chapter 5

Lab-Scale Synthesis of Isotopically Labeled Formaldehyde for the Production of Formaldehyde-Based Wood Adhesives

5.1 Introduction

Solid-state nuclear magnetic resonance spectroscopy employing cross polarization and magic angle spinning (CP/MAS NMR) has proven a powerful tool in the characterization of phenolic and isocyanate adhesives at the wood bondline (see Chapter 4 and ref. 1). Information with regards to extent of cure and adhesive-adherend interactions can be obtained. In order to use these techniques, it is necessary that the adhesives are synthesized with a nucleus active in the NMR. This is easily accomplished through the use of ^{13}C labeled formaldehyde during synthesis. While unlabeled formaldehyde is relatively cheap and easy to obtain commercially, labeled materials are typically characterized by high costs and low availability. It is beneficial therefore, to have the in-house capability to synthesize labeled formaldehyde. The objective of this study is to revisit established methods of laboratory preparation of isotopically labeled formaldehyde and determine a suitable synthetic technique for the production of labeled formaldehyde-^{13}C-d_2. This technique could theoretically be applied to the synthesis of other types of labeled formaldehyde.

5.2 Background

The synthesis of formaldehyde singly labeled with ^{14}C is well documented in the literature (2). There is little information however, on the synthesis of formaldehyde labeled with either ^{13}C or deuterium. A review of the literature revealed that two main procedures are used in the lab-scale synthesis of labeled formaldehyde: reduction of carbon dioxide with lithium aluminum hydride; and catalytic oxidation of methanol. Both synthetic methods were investigated in order to identify the most suitable technique for the synthesis of isotopically labeled formaldehyde for the production of formaldehyde based wood adhesives.

Reduction of Carbon Dioxide

Carbon dioxide can be readily absorbed into solutions of lithium aluminum hydride (LAH) in tetrahydrofuran (THF), where it is subject to reduction. An overview of this reaction is shown in Figure 5.1 for the reduction of CO_2 to formaldehyde.

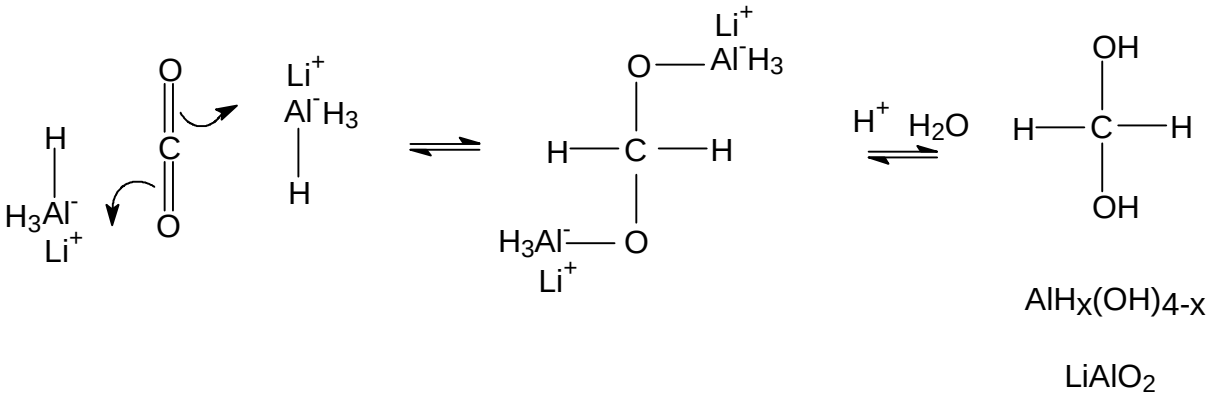

Figure 5.1: Reaction Mechanism Involved in the Reduction of CO_2 to formaldehyde in the presence of LAH

Two mols of hydride are required for reduction of carbon dioxide to formaldehyde. An aluminum complex species is initially formed. As the reaction proceeds, a metal oxide network is formed as the aluminum complexes continue to reduce CO_2. This network can be hydrolyzed by dilute acid to form methylene glycol (hydrated formaldehyde), lithium aluminate and various aluminum hydroxide species. The reduction can also lead to alternate products, depending on the molar ratios of CO_2:LAH and the reaction time. These reactions are outlined in Figure 5.2.

$$4CO_2 + 3LiAlH_4 \rightleftharpoons LiAl(OCH_3)_4 + 2LiAlO_2 \rightleftharpoons CH_2OH$$

$$2CO_2 + LiAlH_4 \rightleftharpoons LiAl(OCH_2)_2 \rightleftharpoons CH_2O$$

$$4CO_2 + LiAlH_4 \rightleftharpoons LiAl(OCH_3)_4 \rightleftharpoons COOH$$

Figure 5.2: Possible Reactions from the Reduction of CO_2 in the presence of LAH

If only one mol of hydride is transferred per mol of CO_2, formic acid results. This technique has been used to synthesize formic acid in appreciable yields (3). If three mols of hydride are transferred per mol of CO_2, methanol is the product. Methanol has also been synthesized in appreciable yields by this method (4). It has been found that molar ratio of CO_2:LAH of 1:1 gives higher yields of formaldehyde than CO_2:LAH of 2:1 (5). LAH can theoretically transfer 4 mols of hydride to CO_2. These results indicate that this does not occur for this system. It is likely that the complexes formed during the initial stages of reaction are hindered sterically, which would reduce their subsequent reactivity. The same study also found that reaction time of 0.5 hours produced optimum yield. Short reaction times presumably lead to formic acid while long reaction times would lead to methanol. A compositional analysis of the products however, was not performed (5).

Oxidation of Methanol

Primary alcohols such as methanol can be oxidized in the presence of metals or metal oxide catalysts. Industrially, the catalysts used to oxidize methanol to formaldehyde are silver, copper or molybdenum-iron oxide (6). The reaction mechanism has been investigated for the metal oxide catalyst (7-10) and the proposed mechanism is shown in Figure 5.3.

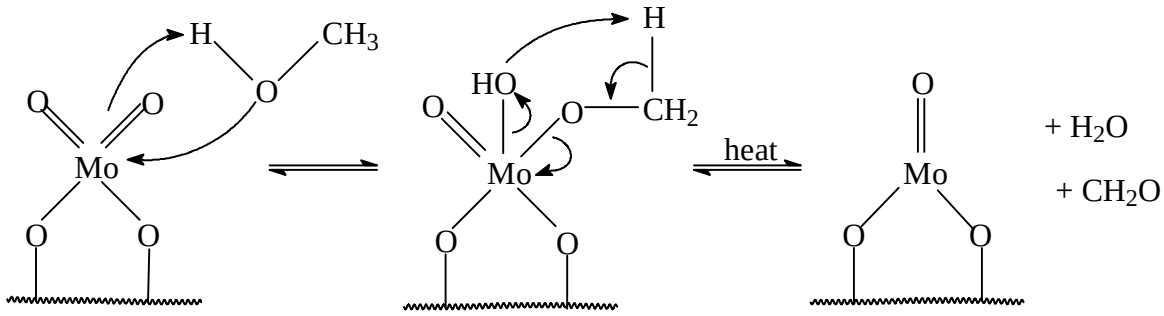

Figure 5.3: Reaction Mechanism involved in the oxidation of methanol in the presence of a molybdenum oxide catalyst

The reaction proceeds by the adsorption of methanol onto the oxidized catalyst where it forms methoxy groups. Reduction of the catalyst coupled with methoxy decomposition to formaldehyde and water occurs when the catalyst temperature is raised above 100^{o}C (8). The catalyst is then re-oxidized by molecular oxygen. The formaldehyde produced does not undergo further oxidation due to the presence of water and unreacted methanol, which successfully compete for available oxidation sites (9).

5.3 Experimental

Reduction of Carbon Dioxide

All materials were purchased from Aldrich Chemicals and used as received. A 1 molar solution of lithium aluminum hydride (LAH) in tetrahydrofuran (THF) (15 mL, 0.015 mol) was transferred via cannula under nitrogen to a dry 500 mL round bottomed flask. The flask was purged with nitrogen and then immersed in a Dewar flask filled with liquid nitrogen. After the LAH froze, the flask was evacuated at a pressure of 3 mm Hg. Carbon dioxide was introduced from a lecture bottle via a triple-necked alternate two-way flow stopcock. An ordinary balloon, connected to the stopcock, was inflated with CO_2 to approximately the volume of the 500 mL flask and then introduced into the flask containing the frozen LAH. The mixture was allowed to sit for 5 minutes, after which time it was placed in an ice-bath and gently swirled for 30 minutes. After the reaction time had elapsed, the excess LAH was decomposed with the careful dropwise addition of 0.1 normal sulfuric acid, which caused some foaming. After foaming had ceased, additional acid (30 mL, 0.003 mol) was added to hydrolyze the alumina complexes. The THF was removed by rotational evaporation. The remaining slurry was distilled at atmospheric pressure to isolate the formaldehyde-water solution. Three times during the distillation, just prior to the pot boiling dry, an additional 20 mL of distilled water was added to ensure complete removal of

formaldehyde. Yield was determined by gas chromatography. The gas chromatograph was calibrated with formaldehyde calibration samples produced from a formaldehyde solution which had been standardized by sodium sulfite titration.

A fractional condensation column was constructed consisting of a 26" long 3" OD tube. An arm ending in a 24/40 adapter was positioned 3" from the bottom end. An arm ending in a 19/22 adapter, 2" from the top end, was connected to a secondary condenser coil and receiver flask. The bottom was closed with a hose nipple adapter. A 6" coil of 1/4" copper tubing was inserted at the top of the column through a rubber stopper as the primary condenser. A thermometer extended 0.5" past the end of the coil. The remainder of the column was packed with 5 mm glass beads. The design of the column was adapted from the patent literature (11,12).

Oxidation of Methanol

Methanol, purchased from Fischer Scientific, was distilled prior to use to remove impurities. Methanol-^{13}C-d_4 was purchased from Cambridge Isotopes and used as received. Iron Molybdenum Oxide, manufactured by Perstorp Polyols was obtained from Neste Resins Corp. The catalyst was pulverized using a mortar and pestle prior to use. The particles were screened and only those greater than 18 mesh were utilized. Compressed air was used throughout.

The apparatus used to perform the oxidation was a modified version of that described by Murray et al. (13). The apparatus is shown in Figure 5.4.

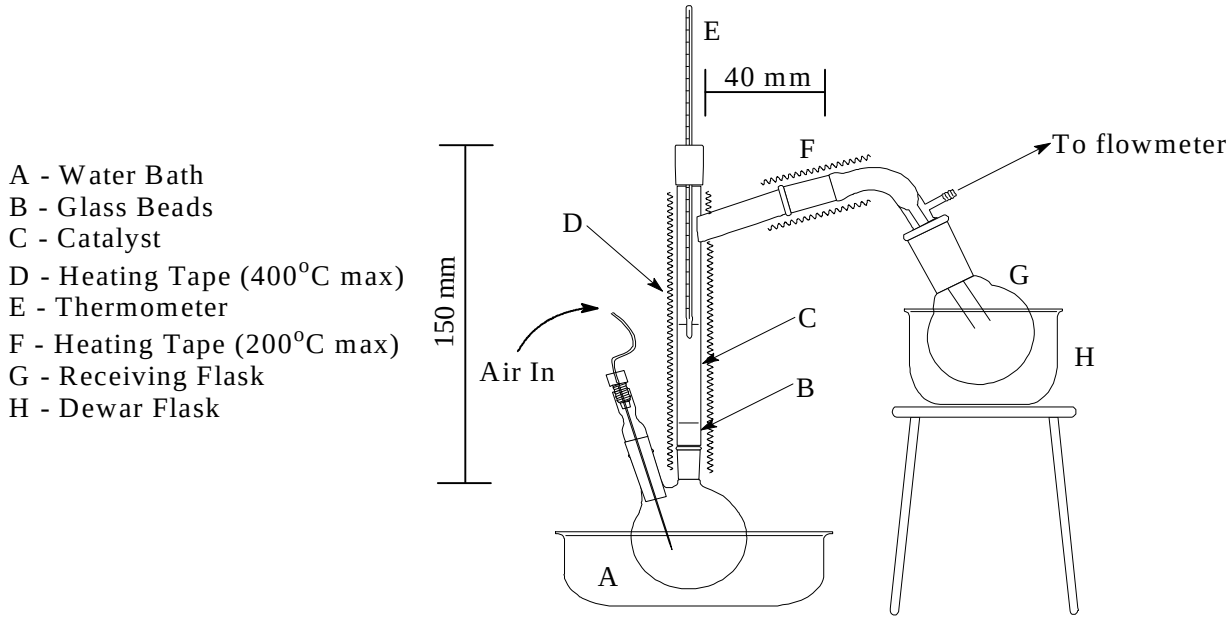

Figure 5.4: Apparatus used in the synthesis of labeled paraformaldehyde

The air was dried by passing it through gas bubblers filled with concentrated sulfuric acid, calcium chloride pellets and potassium hydroxide pellets. A safety trap separated the H_2SO_4 from the $CaCl_2$. The dried air was passed into a double necked (19/33) 50 mL round bottomed flask containing methanol at the base of the oxidation chamber. The oxidation chamber consisted of a 20 mm OD piece of Pyrex tubing with a single outlet arm. A 40 mm high column of 5 mm diameter glass beads were used to ensure mixing of methanol vapors and air. 5 g of catalyst was used, separated from the glass beads with a small plug of glass wool. The bulb of a 500°C thermometer extended into the catalyst. The outlet arm (19/22) was also filled with glass wool. A receiver adapter was manufactured so that the outlet tube extended 40 mm past the edge of the 19/22 male adapter. The receiver adapter was connected to a Cole-Parmer teflon flowmeter. The receiver flask was partially immersed in liquid nitrogen. The oxidation chamber was wrapped in a glass heating tape and heated to 340°C (±5°) prior to reaction. The receiver adapter was wrapped in a heating tape and maintained at a temperature of 120°C (± 5°) throughout the reaction. Air flow rate was adjusted to maintain a flow rate of approximately 170 mL/min. throughout the reaction.

In a typical run, the catalyst was heated to temperature with air blowing through an empty double necked 50 mL round bottomed flask with the receiver flask in place submerged in liquid N_2. After the catalyst temperature had stabilized, the empty flask was replaced with one containing a known quantity of methanol. The reaction was exothermic,

producing a reaction temperature of 370 ^{o}C (± 5 ^{o}C). After the methanol had been consumed and the catalyst temperature had returned to 340^{o}C (±5^{o}), the receiver adapter and flask were removed from the apparatus. The adapter was allowed to air dry overnight. The product in the receiver flask was dried with a steady stream of air overnight. Some paraformaldehyde was condensed in the adapter. This was easily removed and collected. The product was then vacuum dried for 4 hours. Yield was determined by the weight of paraformaldehyde. Formaldehyde solutions were prepared by combining appropriate amounts of water and paraformaldehyde and heating at 120 ^{o}C in a pressurized test tube for 24 hrs.

Yield Determination from Hydride Reduction

All materials were purchased from Fischer Scientific and used as received. The procedure was taken from Walker (6). A 1 molar solution of sodium sulfite was prepared by placing 126 g of anhydrous Na_2SO_3 in a 1 L volumetric flask and filling it to the mark with distilled water. 50 mL of this solution were pipetted into a 250 mL Erlenmeyer flask containing a stir bar. 6 drops of 0.05 % thymolphthalein (in ethanol) were added. 3 g of neutral formaldehyde solution were then added which turned the solution blue. The solution was titrated with standardized 1 N HCl until all blue color disappeared. Percent formaldehyde was calculated by:

$$\% \, formaldehyde = \frac{V * N * 30.03}{V_s}$$

where V is the volume of 1 N HCl added to remove indicator color, N is the normality (equivalents/mL) of the HCl solution, 30.03 is the number of milligrams per milliequivalent and V_s is the volume of sample tested.

These solutions were then analyzed by gas chromatography (HP 6890) using a capillary column (HP-5). Peak integrals were determined. A calibration curve was constructed by plotting the GC peaks integrals vs. percent formaldehyde.

To determine the concentration of a labeled solution, 1 uL was injected into the GC column and the peak integral measured. The calibration curve was then utilized to determine formaldehyde concentration.

NMR Experiments

The product from the methanol oxidation was hydrolyzed in D_2O (10% w/w) in a sealed tube for 4 hrs. ^{13}C and ^{1}H solution NMR spectra were obtained on a Varian Unity 400 MHz Spectrometer operating at a frequency of 100.577 MHz for ^{13}C. 64 scans were accumulated. Proton decoupling was used throughout.

Mass Spectroscopy

The product from the methanol oxidation was hydrolyzed in D_2O (10% w/w) in a sealed tube for 4 hrs. A mass spectrum was obtained on a VG Analytical Organic Mass Spectrometer Model 7070E.

5.4 Results and Discussion

Yield of formaldehyde from the reduction of carbon dioxide in the presence of lithium aluminum hydride was 68% (average of 3 replications, ± 2%). The isolation of the product into a form suitable for the synthesis of formaldehyde-based resins however, proved problematic. A number of techniques were attempted to isolate the product. Filtering the alumina-based solids from the aqueous phase resulted in a substantial loss of yield. The filtered material had a strong odor of formaldehyde. Presumably the polar alumina compounds present were strongly associated with the product.

Simple fractional distillation attempts were unsuccessful at obtaining sufficient fractionation of the THF from the remainder of the aqueous phase. A highly efficient column would be required to accomplish this. Removal of THF from the reaction flask by vacuum drying was attempted however, an explosion occurred when atmospheric pressure was restored. It has been found that the volatility of LAH is enhanced after treatment with CO_2 (14). This technique therefore, is not recommended.

Once the formaldehyde-water mixture had been distilled from the alumina solids, the concentration was in the range of 1 - 3 % (as determined by GC peak integrals). Concentrating formaldehyde solutions is problematic due to their somewhat unusual properties. It has been found that at low concentrations (< 5%), the distillate is always more concentrated than the residue while at high concentrations (> 5%), the reverse is the case, the residue is more concentrated (15). The reason for this is that at higher concentrations, a greater proportion of hydrated formaldehyde is in oligomeric form. These species will have a relatively low vapor pressure and hence will remain in the residue during distillation. At low concentrations, the formaldehyde hydrate is present in monomeric form. These species have a relatively high vapor pressure and therefore will volatilize much more readily during distillation.

In order to concentrate solutions less than 1 %, the most effective way is through fractional condensation (16). This has been described in the patent literature (11,12). Unfortunately, the size of the column required for such a distillation required a large amount of starting material. The scale within which the reductions were performed did not make this feasible. For the above reasons, the synthesis of formaldehyde, for the production of formaldehyde-based resins via reduction of CO_2 with LAH was deemed unsuitable.

The yield of paraformaldehyde from the reduction of methanol was 49% (average of three replications ± 3%). The major source of product loss was formaldehyde gas escaping through the end of the flowmeter. A midget bubbler was placed between the receiver adapter and the flowmeter, although the yield increase was minimal and served to dilute the product.

The ^{13}C NMR spectrum for the product of the $^{13}CD_2OD$ oxidation is shown in Figure 5.5. An expanded view of the region from 95-75 ppm is shown in Figure 5.6.

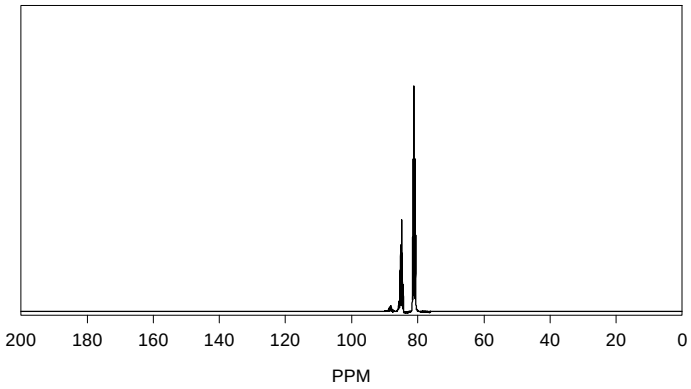

Figure 5.5: ^{13}C solution NMR spectrum of $^{13}CD_2O$.

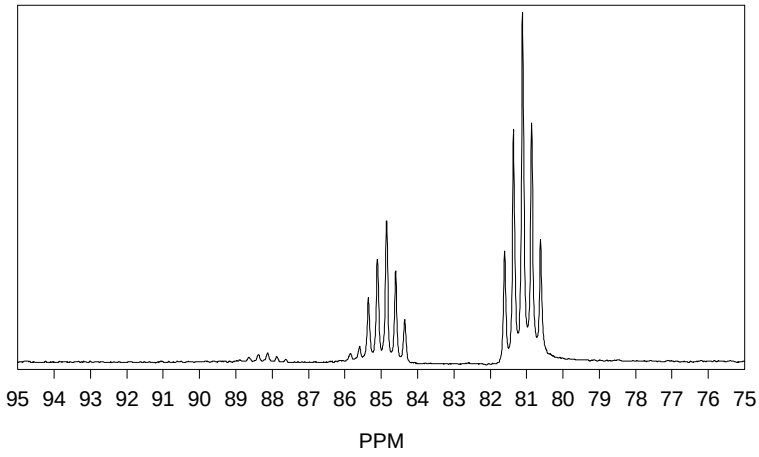

Figure 5.6: ^{13}C solution NMR spectrum of $^{13}CD_2O$.
Expanded view of the 95-75 ppm range.

Three peaks are evident, centered at 81, 85 and 88.3 ppm. Formaldehyde monohydrate and its oligomers have been identified in this region in aqueous formaldehyde resins (17,18). The dominant species of formaldehyde present in aqueous solution is the monohydrate form (i.e. $CH_2(OH)_2$) (6). The peak centered at 81 is therefore the monodeuterate form of $^{13}CD_2O$, $^{13}CD_2(OD)_2$. The splitting pattern of this peak (shown in Figure 5.6) confirms this assignment. The peak appears as a pentet, which is what would be expected following the 2n + 1 rule (deuterium being a spin 1 nucleus). The two peaks appearing downfield are likely oligomeric forms of $^{13}CD_2O$. The spitting pattern of the peak centered at 85 ppm appears as a septet, but due to its asymmetry, is likely two overlapping pentets from the dimeric species. The peak centered at 88.3 ppm appears as a pentet but its intensity makes assignment difficult. This peak most likely corresponds to the trimeric

species. A ^{1}H solution NMR spectrum of the product revealed no significant source of protons in the sample.

The mass spectrum for the product of methanol oxidation demonstrated a peak is at 33 m/e which corresponds to the molecular weight of $^{13}CD_2O$. The most common fragments produced are ^{13}CDO and ^{13}CO (19) and these were also identified.

5.5 Conclusions

The literature dealing with the laboratory-scale synthesis of isotopically labeled formaldehyde has been reviewed and the two main techniques revisited. A technique has been established for the in-house synthesis of labeled formaldehyde for the synthesis of labeled, formaldehyde-based wood adhesives. Reduction of carbon dioxide in the presence of lithium aluminum hydride resulted in good yields of formaldehyde however the product was in very dilute solution which proved problematic to convert into a useable form. Oxidation of methanol resulted in lower yields than the reduction of carbon dioxide however the product was in the form of paraformaldehyde which is easily converted into a useable form. For this reason, oxidation of methanol is favored over carbon dioxide reduction for the production of formaldehyde for use in synthesizing formaldehyde-based wood adhesives. Using this technique, paraformaldehyde-^{13}C-d_2 was produced in appreciable yields by the oxidation of methanol-^{13}C-d_4.

5.6 References

1. Wendler, S.L. and C.E. Frazier. International Journal of Adhesives and Adhesion. 16, 179-186. 1996.

2. Murray, A. and D.L. Williams. Organic Syntheses with Isotopes. Interscience Publishers. New York. 1958.

3. Finholt, Albert E. and Eugene C. Jacobson. Journal of the American Chemical Society. 70, 1948.

4. Nystrom, Robert F., William H. Yanko and Weldon G. Brown. Journal of the American Chemical Society. 70, 441. 1948.

5. Weygand, F. and H. Linden. Angewandte Chemie. 66, 6, 174-175. 1954.

6. Walker, J. Frederick. Formaldehyde. 3rd ed. R.E. Krieger Publishers. Huntington, New York. 1975.

7. Edwards, James., M.B. Cutlip and C.O. Barnett. Journal of Catalysis. 50, 24-34. 1977.

8. Cheng, W-H., U. Chowdry, A. Feretti, L.E. Firment, R.P. Groff, C.J. Machiels, E.M. McCarron, F. Ohuchi, R.H. Staley and A.W. Sleight. 165-181 In Heterogeneous Catalysis. B.L. Shapiro ed. Texas A&M University Press. College Station, Texas. 1984.

9. Cheng, Wu-Hsun. Journal of Catalysis. 158, 477-485. 1996.

10. Tatibouet, J.M. and J.E. Germain. Journal of Catalysis. 72, 375-378. 1981.

11. Walker, Frederick. U.S. Patent 1,871,019. Mar. 26, 1930.

12. Zimmerli, Adolph. U.S. Patent 1,662,179. Jan. 28, 1924.

13. Murray, Arthur III., C. Wayne Bills and Anthony R. Ronzio. Journal of the American Chemical Society. 74. 2405-2406. 1952.

14. Barbaras G., G.D. Barbaras, A.E. Finholt and H.I. Schlesinger. Journal of the American Chemical Society, 70, 877. 1948.

15. Wilkinson, John A. and I.A. Gibson. Journal of the American Chemical Society. 43, 4, 695-700. 1921.

16. Zimmerli, Adolph. Industrial and Engineering Chemistry. 19, 4, 524-525. 1927

17. Werstler, D.D. Polymer, 27, 757-764. 1986.

18. Tomita, Bunichiro and Shiro Hatono. Journal of Polymer Science: Polymer Chemistry Edition, 16, 2509-2525. 1978.

19. Pritchard, Howard and A.G. Harrison. Journal of Chemical Physics. 48, 12, 5620-5630. 1968.

Chapter 6

Characterization of Phenol-Formaldehyde Resin within a Cured Wood-Based Composite Panel

6.1 Introduction

The strength and durability of wood-based composite materials are known to be a function of the cured state of the adhesive. The properties of the composite are therefore strongly dependent on the adhesive curing conditions. Cure variables such as temperature, time and wood moisture content will all play a role in determining the structure and properties of the adhesive. A technique which would allow the characterization of the properties of adhesive cured within a composite material, would be of great benefit for the understanding of composite performance.

Previous work has shown that ^{13}C CP/MAS NMR is ideally suited for the characterization of intact wood-PF bondlines (see Chapter 4). Qualitative estimates of degree of resin conversion were obtained by monitoring corrected ratios of the resin methylene and hydroxymethyl carbon signals. It was shown that rotating frame spin-lattice relaxation times ($^{H}T_{1\rho}$) of the resin protons were correlated to glass transition temperature and crosslink density in neat PF. While those correlations were clear, they were not highly sensitive to changes in cure state (see Chapter 3). The reason for this lack of sensitivity was thought to be due to the obscuring effects of spin diffusion. It was shown that the effects of spin diffusion are minimized in neat PF by partial replacement of the resin protons with deuterium. Deuterium enrichment reduces the effects of spin diffusion and increases the sensitivity of $^{H}T_{1\rho}$ to changes in cure state. The combined use of deuterium and ^{13}C labeling may therefore improve the sensitivity of $^{H}T_{1\rho}$ of the resin protons to the effects of cure conditions. This would allow relative estimates of PF resin cure to be made in the presence of wood.

The purpose of this paper is twofold. First, to use ^{13}C labeling and deuterium enrichment of PF to evaluate the use of $^{H}T_{1\rho}$ for characterizing the properties of the resin cured in wood flake sandwich composites. Second, to extend this analysis to the evaluation of resin cured within a panel manufactured in a pilot-scale hotpress operation.

6.2 Experimental

6.2.1 Materials

Phenol (99 + %) and 50% aqueous NaOH were purchased from Aldrich and used as received. 99% paraformaldehyde-^{13}C, 99% phenol-d_6 and 98% methanol-^{13}C-d_2 were purchased from Cambridge Isotopes and used as received. A molybdenum oxide – iron molybdate catalyst, manufactured by Perstorp Polyols, was obtained from Neste Resins Corp.

Flakes of yellow-poplar (*Liriodendron tulipifera*) were hand turned from 5 x 5 x 20 cm blocks using a CAE disk flaker. The blocks had previously been soaked in distilled water for 24 hours. Final dimensions of the flakes were 5 x 2.5 cm x 0.38 mm.

Flakes were oven dried at 105 ^{o}C (± 3 ^{o}C) for 24 hrs and subsequently conditioned to a moisture content of approximately 5 %. This was accomplished by placing the flakes in a sealed dessicator over a saturated sodium sulfate solution for 24 hrs.

Oriented strand board (OSB) Core Flakes were obtained from Weyerhauser Corp., Elkin, NC. Flake moisture content was 5 %. Phenol-formaldehyde OSB resin (Chembond 1527) was obtained from Neste Resins Corp. Resin solids was 44.8%.

6.2.2 Methods

Resin Synthesis

^{13}C labeled phenol formaldehyde

^{13}C labeled resole phenol formaldehyde resin (100% labeling of the hydroxymethyl and methylene carbons) was synthesized using a P : F : Na molar ratio of 1 : 2 : 0.2. Paraformaldehyde-^{13}C (1.6 g, 0.0532 moles) was hydrolyzed in 4.2 mL of distilled water at 120 ^{o}C is a sealed tube for 4 hours. Phenol (2.5 g, 0.0266 moles) was added to a 10 mL round bottomed flask. The formaldehyde-^{13}C solution was then added. 50 % aqueous NaOH solution (0.213 g, 0.00266 moles) was added. The mixture was heated at atmospheric pressure and allowed to reflux for 30 mins. Subsequently, the reaction was quenched by immersion in a cold water bath.

Paraformaldehyde-^{13}C-d_2 was synthesized via catalytic oxidation of methanol-^{13}C-d_2 over a molybdenum oxide iron-molybdate catalyst. A detailed description of this procedure is given in Chapter 5.

^{13}C labeled and deuterium enriched phenol formaldehyde

^{13}C and 50 % deuterium labeled resole phenol formaldehyde resin (100% ^{13}C labeling of the hydroxymethyl and methylene carbons) was synthesized using a P : F : Na molar ratio of 1 : 2 : 0.2. Paraformaldehyde-^{13}C-d_2 (0.25 g, 0.0076 moles) was combined with paraformaldehyde-^{13}C (0.236 g, 0.0076 moles) and hydrolyzed in 1.3 mL of deuterium oxide at 120 ^{o}C is a sealed tube for 4 hours. Phenol (0.353 g, 0.00375 moles) and phenol-d_6 (0.376 g, 0.00375 moles) were added to a 10 mL round bottomed flask. The isotopically labeled formaldehyde solution was then added. 50 % aqueous NaOH solution (0.12g, 0.0015 moles) was added. The solution was heated at atmospheric pressure and allowed to reflux for 30 mins. The reaction was subsequently quenched by immersion in a cold water bath.

Wood Flake Sandwich Composite Preparation

Wood flake sandwich composites were prepared by spraying the isotopically labeled phenol formaldehyde resin onto a single flake, placing a second flake on top and then hot-pressing. Cure temperatures used were 110, 135 and 175 ^{o}C. At each cure temperature, three different cure times were employed: 1 min, 5 min and 10 min. Replications were made for the following cure conditions: 110 ^{o}C, 1min; 135 ^{o}C, 10 mins; and 175 ^{o}C, 10 mins. Pressing was performed on a Micromet Instruments MP-2000 Minipress with a pressure of 1.28 MPa (184 psi). The average post-cure resin

content was determined gravimetrically to be 5% of the oven dry weight of wood, with a range of 4.2 – 7 %. Cured samples were stored at 10 ^{o}C in a dessicator prior to NMR analysis. Moisture content of the cured flake composites was not measured. It was assumed that minimal moisture was present in the samples due to the combined effects of hot pressing and storage in the presence of a dessicator.

Panel Manufacture

Panels were manufactured with a target density of 0.61 g/cm^3 (38 lbs/ft^3). Resin solids content (on an oven dry wood basis) was 7%. Two different types of panels were made based on furnish moisture content. The moisture in the furnish consisted of water in the wood flakes, water in the liquid resin and any additional water which was added to attain the desired moisture content. The first series was made with a furnish moisture content of 13% and the other was made with a furnish moisture content of 24%. Material amounts used for both types of panels are shown in Table 6.1.

Table 6.1 Materials used in the manufacture of pilot-scale waferboard

Furnish Moisture Content	13 %	24 %
Density	0.61 g/cm^3 (38 lbs/ft^3)	0.61 g/cm^3 (38 lbs/ft^3)
Wood with 5% MC	3200 g	3200 g
Neat resin	463 g	463 g
Additional Water	0	317 g
OD Furnish + Moisture	3330 g	3619 g

Wood flakes were sprayed with commercial liquid PF and blended in a laboratory drum blender for approximately 4 minutes. For boards with 24% MC furnish, additional water was sprayed onto the flakes prior to the resin. After application, 50 % of the furnish was hand felted onto a steel caul plate, surrounded by a forming box. An uncured flake composite, prepared with isotopically labeled resin was placed between two pieces of teflon mesh. This allowed for easy isolation and removal of the specimens from the cured panel. The labeled composite and teflon mesh was positioned in the center of the panel. A thermocouple (type K) was placed beside the sandwich composite. The remaining 50% of the furnish was added to the forming box. A second uncured flake composite, prepared with isotopically labeled resin was also placed between teflon mesh. This sample was positioned at the center of the face of the mat. The mat was then covered with a second steel caul plate. The caul plates and mat were placed in a 61 x 61 cm (2 x 2 foot) press.

In-house designed software was used for data acquisition and press control. A displacement controlled press schedule was used. Final mat thickness was 1.27 cm (0.5 inches). Platen temperature was 200 ^{o}C. Closed press time was 5 minutes, with 30 second compression and decompression cycles at the beginning and end of the schedule. Three panels at each furnish moisture content were made with flake sandwich specimens containing ^{13}C labeled PF resin. Five additional panels at each furnish moisture content were made with flake sandwich specimens containing ^{13}C (100% labeling of hydroxymethyl and methylene carbons) and 50 % deuterium labeled PF resin.

Once the press had opened, the labeled sandwich composites on the face were immediately removed. The panels were broken in half and the labeled sandwich composites were removed from the core within 90 seconds. The samples were weighed and then stored at 10 ^{o}C until NMR analysis. Samples, which contained ^{13}C and 50 % deuterium labeled PF resin were dried under high vacuum (3 mmHg) in the presence of phosphorus pentoxide for 72 hours. These samples were analyzed by ^{13}C CP/MAS NMR prior to and after drying.

NMR Experiments

Samples for solid-state NMR analysis were made by cutting small disks out of the flake composites using a paper hole puncher. These disks were randomly loaded into a zirconium oxide rotor and filled in and around with aluminum oxide powder. Kel-f caps were used to seal the rotors.

NMR measurements were performed on a Bruker MSL-300 MHz spectrometer using a 7 mm Probenkopf MAS.07.D8 probe. The spectrometer operated at a frequency of 75.47 MHz for ^{13}C nuclei. The proton spin-lock field strength was approximately 56 kHz. The Hartmann-Hahn match was established using adamantane. Standard phase cycling was used during acquisition.

Proton spin-lattice rotating frame relaxation times ($^{H}T_{1\rho}$) were obtained by two different methods. Samples, which were made with ^{13}C labeled resin, were analyzed using a standard cross polarization pulse with a variable contact time. Contact times ranged from 75 μsec to 7 msec. Samples, which were made with ^{13}C labeled and 50 % deuterium enriched resin, were analyzed using a variable spin-lock pulse prior to a fixed contact time. Spin-lock times ranged from 100 μsec to 7 msec. 400 scans were accumulated for each delay time. Recycle delay was 3.75 seconds and all samples were spun at 4 kHz (± 20 Hz).

6.3 Results and Discussion

Laboratory Scale Flake Composites

Flake composite samples were prepared with isotopically labeled PF resin. These specimens were cured at temperatures of 110, 135 or 175 ^{o}C and times of 1, 5 or 10 minutes under 1.28 MPa.

A series of ^{13}C CP/MAS NMR spectra are shown in Figure 6.1.

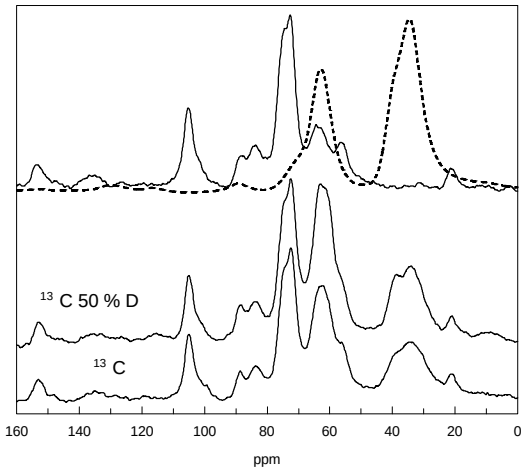

Figure 6.1: ^{13}C CP/MAS NMR Spectra for Yellow poplar (top – solid), ^{13}C labeled, neat PF resin (top - dashed), ^{13}C labeled PF cured in the presence of wood (bottom) and ^{13}C and 50% deuterium labeled PF resin cured in the presence of wood (middle).

The top two spectra show yellow-poplar flakes (solid line) and neat, cured ^{13}C labeled PF (dashed line). The main peaks of interest in the cured PF spectrum are centered at 63 ppm (unreacted hydroxymethyl carbons) and 35 ppm (methylene bridge carbons). It is shown that the methylene bridge peak does not overlap with any wood resonances. The hydroxymethyl peak however, does overlap with the C_6 carbon of cellulose and hemicellulose. The intensities of the resin peaks are so strong due to ^{13}C labeling that overlap is not a significant problem. The bottom two spectra are of flake composites made with either ^{13}C labeled PF or ^{13}C and 50% deuterium labeled PF (7% resin solids).

Figure 6.2 shows an expanded view of the methylene (35 ppm) and hydroxymethyl (63 ppm) regions for samples made with ^{13}C labeled PF (bottom) and ^{13}C and 50% deuterium labeled PF (top).

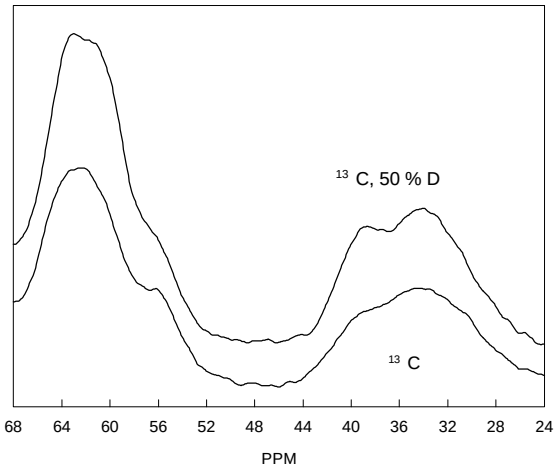

Figure 6.2: Expanded ^{13}C CP/MAS NMR Spectra for ^{13}C labeled (bottom) and ^{13}C and 50% deuterium labeled (top) PF resin showing the fine structure of the methylene and hydroxymethyl regions.

It is clear that samples, which contain ^{13}C labeled and 50% deuterated resin, show greater detail in the fine structure of these peaks than samples, which contain ^{13}C labeled resin. The dominant interactions in the ^{13}C CP/MAS NMR experiment which give rise to broad lineshapes are the chemical shift anisotropy, heteronuclear coupling of ^{1}H and ^{13}C nuclei and homonuclear dipolar interactions (1). High-powered decoupling fields, applied at the proton resonance frequency, are used to minimize the effects of heteronuclear coupling. Magic angle spinning is used to minimize the effects of chemical shift anisotropy. Even so, fine structural details are often obscured in ^{13}C CP/MAS specta. The replacement of protons in a sample with deuterium acts to reduce the effects of homonuclear dipolar coupling and allows enhanced resolution of the fine structure of the peaks. This effect is observed in Figure 6.2. It appears that two resonances within the methylene peak are observable in samples containing ^{13}C labeled and 50% deuterated resin, centered at 41 ppm (range: 44-37 ppm) and 32 ppm (range: 37-26 ppm). Two resonances are also evident, but less obvious, in the hydroxymethyl peak, centered at 61 ppm (range: 62.4-60 ppm) and 64 ppm (range: 68 – 62.4 ppm). Quantitative ^{13}C solution NMR of phenol formaldehyde prepolymers has shown that ortho-ortho (o-o') methylene bridges resonate in the range of 30-32 ppm, while para-para (p-p') methylene bridges resonate in the range of 40-41 ppm (2). Ortho-para (o-p) methylene bridges resonate in the range of 36-37 ppm (2). Ortho hydroxymethyl groups resonate in the range of 61.4 – 61.5 ppm, while para hydroxymethyl groups resonate in the vicinity of 65.5 ppm (2). Deuterium enrichment of the resin therefore, allows the relative evaluation of the o-o' or p-p' nature of the crosslink units.

The ratios of intensities of the o-o' : p-p' peaks in the methylene region as a function of cure time and temperature are shown in Figure 6.3. It appears that o-o’ methylene bridges are more predominant than p-p’ methylene bridges at higher cure

temperatures, which is not unexpected. Although the para site of the phenolic hydroxyl is more reactive to substitution than the ortho sites, the fact that there are two ortho sites per repeat unit means that as cure progresses, more ortho-ortho methylene bridges are formed than para-para methylene bridges. An attempt was made to characterize the fine structure within the hydroxymethyl peak. Unfortunately, the resolution was insufficient to distinguish more than a single peak.

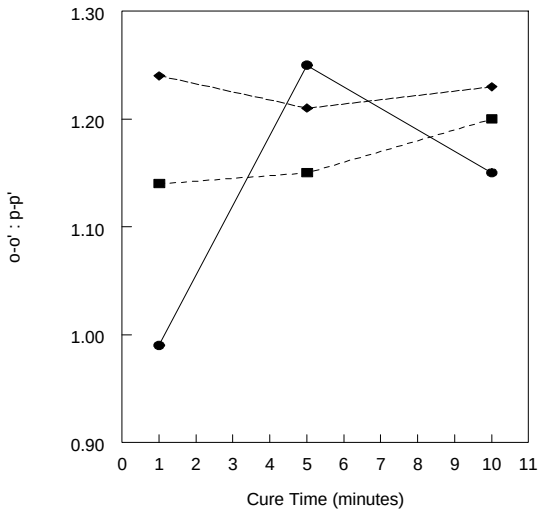

Figure 6.3: Ratios of ortho-ortho : para-para methylene bridges as a function of cure time and temperature. Cure Temperatures: ● - 110 °C, ■ - 135 °C, ♦ - 175 °C.

Proton spin-lattice rotating frame relaxation times ($^{H}T_{1\rho}$) from the resin methylene carbons in wood flake sandwich composites made with either ^{13}C labeled or ^{13}C and 50 % deuterium labeled PF are compared in Figure 6.4. Increased values of $^{H}T_{1\rho}$ have been correlated with both increased glass transition temperatures and crosslink densities for neat PF (see Chapter 3). The bottom graph of Figure 6.4 shows that $^{H}T_{1\rho}$ shows minimal sensitivity to state of resin cure. The sensitivity to cure temperature is more evident than to cure time. This is attributed to the fact that spin diffusion reduces the observed value of $^{H}T_{1\rho}$. Spin diffusion is a non-motional process, the result of static energy exchange between protons in a sample. The presence of spin diffusion acts to obscure motional contributions to $^{H}T_{1\rho}$. In the case of neat PF, it has been shown that the effects of spin diffusion can be diminished by replacing protons in a sample with deuterium (see Chapter 3).

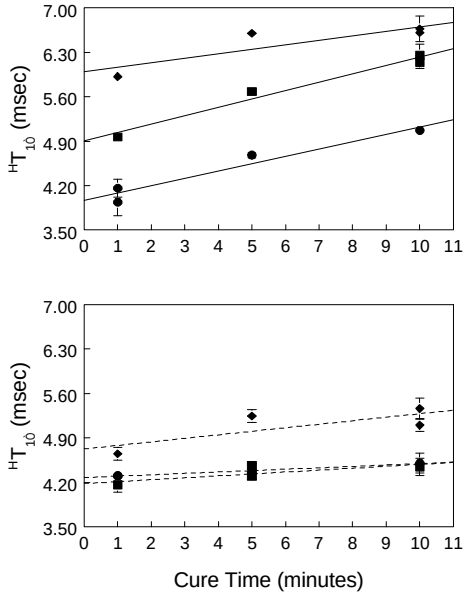

Figure 6.4: Proton Spin-Lattice Rotating Frame Relaxation Times (in msec) for ^{13}C labeled (bottom) and ^{13}C and 50% deuterium labeled PF resin (top) cured in the presence of wood. Cure Temperatures: ● - 110 °C, ■ - 135 °C, ♦ - 175 °C.

By diluting the protons with deuterium, the static transfer of energy between protons can be reduced or eliminated (3). The top graph in Figure 6.4 shows that the $^{H}T_{1\rho}$ of ^{13}C and deuterium labeled PF displays enhanced sensitivity to both cure time and cure temperature. The increased sensitivity to cure conditions for the ^{13}C labeled and 50 % deuterated resin over ^{13}C labeled resin indicates that the contribution of spin diffusion in this system has been reduced by the deuterium enrichment. The use of ^{13}C and 50% deuterium labeling then, improves our ability to evaluate cure using NMR relaxation measurements.

Pilot Scale Panel Experiments

The use of labeled PF to evaluate differences in resin cure and properties as a function of position in a pilot-scale panel were investigated. Flake composites, prepared with isotopically labeled resin were positioned at the center of the core and face of panels. These were removed after panel hotpressing and analyzed by ^{13}C CP/MAS NMR. Typical core temperatures reached during pressing of panels manufactured with isotopically labeled samples are shown in Figure 6.5.

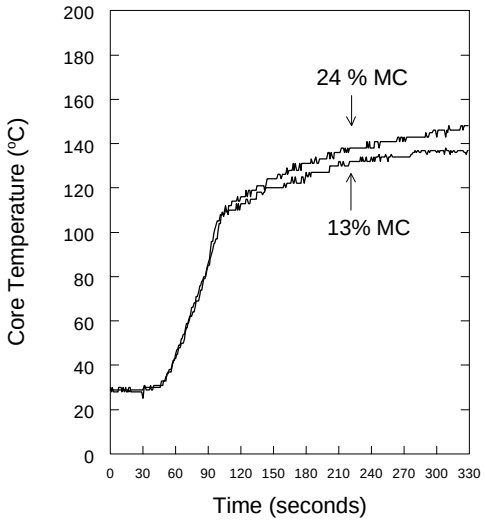

Figure 6.5: Typical core temperatures of panels made with isotopically labeled PF samples.

It is shown that the core temperatures in both types of panels are significantly lower than the platen temperature of 200 ^{o}C. It has been found that conditions of saturated steam are present in similar OSB panels made with 15% MC furnish (4). It is likely therefore, that conditions of saturated steam are present in the cores of both types of panels made in this work, although gas pressures within the mat were not measured.

^{13}C CP/MAS NMR spectra for ^{13}C labeled core and face specimens removed from both types of panels are shown in Figure 6.6.

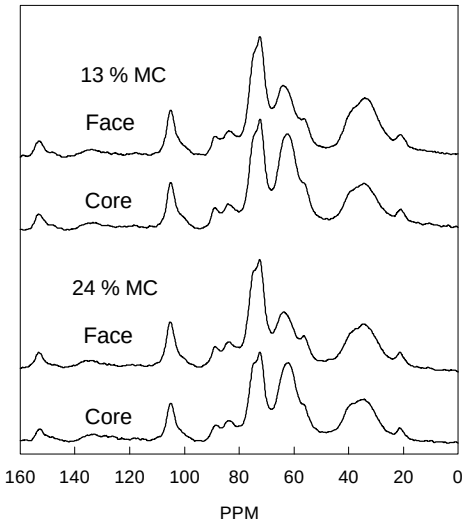

Figure 6.6: Typical ^{13}C CP/MAS NMR Spectra for ^{13}C labeled PF samples made from 13% and 24% MC furnish removed from the core and face of test panels.

Figures 6.6 clearly shows that samples removed from the face of the panels possess increased methylene (35 ppm) and diminished hydroxymethyl (63 ppm) signals as compared with those of the core samples. This indicates that the samples at the face of the panel have a higher degree of conversion than those at the core. These changes are more accurately followed by correcting the peak integrals for differences in cross polarization and proton spin-lattic relaxation rates (5).

The ratios of corrected peak integrals for methylene to hydroxymethyl carbons for panels made with 13 and 24 % MC furnish are shown in Table 6.2.

Table 6.2: Corrected Ratios of Methylene:Hydroxymethyl Peak Integrals for Panel Samples Cured with ^{13}C labeled PF.

Furnish Moisture Content	Sample Position	CH_2/CH_2OH (corrected)	Sample Position	CH_2/CH_2OH (corrected)
13%	Core	0.8 0.8 0.9 Mean = 0.8	Face	1.5 1.3 1.9 Mean = 1.6
24%	Core	0.8 1.1 1.0 Mean = 1.0	Face	1.9 1.8 1.8 Mean = 1.8

The average methylene to hydroxymethyl ratio for core and face specimens for all panels are 0.9 and 1.7 respectively. A paired t-test shows that the corrected signal ratios are significantly different ($t = 9.79$, $p < 0.001$). This confirms that differences in resin conversion can be monitored as a result of position in a wood based composite panel. The difference in degree of conversion between face and core samples is not unexpected due to the difference in maximum temperatures occurring during pressing. The maximum face temperatures reached were assumed to be at or near the platen temperature of 200 ^{o}C, while the core temperatures did not exceed 150 ^{o}C (Figure 6.5). No statistically significant difference in corrected signal ratios however, was noted between the two furnish moisture contents. This can be explained based on the conditions existing in the cores of the two types of panels. During hotpressing, water is vaporized and forced into the core of the panel due to convection. Conditions of saturated steam may or may not be present, depending on the initial furnish MC (4). Specimens cured at the face of both types of panels are likely exposed to similar conditions of temperature and water vapor pressure, since most of the moisture is driven into the core of the panel. If saturated steam is present in the core of both types of panels, the gas pressure is a function of temperature, not furnish MC. The temperatures in the core of the panel (compared with the platen) are similar. Therefore, the core gas pressures of both types of panels will be similar (Figure 6.5). If the conditions specimens in both types of panels are the same, the degree of conversion of the resin should also be the same. This explanation assumes that saturated conditions are present however, as already mentioned, gas pressures were not measured in the core of the panels.

$^{H}T_{1\rho}$ values obtained for the resin methylene and hydroxymethyl protons are shown in Table 6.3.

Table 6.3: Proton Spin-Lattice Relaxation Times in msec, for resin methylene (35 ppm) and cellulose/hemicellulose $C_{2,3,5}$ (72 ppm) from panel samples made with ^{13}C labeled PF. Standard errors are shown in parenthesis.

Furnish Moisture Content	Sample Position	$^{H}T_{1p}$ 35 ppm, in msec (error)	Sample Position	$^{H}T_{1p}$ 35 ppm, in msec (error)
13%	Core	6.5 (0.3) 6.6 (0.3) 6.4 (0.3)	Face	6.1 (0.3) 6.3 (0.3) 6.1 (0.3)
24%	Core	6.1 (0.2) 6.6 (0.2) 6.4 (0.2)	Face	5.6 (0.2) 6.2 (0.2) 6.2 (0.2)

^{13}C CP/MAS spectra for ^{13}C labeled and 50% deuterated core and face samples removed from both types of panels are shown in Figure 6.7.

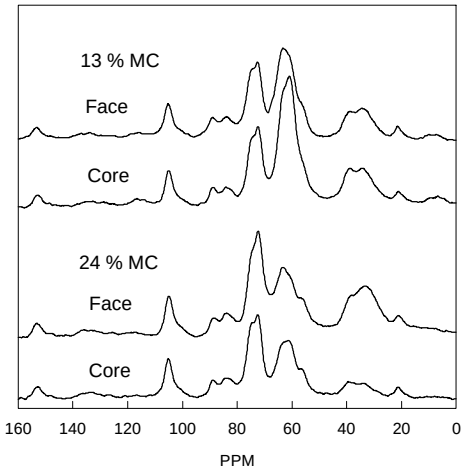

Figure 6.7: Typical ^{13}C CP/MAS NMR Spectra for ^{13}C and 50% deuterium labeled PF samples made from 13% and 24% MC furnish, removed from the core and face of test panels.

Differences in degree of conversion are again noted between core and face samples by observing the signal intensities of the methylene (35 ppm) and hydroxymethyl (63 ppm) signals. Variable contact time experiments were not performed on these samples however, so corrected signal intensities could not be determined.

The use of ^{13}C and 50% deuterium labeling allows elucidation of the methylene fine structure, as with the wood-flake composite samples. Values of o-o' : p-p' calculated for samples removed from panels are shown in Table 6.4.

Table 6.4: Ratios of ortho-ortho : para-para methylene bridges as a function of Furnish Moisture Content and Position in Board for ^{13}C and 50% deuterium labeled Specimens.

Furnish Moisture Content	Sample Position	o-o':p-p' methylene	Sample Position	o-o':p-p' methylene
13%	Core	1.0 1.1 0.8 0.9 Mean = 1.0	Face	1.2 1.2 1.1 1.2 Mean = 1.2
24%	Core	1.0 0.9 1.0 0.9 0.9 Mean = 0.9	Face	1.2 1.1 1.2 1.1 1.1 Mean = 1.2

The average values of o-o' : p-p' for the core and face samples are 0.9 and 1.2 respectively. A paired t-test showed that these differences are statistically significant ($t = 5.69$, $p < 0.001$). No difference was noted in o-o' : p-p' ratios between the different furnish moisture contents. These results indicate that resin cured in the core of the panel shows greater o-o' methylene bridge character than resin cured in the face, which shows greater p-p' methylene bridge character. Increase in o-o' : p-p' ratios with cure temperature is in agreement with the results obtained from the laboratory scale flake composites.

$^{H}T_{1\rho}$ values, obtained for resin and wood resonances from samples which were removed from panels and contained ^{13}C and 50 % deuterium enriched resin, are shown in Table 6.5.

Table 6.5: Proton Spin-Lattice Rotating Frame Relaxation Times, in msec, (standard error) and Mass Increases (% of oven dry weight) as a Function of Furnish Moisture Content and Position in Board for ^{13}C and 50% deuterium labeled Specimens. ** - no resin was detected in this sample.

Furnish Moisture Content	Sample Position	35 ppm	72 ppm	Mass Increase (%)	Sample Position	35 ppm	72 ppm	Mass Increase (%)
13%	Face	6.2 (0.2)	8.1 (0.2)	5	Core	**	9.6 (0.2)	8
		6.3 (0.1)	7.7 (0.1)	3		5.9 (0.2)	9.1 (0.1)	8
		6.4 (0.1)	7.8 (0.1)	6		6.6 (0.1)	8.8 (0.2)	13
		5.6 (0.2)	9.2 (0.1)	7		6.4 (0.1)	10.2 (0.1)	19
		6.4 (0.3)	9.0 (0.2)	5		7.5 (0.2)	10.8 (0.2)	12
24%	Face	6.3 (0.1)	8.0 (0.2)	8	Core	7.0 (0.2)	9.5 (0.2)	22
		6.0 (0.2)	8.1 (0.1)	11		6.0 (0.2)	8.8 (0.2)	15
		6.1 (0.1)	8.4 (0.1)	4		6.1 (0.3)	9.0 (0.4)	17
		6.2 (0.6)	9.5 (0.3)	8		6.2 (0.1)	8.5 (0.1)	15
		6.8 (0.3)	9.0 (0.1)	8		6.8 (0.3)	9.3 (0.2)	20

It is shown that NMR analysis failed to detect any labeled resin in one of the core samples. This means that the labeled resin was washed from this sample during panel manufacture. This indicates significant amounts of mass transfer within the cores of the panels. Figure 6.6 show differences in signal intensities for the resin peaks between core and face samples. Core samples demonstrated diminished methylene and hydroxymethyl signals. This may also be an indication of resin migration during cure.

Figure 6.4 showed that the use of ^{13}C and 50 % deuterium enriched PF resin in laboratory prepared wood-flake sandwich composites allowed qualitative estimates of resin cure to be made from methylene $^{H}T_{1\rho}$'s, as a function of cure conditions. In this case however, no significant differences are seen between methylene $^{H}T_{1\rho}$'s (35 ppm) of the face and core samples. This means that, as in the case of samples cured with ^{13}C labeled resin, $^{H}T_{1\rho}$ in this case, is not sensitive to the effects of cure conditions. There are several possible reasons for this observation. It is known that the environment, which exists in the interior of a wood-based composite mat is very complex, with variations in temperature as well as water vapor pressure, as a function of position within the mat (4). Water vapor pressure was not an important variable in the manufacture of the laboratory prepared wood-flake sandwich composites because of the insufficient amounts of moisture. Table 6.5 also shows the values of mass increases (on an oven dry basis) of the cured samples, recorded immediately after they had been removed from the panels. The same amount of resin was applied to each flake. The increased mass of the samples therefore, is a combination of resin solids (4-6 %) and water. It is shown that face samples had lower mass increases than core samples, presumably due to higher water vapor pressures (possibly saturated) occurring in the cores of the panels. Any significant source of protons within the resin would act to obscure the contribution of motional processes to the value of $^{H}T_{1\rho}$ by increasing the contribution of spin diffusion (non-

motional) processes. Water within the flakes or the resin could then reduce the effectiveness of the deuterium enrichment.

In order to test this hypothesis, samples were vigorously dried under vacuum in the presence of phosphorus pentoxide for 72 hrs and then re-analyzed with ^{13}C CP/MAS NMR. $^{H}T_{1\rho}$ values obtained for the dried specimens are shown in Table 6.6. $^{H}T_{1\rho}$'s for the cellulose and hemicellulose $C_{2,3,5}$ peak (72 ppm) showed marked decreases in $^{H}T_{1\rho}$ upon drying. Core samples, on average, demonstrated greater decreases than those of the face (1.5 msec compared with 0.8 msec). This can be explained on the basis of the moisture content differences of the face and core samples prior to drying. $^{H}T_{1\rho}$'s for the resin methylene bridge carbon (35 ppm) also showed differences between untreated and dried samples, although consistent trends were not evident. Drying appeared to enhance the sensitivity of the methylene $^{H}T_{1\rho}$ to the effects of cure conditions. The differences in the methylene $^{H}T_{1\rho}$ between core and face (6.2 and 6.8 msec) are significant ($t = 3.75$, $0.005 > p > 0.001$), however the sensitivity is much lower than those shown for the laboratory prepared wood flake sandwich composites.

Table 6.6: Proton Spin-Lattice Rotating Frame Relaxation Times, in msec, (standard error) as a Function of Furnish Moisture Content and Position in Board for dried ^{13}C and 50% deuterium labeled Specimens.

Furnish Moisture Content	Sample Position	35 ppm	72 ppm	Sample Position	35 ppm	72 ppm
13%	Face	6.4 (0.2) 7.0 (0.2) 7.2 (0.4) 6.8 (0.3) Mean = 6.9	8.0 (0.1) 7.7 (0.2) 7.9 (0.2) 8.0 (0.2)	Core	6.4 (0.2) 6.3 (0.3) 5.2 (0.3) 6.4 (0.3) Mean = 6.1	8.6 (0.1) 8.0 (0.3) 7.8 (0.2) 7.7 (0.2)
24%	Face	6.8 (0.3) 6.9 (0.3) 6.7 (0.1) 6.5 (0.2) 7.0 (0.3) Mean = 6.8	7.3 (0.3) 7.8 (0.1) 8.1 (0.1) 7.7 (0.2) 7.5 (0.4)	Core	6.5 (0.3) 6.5 (0.3) 6.4 (0.3) 5.8 (0.3) 6.2 (0.3) Mean = 6.3	7.9 (0.2) 7.2 (0.2) 7.7 (0.1) 7.6 (0.2) 8.2 (0.2)

The relative insensitivity of methylene $^{H}T_{1\rho}$'s of the ^{13}C labeled, 50% deuterated samples from the panels as compared with the laboratory prepared flake composites is most likely a result of differences in moisture environments during cure however, the mechanism is not clear. The samples cured in the core of the panels were thought to be subjected to saturated conditions during cure while the flake composite samples were not. Presumably, most of the moisture contained in the panel samples is in the form of water associated with the wood. It is also possible that water is also present due to resin

solvent, which had not been evaporated during cure. It is known that PF polymerization proceeds via multiple sequential and simultaneous condensation equilibria. Saturated conditions during cure may influence these equilibria, resulting in changes in cure chemistry. It has been shown that structural differences do occur between resin cured in the face and core of the panels. These differences may manifest themselves as changes in the amount and nature of the crosslinking units, significantly altering the motional processes, which occur in the cured resin, making comparisons of $^{H}T_{1\rho}$ complicated. Pressure on the PF condensation equilibria may also result in water being trapped in the growing network during cure. If this water had been incorporated into the cured network, it would be very difficult to remove without changing the network structure. Water trapped in the cured network may enhance the effects of spin diffusion within the system, acting to obscure motional contributions. This would result in the observed insensitivity of the methylene $^{H}T_{1\rho}$'s to cure conditions in the panel specimens.

6.4 Conclusions

^{13}C CP/MAS NMR can be applied as a technique to determine differential degrees of PF resin cure within a wood based composite panel. The use of ^{13}C labeled PF allows the relative state of resin cure to be monitored by measurement of the resin methylene and hydroxymethyl carbons. It was shown that samples cured at the face of panels had higher degrees of resin conversion than those cured at the core. The use of ^{13}C labeled and 50% deuterium enriched PF allows fine structural differences in the cured resin to be assessed. It was shown that samples cured at the face of panels had a greater proportion of ortho-ortho resin methylene ratios. Proton rotating frame spin-lattice relaxations are relatively insensitive to changes in resin network motions. They do reveal however, the important and complicated role moisture plays during cure of phenol formaldehyde.

6.5 References

1. Fyfe, C.A. 1983. Solid State NMR for Chemists. CFC Press. Guelph, Ontario Canada.

2. Werstler, D.D. 1986. Polymer 27, 750-756.

3. Parmer, J.F., L.C. Dickinson, J.C.W. Chien and R.S. Porter. 1987. Macromolecules 20, 2308-2310.

4. Kamke, F.A. and L.J. Casey. 1988. Forest Products Journal. 38 (3) 41-43.

5. Mehring, M. 1983. High Resolution NMR Spectroscopy in Solids. 2nd ed., Springer-Verlag, Berlin.

Chapter 7

Molecular Aspects of Wood-Adhesive Interactions

7.1 Introduction

The two main types of adhesives used in the production of structural wood-based composites are phenol formaldehyde (PF) and polymeric isocyanate (pMDI) resins. Processing and the properties of materials produced using these two types of resins are known to be significantly different. The use of pMDI allows shorter press times, and also permits higher wood moisture tolerances during pressing (1). pMDI bonded products also possess superior mechanical performance compared with those made with PF (2,3). Recently, there has been a great deal of interest in an explanation of the superior performance of pMDI-bonded products from a molecular standpoint (4,5). These studies have attempted to elucidate fundamental interactions between pMDI and wood on a molecular scale.

It is generally accepted that the mechanism through which PF adheres to wood is a combination of secondary interactions (i.e. hydrogen bonds) and mechanical interlocking forces (6). pMDI is also capable of adhering to wood through these mechanisms but because of the reactive nature of the isocyanate functionality in pMDI resins, it has been postulated that covalent linkages may be formed between the resin and wood during cure. Recent ^{15}N CP/MAS NMR studies have found indirect evidence of this type of interaction, but it appears that it may not be a major contributing factor under common industrial processing conditions (7).

A major difference between PF and pMDI resins is their molecular weight at application. Typically pMDI resins are applied with a weight average molecular weight (M_w) < 500 g/mol, as compared with PF resins which have a M_w > 1500 g/mol at application. A recent study (4) found that liquid pMDI has the ability to plasticize wood. This indicates that liquid pMDI must be miscible, on a molecular scale, with wood polymers. If this is the case, one could envision an interpenetrating network (IPN) morphology existing at the wood-pMDI bondline, resulting from penetration of the adhesive monomers into the cell wall prior to polymerization.

A recent study was conducted on the swelling of wood with organic liquids (8). The primary factors which influenced swelling were found to be: molar volume, hydrogen bonding capacity and basicity. An interesting finding was that benzyl alcohol was found to be more effective than water at swelling quaking aspen (*Populus tremuloides)* (8). Benzyl alcohol is similar in size and structure to monomeric PF (i.e. hydroxymethylated phenol). These results suggest that PF monomers in addition to pMDI, may possess the capability to swell wood. If this were the case, it could be possible that an IPN exists at the molecular interphases of both wood-pMDI and wood-PF. A possible form of this morphology is shown in Figure 7.1 to illustrate the scale of interactions which may exist between wood and adhesive.

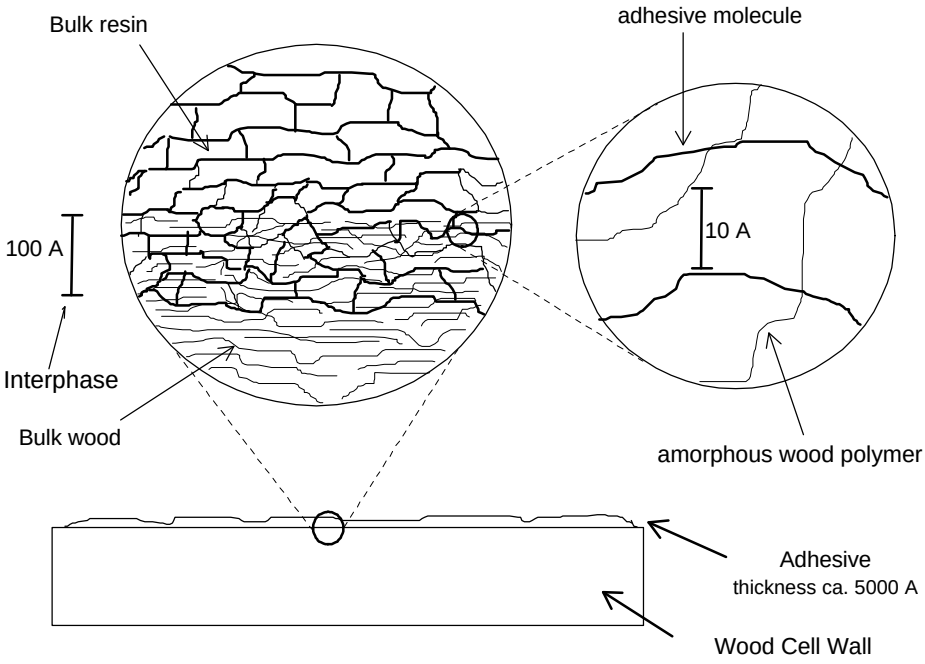

Figure 7.1: The hierarchical nature of the wood-adhesive interphase

Solid-state NMR employing cross polarization (CP) and magic angle spinning (MAS) has been used to characterize the molecular level interactions in a variety of polymeric blends (9). The primary method of obtaining this type of information is to make use of cross polarization measurements. Cross polarization is a method of signal enhancement in solid-state NMR where magnetization is transferred from abundant spins (usually ^{1}H) to rare spins (usually ^{13}C). The efficiency of cross polarization is determined by the strength of the ^{1}H-^{13}C magnetic coupling, which is a function of the proximity of the cross polarizing nuclei and their mobility with respect to the main magnetic field (10). Cross polarization probes very low frequency, near static motions, and will occur only if the average proton-carbon distances of 0-20 angstroms (11). Molecular interactions have been probed in blends by replacing the protons in one component with deuterons (11-16). Removal of the protons from one component prevents any cross polarization from occurring within that component. The only CP which can then occur would be from the protonated component to the deuterated component. In order for this to occur, the two components must be within approximately 10-20 angstroms of one another (i.e. molecularly miscible). Therefore, monitoring the signal intensities of the carbons of the deuterated component due to CP can give information with regards to its interactions with the protonated component.

The purpose of this study is to examine molecular level interactions between wood and phenol formaldehyde (PF) and polymeric isocyanate (pMDI) resins. This will be accomplished through the synthesis of perdeuterated resins. Wood flake sandwich composites will then be manufactured using the labeled resins and the cross polarization behavior of the resin carbons will be assessed.

7.2 Experimental

7.2.1 Materials

Phenol (99%) and hydrochloric acid (12.2 N) was purchased from Fischer Scientific and used as received. Aniline was also purchased from Fischer Scientific and was vacuum distilled prior to use. Paraformaldehyde (95 %) was purchased from Aldrich Chemicals and used as received. Methanol-^{13}C-d_4, Phenol-d_6, aniline-d_7 and paraformaldehyde-^{13}C were purchased from Cambridge Isotopes and used as received. A molybdenum oxide – iron molybdate catalyst, manufactured by Perstorp Polyols and obtained from Neste Resins Corp. was used as received.

7.2.2 Methods

Resin Synthesis

Paraformaldehyde-^{13}C-d_2 was synthesized via catalytic oxidation of methanol-^{13}C-d_4 over a molybdenum oxide – iron molybdate catalyst. A detailed description of this procedure is given in Chapter 4.

^{13}C labeled and 85 % deuterium enriched phenol formaldehyde

^{13}C labeled and 85 % deuterium enriched phenol formaldehyde (PF) was synthesized using a 1 : 2 : 0.2 molar ratio of P : F : Na. Target resin solids was 50 %. Two different resins were synthesized, based on reaction time.

1 g (0.0303 mol) of paraformaldehyde-^{13}C-d_2 and 0.162 g (0.0054 mol) of paraformaldehyde-^{13}C were added to 3 g (0.15 mol) of deuterium oxide and hydrolyzed at 120 ^{o}C in a sealed tube for 4 hours. 0.254 g of phenol (0.0027 mol) and 1.52 g of phenol-d_6 were added to a dry 10 mL round bottom flask connected to a condenser. 0.28 g (0.00357 mol Na) of 50 % NaOH was then added followed by the labeled formaldehyde solution. The reaction mixture was allowed to reflux followed by quenching in a cold water-acetone bath. One PF resin was made using a reaction time of 20 minutes (designated PF-low) and a second was made using a reaction time of 45 minutes (designated PF-high). The resins were stored at – 10 ^{o}C until use.

Polymeric diphenylmethane diisocyanate

^{13}C labeled and 85 % deuterium enriched polymeric diphenylmethane diisocyanate (pMDI) was synthesized via a two step reaction using a 4 : 1 molar ratio of aniline : formaldehyde and a 1 : 1.5 molar ratio of aniline : HCl.

In the first step, 4.246 g (0.0424 mol) of aniline-d_7, 0.697 g (0.0075 mol) of aniline, 0.35 g (0.0106 mol) paraformaldehyde-^{13}C-d_2, 0.06 g (0.0019 mol) paraformaldehyde-^{13}C, 6.2 mL of 12.2 N HCl (0.075 mol) and 6.3 g (0.35 mol) of distilled water were added to a 50 ml round bottomed flask connected to a condenser. The mixture was heated and allowed to reflux for 8 hours. The reaction was quenched by immersion in a cold water-acetone bath.

The resulting polyamine/aniline/water mixture was transferred to a 250 mL separatory funnel. 30 mL of distilled chloroform was added. The aqueous phase was neutralized with 5 mL of 10 N NaOH. The organic phase was collected. The aqueous phase was washed twice with 30 mL quantities of chloroform, which were also collected. The aqueous phase was discarded. The organic layer was then washed three times with 20 mL double distilled water to remove any excess caustic and dried with anhydrous sodium sulfate. The mixture was then filtered and the chloroform was removed by rotational evaporation. The polyamine was subsequently isolated by vacuum distillation of the residual aniline (120 ^{o}C, 3mmHg) and stored overnight.

In the second step, the polyamine was phosgenated using a 1.14 : 3 molar ratio of triphosgene : polyamine. Theoretically, 1 mol of triphosgene is capable of converting 3 mols of polyamine to polyisocyanate. Amine content of the polyamine was determined by assuming complete conversion of formaldehyde to methylene dianiline. The total weight of methylene groups (i.e. mass of formaldehyde used) was subtracted from the weight of the polyamine to obtain the weight of dehydroaniline, from which moles of amine groups could be estimated. 2.3 g of polyamine (93% yield of methylene dianiline-0.023 mol dehydroaniline) was recovered.

The polyamine was first dissolved in 11 times its weight of orthodichlorobenzene (ODCB) (25.3 g). This solution was transferred via cannula under nitrogen to a flamed 250 mL triple necked flask connected to a condenser with an attached gas adapter. Triphosgene (2.6 g, 0.0087 mol) was dissolved in 10 times its weight of ODCB (26 g) and added to the reaction vessel under nitrogen with vigorous stirring. The reaction mixture was allowed to reflux under nitrogen for 2 hours. The mixture was allowed to cool and was then transferred via cannula to a flamed 100 mL round bottomed flask. Residual ODCB was removed by vacuum distillation. The remaining polyisocyanates were heat treated at 205 ^{o}C for 10 minutes followed by quench cooling. Amount of polyisocyanate recovered was 2.91 g (90 % yield from the phosgenation).

The overall reaction was performed twice. The yields of polymeric isocyanate from the two reactions were 84 and 63 % respectively. Both products were mixed prior to analysis and use. The product was stored under N_2 at – 10 ^{o}C until use.

Resin Characterization

PF and pMDI resins were derivatized for molecular weight determination. PF resin was acetylated in a 1 : 1 molar mixture of pyridine : acetic anhydride at room temperature for 72 hours. The reaction mixture was then added to a 250 mL separatory funnel. 20 mL distilled water was added to decompose excess acetic anhydride followed by 20 mL of saturated NaCl solution. 25 mL of chloroform was added. After vigorous shaking, the organic layer was collected. The aqueous layer was washed twice with 25 mL chloroform, which was also collected. The organic phase was dried with anhydrous sodium sulfate and then filtered. The chloroform was removed by rotational evaporation. The product was an oil with the odor of pyridine. The pyridine was removed by addition of 200 mL of toluene and rotational evaporation.

pMDI resin was derivatized by reaction with diethylamine in chloroform at room temperature for 30 minutes. Residual diethylamine and chloroform were removed by rotational evaporation.

Molecular weights were determined using gel permeation chromatography. Detection was accomplished with a Viscotek viscometer (Model 100) and a Waters differential refractometer (Model 410). Waters ultrastyrogel columns were used. Three columns used in sequence with pore sizes of 10^3, 10^4 and 10^6 angstroms respectively. Samples were run at 40 ^oC in tetrahydrofuran.

^{13}C and ^1H spectra were obtained for derivatized resins in chloroform-d_6. Spectra were obtained using a Varian Unity 400 MHz spectrometer at a frequency of 100.577 MHz. 196 scans were accumulated for each sample and the spectra were internally referenced to tetramethylsilane.

Isocyanate content for the labeled pMDI was obtained using ASTM Standard D 5155-91 – Standard Test Method for Polyurethane Raw Materials: Determination of the Isocyanate Content of Aromatic Isocyanates. Test method C (unheated trichlorobenzene-toluene-dibutylamine) was used. A 2N dibutylamine solution was prepared by diluting 130 g of dibutylamine to 500 mL with toluene. 40 g of type 4A molecular sieves were added. A 1 N methanolic HCl solution was prepared by adding 78.9 mL (0.8 mol) of 37 % HCl to 734 mL of methanol. Three standard solutions of sodium carbonate were prepared, consisting of 0.20, 0.22 and 0.25 g of Na_2CO_3 in 50 mL water. The mean normality of the methanolic HCl solution was determined to be 0.952 N.

In order to conserve the labeled pMDI resin, the procedure was scaled down to 10% of that specified in the ASTM Standard. Isocyanate content of the ^{13}C and deuterium labeled pMDI was determined to be 32.1 %.

Flake Composite and Neat Resin Sample Preparation

Yellow poplar (*Liriodendron tulipifera*) flakes were hand turned on a CAE disk flaker from 5 cm x 5 cm x 15.3 cm (length) blocks which had been soaked in distilled water overnight. Final flake dimensions were 5 cm x 5 cm x 0.38 mm. The flakes were oven-dried for 24 hrs at 103 ^oC (± 2 ^oC). The flakes were then equilibrated to a moisture content of 5 % by placing them in a sealed dessicator over a saturated sodium sulfate solution for 24 hours.

Flake composites were prepared by spraying labeled resin onto a single flake, placing a second flake on top and then hot pressing. Cure temperatures were 135 and 175 ^oC. Cure time was 10 minutes. PF samples at both cure temperatures and pMDI samples cured at 135 ^oC were cured within 30 seconds of the application of resin. Three different types of pMDI bonded samples were prepared for cure at 175 ^oC. One sample was cured within 30 seconds of the application of resin (designated pMDI-0). A second sample was prepared by spraying the resin onto the flake and pressing after 30 minutes in the open atmosphere (designated pMDI-30). A third sample was prepared by spraying the resin onto the flake and pressing after 24 hours in the open atmosphere (designated pMDI-24). One replicate was made for each resin/cure temperature combination. Post-cure resin content ranged from 4 – 6.5 % (oven-dry wood basis). Pressing was performed on a Micromet Instruments MP-2000 Minipress with a pressure of 1.28 MPa (184 psi). Cured samples were stored in a dessicator in the presence of Drierite^{TM} at –10 ^oC prior to NMR analysis.

In order to obtain neat resin samples produced under similar conditions to the resin cured in the composite specimens, the same amount of resin applied to the

composite was used to make neat samples. The curing apparatus consisted of a test tube preheated in a silicone oil bath to either 135 or 175 ^{o}C. Neat labeled PF resin samples were prepared by curing 0.05 g of resin for 10 minutes in the reaction vessel. One sample was made for each cure temperature. In the case of the pMDI samples, the amount of water present in an uncured wood-flake composite was also added to the curing vessel. Neat labeled pMDI resin samples were prepared by vigorously stirring 0.05 g of resin and 0.03 g of water in the reaction vessel for 10 minutes. One sample was made for each cure temperature. After curing, the samples were removed from the tube and stored at – 10 ^{o}C until analysis.

^{13}C CP/MAS NMR Measurements

Flake composite samples for NMR analysis were prepared by cutting small disks out of the composite using a paper hole puncher. These disks were randomly loaded into a zirconium oxide rotor and filled in and around with aluminum oxide powder. Neat resin samples, as obtained after cure, were placed in a zirconium oxide rotor which was filled with aluminum oxide powder. Kel-f caps were used to seal the rotos.

NMR measurements were performed on a Bruker MSL-300 MHz spectrometer using a 7 mm Probenkopf MAS.07.D8 probe. The spectrometer operated at a frequency of 75.47 for ^{13}C nuclei. The proton spin-lock field strength was approximately 56 kHz. The Hartman-Hahn match was established using adamantane. Standard phase cycling was used during acquisition.

Two different relaxations were performed for each specimen. Proton spin-lattice rotating frame relaxation times ($^{H}T_{1\rho}$) were obtained by employing a variable spin-lock prior to a fixed contact time pulse. Contact time was 5 msec. Spin-lock times ranged from 100 usec – 5 msec.

Cross polarization (CP) signal enhancement was monitored at room temperature using a standard cross polarization pulse with a variable contact time. Contact times ranged from 25 usec – 5 msec.

For each type of experiment, 600 scans were accumulated at each delay time. Recycle delay was 3.75 seconds and all samples were spun at 4 kHz (± 20 Hz).

Transmission Electron Microscopy

Bondline sections (60-90 nm in thickness) were observed using a JEOL TEM-100CXII Electron Microscope. Sections were imbedded in Polybed^{TM}, a 4-part commercial epoxy embedding material. Embedded sections were placed on grids and sequentially stained with uranyl acetate and lead citrate. Staining consisted of immersion in 2 % aqueous uranyl acetate for 12 minutes followed by immersion in Reynolds^{TM} lead citrate for 5 minutes. Between stains the sections were rinsed with distilled water and dried with filter paper.

7.3 Results and Discussion

Results from molecular weight characterization (pMDI corrected for derivatization) are shown in Table 7.1.

Table 7.1 : Molecular weights obtained for the three resins used in this study

Sample	M_n (g/mol)	M_w (g/mol)
PF-low	190	410
PF-high	350	1020
PMDI	180	280

A series of ^{13}C CP/MAS NMR spectra for samples cured at 135 ^{o}C are shown in Figure 7.2. The top two spectra show neat, labeled pMDI and a wood-pMDI composite. The bottom two spectra show neat, labeled PF and a wood-PF composite. The main peak of interest in the neat pMDI spectrum is the methylene carbon (40 ppm). The use of ^{13}C labeling allows detection of the methylene carbon in the composite spectrum. The small peak appearing upfield from the methylene carbon signal may be due to the presence of aminobenzyl aniline.

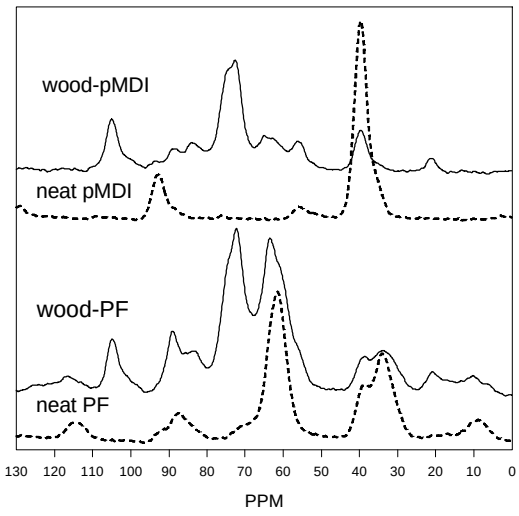

Figure 7.2: ^{13}C CP/MAS NMR spectra of neat labeled resins (dashed lines) and labeled resin composites (solid lines).

The main peaks of interest in the neat PF spectrum are the resin methylene bridge carbons (35 ppm) and the resin hydroxymethyl carbons (63 ppm). It is shown that some signal overlap occurs between the resin hydroxymethyl signal and the cellulose and hemicellulose C_6 signal (60 ppm). No overlap is seen in the case of the resin methylene signal. Structural differences between the neat PF and PF cured in the presence of wood are noted. The use of deuterium labeling of PF resin has been shown to allow observation of the fine structure of methylene and hydroxymethyl structures (see Chapter 6).

Wood-Phenol Formaldehyde Interactions

Proton spin-lattice rotating frame relaxation times ($^{H}T_{1\rho}$) for resin methylene carbons (35 ppm) and the carbons of the cellulose/hemicellulose $C_{2,3,5}$ of wood (72 ppm) for PF composite and neat resin specimens are shown in Table 7.2.

Table 7.2: Proton Spin-Lattice Rotating Frame Relaxation Times, in msec for PF bonded Composites. Standard Error is shown in parenthesis.

Cure Temperature = 135 ^{o}C			
PF-low		PF-high	
Composite		Composite	
35 ppm	8.7 (0.3) 8.2 (0.2)	35 ppm	8.1 (0.3) 8.3 (0.2)
72 ppm	8.4 (0.2) 8.2 (0.3)	72 ppm	8.4 (0.1) 8.9 (0.5)
Neat		Neat	
35 ppm	6.3 (0.4)	35 ppm	15.2 (1.2)
Cure Temperature = 175 ^{o}C			
PF-low		PF-high	
Composite		Composite	
35 ppm	9.1 (0.4) 9.1 (0.5)	35 ppm	6.7 (0.3) 7.3 (0.5)
72 ppm	8.1 (0.3) 8.3 (0.3)	72 ppm	7.8 (0.1) 8.0 (0.2)
Neat		Neat	
35 ppm	14.3 (0.2)	35 ppm	14.5 (1.4)

In all cases, resin methylene carbons of neat specimens display significantly different $^{H}T_{1\rho}$'s than samples cured in the presence of wood. This indicates that the presence of wood during cure has a significant impact on the mid-kHz frequency molecular motions in the cured state of the resin. It is shown that for composite specimens, made with both

PF-low and PF high and cured at 135 ^{o}C, the resin methylene and wood resonances display the same $^{H}T_{1\rho}$. For composite samples cured at 175 ^{o}C however, the wood and resin $^{H}T_{1\rho}$'s are significantly different. $^{H}T_{1\rho}$ is dominated by spin diffusion due to the presence of strongly coupled protons (10). In a single-phase material, spin diffusion causes $^{H}T_{1\rho}$ to be the same for all protons, even if observed through different carbons. The presence of phase boundaries acts to inhibit spin diffusion, which causes each phase to relax independently of one another. This can be identified by bi-exponential decay in signal intensity as a function of contact time. In all cases however, mono-exponential decays in signal intensity as a function of spin-lock time were observed, indicating that in all cases the wood and resin are behaving as single-phase materials. The $^{H}T_{1\rho}$ experiment yields information with regards to domain size on the scale of 10-100 angstroms (9) The fact that the wood and resin protons (PF Low and PF High) for composite samples cured at 135 ^{o}C show the same $^{H}T_{1\rho}$, may indicate that the wood and resin are a homogenous phase on this size scale. If in fact, a homogenous phase does exist it would be comprised of the resin and the amorphous components of wood, since these would be the most accessible to monomer penetration. This conclusion however, can not be confirmed solely based upon $^{H}T_{1\rho}$ measurements since it is also possible that the wood and the resins cured at 135 ^{o}C simply display the same relaxation time but are not in a homogenous phase. It would follow therefore that the results of the $^{H}T_{1\rho}$ measurements indicate that samples (PF-low and PF-high) cured at 175 ^{o}C are not in a homogenous phase on the size scale of 10-100 angstroms.

Signal build as the result of cross polarization (CP) for PF resin methylene carbons in composite specimens are compared with neat resin methylene carbons in Figures 7.3 –7.6. Signals were normalized by setting the peak intensity at the shortest contact time equal to zero and scaling all subsequent peaks with reference to it. Recall that 85 % of the PF resin protons were replaced with deuterium. Signal enhancement in CP/MAS NMR is the result of static energy transfer from protons to carbons. The fact that 15 % of the protons are still present in the samples means that there will be an inherent signal build due to CP in the resin methylene signal as a result of the presence of these protons. Any additional CP in the composite specimens will theoretically be the result of long range CP from any additional source of protons (i.e. wood) to the resin carbons. The comparison between neat and composite specimens therefore attempts to assess the relative contribution of the inherent CP within the resin due to the presence of protons. If signal build due to CP is significantly greater for composite resin methylene carbons compared with neat resin methylene carbons, it is hypothesized that CP has occurred from the wood protons to the resin carbons. CP efficiency is a function of both proximity of the protons and carbons and their rigidity and will only occur if the protons and carbons are within 0-20 angstroms of one another. Therefore if CP occurs between wood protons and resin carbons, then it is possible that the cured resin interpenetrates the wood cell wall.

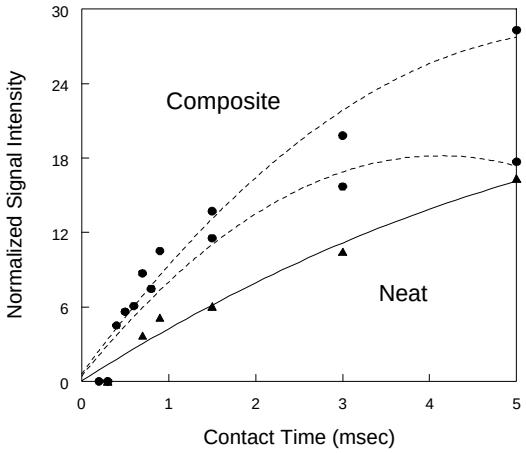

Figure 7.3: Normalized signal intensity plotted as a function of Cross Polarization Contact Time. ● - composite specimens, ▲- neat specimen. Samples were cured with PF-low at 135 ^{o}C.

Figure 7.3 shows the signal build of resin methylene carbons of the composites compared to neat resin carbons for PF-low cured at 135 ^{o}C. The resin methylene carbons of the composites made with PF-low display a stronger signal build due to CP than the neat resin methylene carbons. This indicates that CP is occurring between the wood and the resin and therefore that they are miscible on a scale of 10-20 angstroms.

Figure 7.4 shows that the resin methylene carbons of the composite cured with PF-low (175 ^{o}C) shows weaker signal build due to CP than the neat resin methylene carbons. This indicates that the wood and resin are not miscible on a scale less than 20 angstroms.

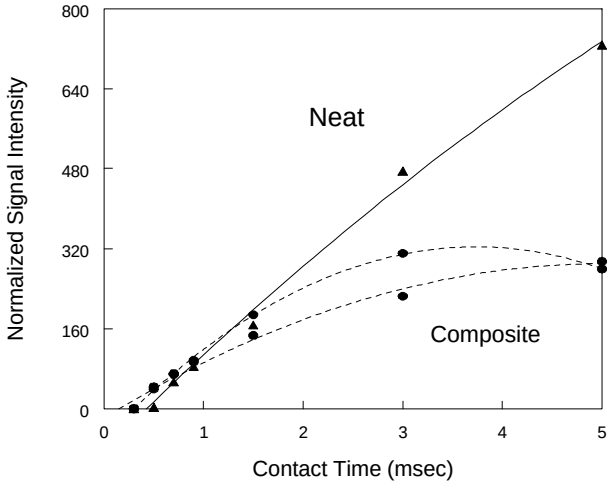

Figure 7.4: Normalized signal intensity plotted as a function of Cross Polarization Contact Time. ● - composite specimens, ▲- neat specimen. Samples were cured with PF-low at 175 ^{o}C.

Recall however that $^{H}T_{1\rho}$ measurements indicated that the wood and resin were homogenous on a scale of 20-100 angstroms. If the size of a domain is smaller than the characteristic scale of a particular observation, a blend appears homogenous (9). Therefore, it appears that PF-low cured at 175 ^{o}C is miscible with wood on a scale of 20-100 angstroms (from $^{H}T_{1\rho}$) but not less than 20 angstroms (from CP).

Figures 7.5 and 7.6 compare the signal build of resin methylene carbons of the composites with neat resin methylene for PF-high cured at 135 ^{o}C and 175 ^{o}C respectively. In both cases, the signal build of the neat resin methylene carbons is significantly stronger than that of the resin methylene carbons of the composites. This indicates that CP does not occur between wood and PF High and that they are not miscible on a space scale detectable by CP measurements. It should be noted that the scaling of signal intensities increases significantly with cure temperature (Figures 7.3 and 7.5 [135 ^{o}C] compared with Figures 7.4 and 7.6 [175 ^{o}C]). This is the result of increased efficiency of cross polarization due to the increased rigidity of the resins cured at higher temperatures.

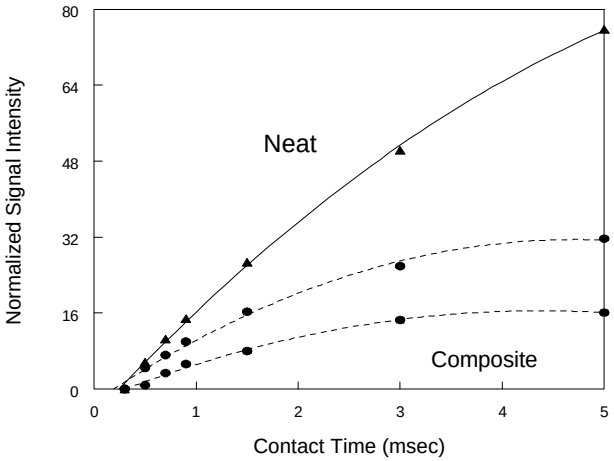

Figure 7.5: Normalized signal intensity plotted as a function of Cross Polarization Contact Time. ● - composite specimens, ▲- neat specimen. Samples were cured with PF-high at 135 ^{o}C.

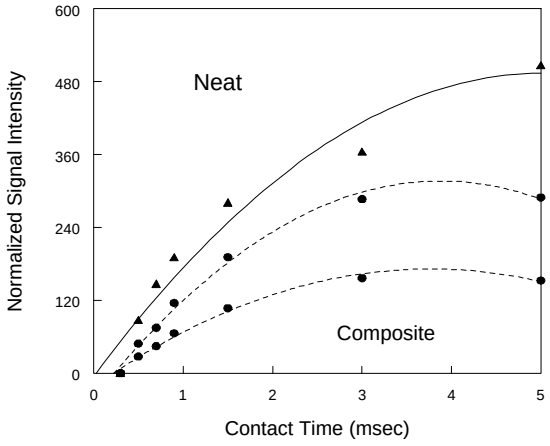

Figure 7.6: Normalized signal intensity plotted as a function of Cross Polarization Contact Time. ● - composite specimens, ▲- neat specimen. Samples were cured with PF-high at 175 ^{o}C.

In order to investigate the influence of moisture on the signal build due to cross polarization, two composite samples were selected, one which showed molecular interactions and one which did not and exposed to high humidity conditions. Composite samples made with PF-low cured at 135 ^{o}C and PF-high cured at 135 ^{o}C were placed in a sealed dessicator in the presence of water for 72 hours. The signal build due to CP from the resin methylene carbons was then monitored. Comparisons of the signal build due to CP for the dry and re-wetted samples are shown in Figures 7.7 and 7.8. Figure 7.7 shows that, moisture affects signal intensity at longer contact times for the sample which displayed molecular interaction (PF-low cured at 135 ^{o}C). At short contact times, the re-wetted samples still possess greater signal intensities than the neat samples, indicating molecular interaction. Figure 7.8 also shows that moisture affect the signal intensities at longer contact times for composites which did not show interaction (PF-high cured at 135 ^{o}C).

The results from Figures 7.7 and 7.8 indicate that moisture does not act to enhance CP of the resin methylene. It may however, play a minor role in masking information with regards to molecular-level interactions obtained from CP experiments. This effect would be most predominant at long contact times.

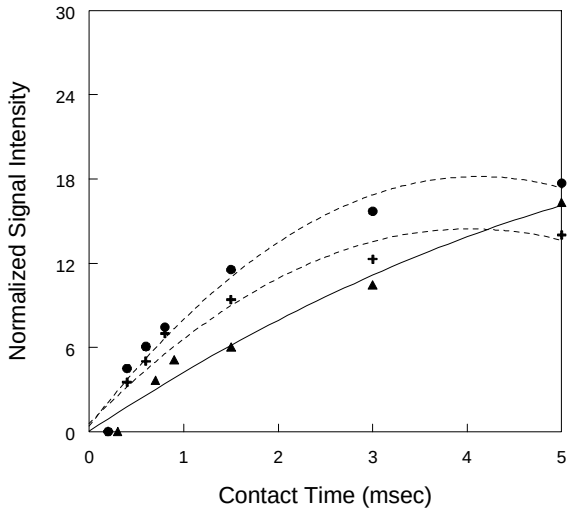

Figure 7.7: Normalized signal intensity plotted as a function of Cross Polarization Contact Time. ● - composite specimen (dry), ✚ - composite specimen (re-wetted), ▲- neat specimen. Samples were cured with PF-low at 135 ^{o}C.

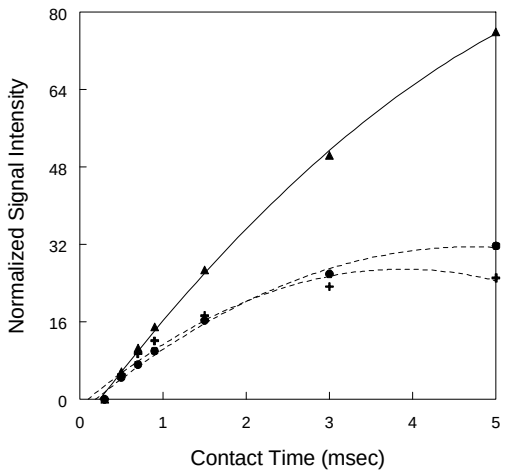

Figure 7.8: Normalized signal intensity plotted as a function of Cross Polarization Contact Time. ● - composite specimen (dry), ✚ - composite specimen (re-wetted), ▲- neat specimen. Samples were cured with PF-high at 135 ^{o}C.

There is a complication in using the CP behavior of neat resins to estimate the inherent CP in the resins within the composite. It was shown in Figure 7.2 that neat PF resin had a different cured structure than PF resin cured in the presence of wood. It was also shown in Table 7.2 that the mid-kHz motions of the neat cured resins were different than resin cured in the presence of wood. It is known that CP efficiency is influenced not only by proximity of the protons and carbons, but also by rigidity of the resin molecules. The molecular rigidity of the cured resin will change as a result of both cure temperature and the presence of wood. If the molecules of the neat resin are more rigid than those of the resin cured in the composite at a given cure temperature, the inherent CP will be stronger in the neat resin. This may mask information with regards to molecular miscibility obtained from the CP experiments.

The fact that PF possesses the ability to penetrate into the cell wall is most likely a result of the size of the monomeric adhesive. Both PF-low and PF-high possess distributions of molecular weight, which include monomers. It has been shown that benzyl alcohol is capable of swelling quaking aspen (*Populus tremuloides*) more effectively than water (8). PF monomers (hydroxymethylated phenols) are similar in structure and molecular size to benzyl alcohol and therefore will also likely be capable of swelling the wood cell wall. They also possess the capability to form hydrogen bonds via the phenolic hydroxyl as well as the hydroxymethyl functionalities. Hydrogen bonding capability of organic liquids has been correlated with their ability to swell wood (8).

Figure 7.9 shows transmission electron photomicrographs of PF-low and PF-high composites cured at 175 ^{o}C.

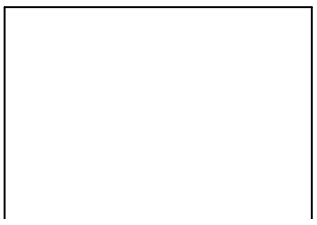

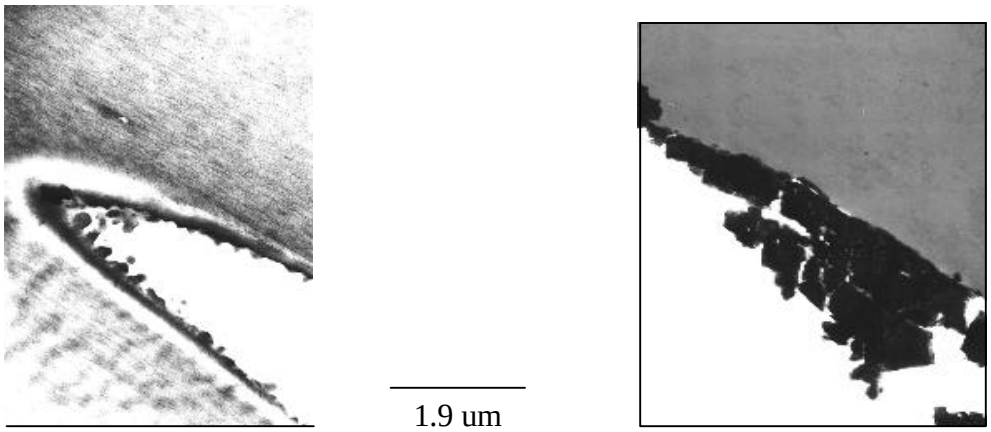

Figure 7.9: Transmission electron photomicrographs of a PF-low sample (left) and a PF-high sample (right). Both samples were cured at 175 ^{o}C. Magnification = 19000 X.

In Figure 7.9, the darkly stained areas are resin. It is seen that the PF-low sample appears to show some interaction with wood, as evidenced by the staining within the wood. This indicates that PF-low has diffused into the wood cell wall. The PF-high sample however, does not appear to be as closely associated with the wood. Staining within the cell wall is not seen, indicating that penetration of the resin has not occurred. It should be pointed out that the practical limit of the resolution of the transmission electron microscopic examination is on the order of 100-200 nm. Therefore the results shown in Figure 7.9 can not be directly related to the results of the NMR experiments which probe angstrom level interactions. However, in order for angstrom scale interactions to occur, it is likely that a higher level penetration of the resin into the cell wall has occurred. Therefore the results shown in Figure 7.9 are consistent with the findings of the NMR experiments.

The degree to which the liquid will be able to penetrate into the cell wall during cure will be strongly dependent on the amount of monomeric material. It will also be a function of the competing rates of diffusion (i.e. penetration) and bulk polymerization (i.e phase separation). The fact that PF is miscible with wood on a molecular level when cured at 135 ^{o}C indicates that the rate of diffusion is faster than the rate of polymerization, allowing penetration into the cell wall. The difference in scale of interaction between PF-low and PF-high is related to the molecular weight distribution. PF-low contains a greater proportion of monomers than PF-high as demonstrated by their molecular weights shown in Table 7.1.

When the cure temperature is raised to 175 ^{o}C, the results of the NMR measurements indicate that PF-low is not miscible with wood on the scale of less than 10 angstroms but appears to be miscible on the order of 10 – 100 angstroms. In this case, the rate of polymerization has increased due to increased cure temperature and competes favorably with the rate of diffusion into the cell wall. Another possible cause is vaporization of monomeric material at the cure temperature of 175 ^{o}C. For PF-high cured at 175 ^{o}C, the combined effects of low amounts of monomer and the increased rate of polymerization prevent miscibility with the wood polymers, on the spatial scale measured by both CP and $^{H}T_{1\rho}$.

Wood-Polymeric Isocyanate Interactions

Proton spin-lattice rotating frame relaxation times ($^{H}T_{1\rho}$) for resin methylene protons (40 ppm) and protons of the cellulose/hemicellulose $C_{2,3,5}$ of wood (72 ppm) for pMDI composite and neat resin specimens are shown in Table 7.3. In all cases, as with the PF samples, neat resin methylene protons display significantly different $^{H}T_{1\rho}$'s than those cured in the presence of wood. This indicates that wood also has a significant influence on the mid-kHz frequency molecular motions in the cured state of pMDI. In all cases, the $^{H}T_{1\rho}$ of the resin methylene protons are significantly different than those of the wood protons, indicating that no interaction on the scale of 20 – 100 angstroms has occurred between the resin and wood.

Table 7.3: **Proton Spin-Lattice Rotating Frame Relaxation Times, in msec for pMDI bonded Composites. Standard Error is shown in parenthesis.**

Cure Temperature = 135 ^{o}C			
Composite			
40 ppm	5.5 (0.3) 7.2 (0.6)		
72 ppm	10.5 (0.1) 10.5 (0.1)		
Neat			
40 ppm	6.2 (0.3) 6.4 (0.3)		
Cure Temperature = 175 ^{o}C			
	PMDI-0	PMDI-30	PMDI-24
Composite			
40 ppm	8.4 (0.8) 7.5 (0.2)	7.3 (0.6) 7.3 (0.4)	6.7 (0.5) 7.1 (0.9)
72	9.7 (0.1) 10.1 (0.2)	8.3 (0.1) 8.2 (0.2)	8.9 (0.1) 9.2 (0.2)
Neat			
40	6.4 (0.1) 6.4 (0.2)		

Build in signal intensity of the methylene carbon as a result of cross polarization is shown in Figures 7.10 and 7.11 for pMDI samples cured at 135 ^{o}C and 175 ^{o}C respectively. Recall that three different types of pMDI bonded specimens were prepared at 175 ^{o}C. One sample was cured immediately upon application of resin (pMDI-0). A second was cured 30 minutes after application of resin (pMDI-30) and a third was cured 24 hours after application of resin (pMDI-24).

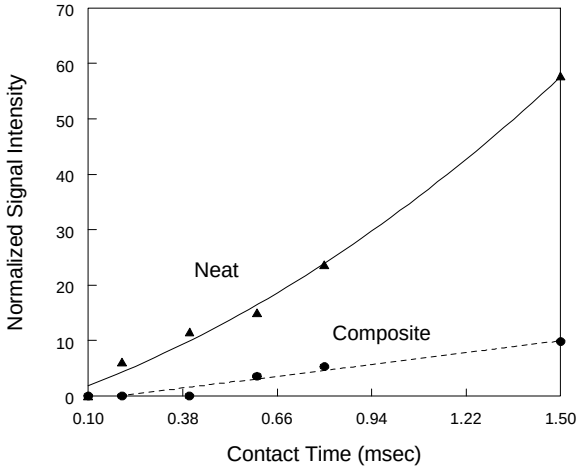

Figure 7.10: Normalized signal intensity plotted as a function of Cross Polarization Contact Time. ● - composite specimens, ▲- neat specimen. Samples were cured with pMDI at 135 ^{o}C.

Figure 7.10 shows that the build in the signal of pMDI-0 cured at 135 ^{o}C is greater than that of the composite sample cured at the same temperature. This indicates that the wood and resin are not miscible on a scale less than 10 angstroms.

Figure 7.11 shows significant differences in the signal build for the composite samples cured at 175 ^{o}C. pMDI-0 and pMDI-30 show significantly lower signal builds due to CP than the neat specimen, indicating that they are not interacting on a scale less than 10-20 angstroms. pMDI-24 shows a significant increase in signal strength compared with that of the neat specimen. The results of the $^{H}T_{1\rho}$ experiments showed that this system is non-interacting on a scale of 10 - 100 angstroms. Since domain size must be smaller than the characteristic scale of the experimental measurement, these results seem counter-intuitive, since molecular miscibility should also be reflected in the $^{H}T_{1\rho}$ experiments. The reason for the disparity between the results of the CP and $^{H}T_{1\rho}$ is unclear at present. Similar observations were found in blends of polyurethane and lignin (6). $^{H}T_{1\rho}$ measurements indicated no miscibility while CP measurements showed interactions (6). This was attributed to the presence of an immiscible blend of the two polymers consisting of three phases, two domains of the lignin and polyurethane and the separating interfacial region. The interactions seen in the CP experiments were attributed to long range CP occurring across the interface. Following this line of reasoning, the results of the $^{H}T_{1\rho}$ and CP measurements for the pMDI bonded specimens, cured 24 hours after application of resin, indicate that the pMDI and wood phases are within 10 angstroms of one another, but not comprised of a single phase region.

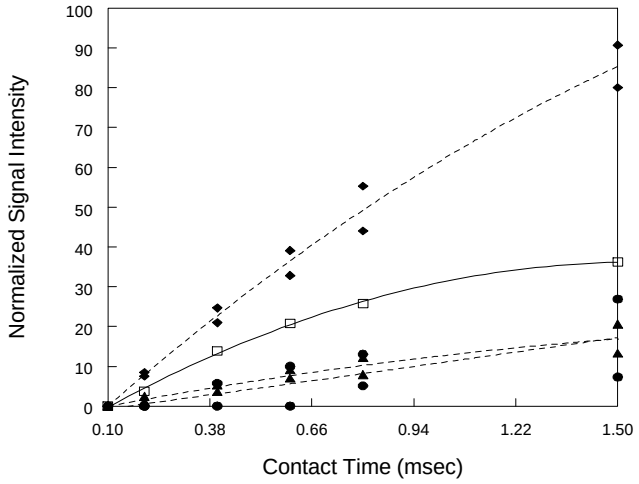

Figure 7.11: Normalized signal intensity plotted as a function of Cross Polarization Contact Time. ● - pMDI-0, ▲- pMDI-30, ◆ - pMDI-24, ❑ - neat specimen. Samples were cured with pMDI at 175 ^{o}C.

While pMDI had lower molecular weight averages than PF Low, it has been shown that the diffusion of monomers into the wood cell wall only occurred after 24 hours. This most likely related to the size of the pMDI monomers. 4-4' diphenylmethane diisocyanate (the predominant monomer of pMDI) has a larger molecular size than hydroxymethyl phenols (the predominant monomers of PF). This would act to decrease the rate of diffusion into the wood polymers. Another factor influencing the rate of diffusion of adhesive into the cell wall will be presence (or absence of solvent). The PF resins were comprised of 50 % water at application. The remainder was a dilute sodium hydroxide solution. Penetration and interaction of PF monomers may be driven by the presence of this solvent. It has been found that organic solvents, which contain small quantities of water as an impurity, act to significantly increase the swelling of wood (8). Wood also has been found to be swollen more readily by basic solutions (8). In the case of pMDI, the resin was comprised of 100 % solids at application. In addition, PF monomers possess greater hydrogen bonding capability than pMDI monomer. Therefore, three explanations exist for the observed time scale differences in PF and pMDI interactions with wood: molecular size, the presence of solvent and hydrogen bonding capability.

Figure 7.12 shows transmission electron photomicrographs of pMDI-0 and pMDI-24 samples.

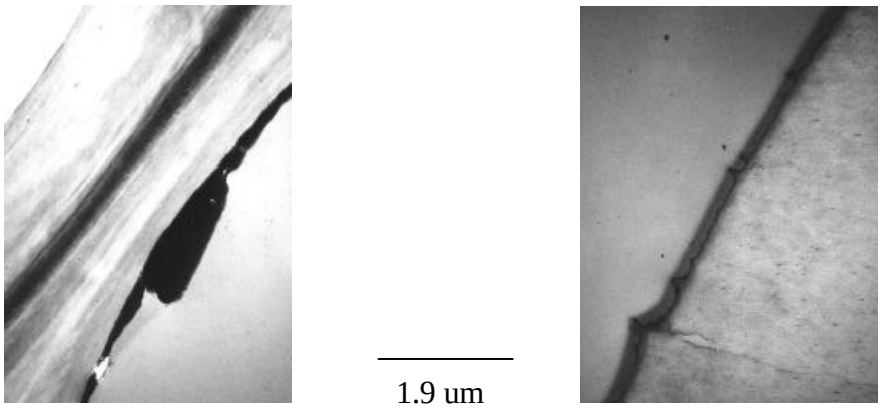

Figure 7.12: Transmission electron photomicrographs of pMDI-0 (right) and pMDI-24 (left). Magnification = 19000 X.

The pMDI-0 sample shows an abrupt transition between the resin and cell wall. This indicates that the resin did not diffuse into the cell wall. The pMDI-24 sample shows a more gradual transition between the resin and the cell wall. This clearly indicates that the resin has diffused into the cell wall. This supports the hypothesis regarding the time dependence of pMDI's ability to diffuse into wood.

7.4 Conclusions

The use of deuterium labeling and NMR relaxation experiments allows the evaluation of relative degrees of molecular interaction between PF and pMDI resins with wood. Results from cross polarization and proton spin-lattice longitudinal relaxation studies indicate that both cured phenol formaldehyde and polymeric isocyanate possess the capability of interacting with wood on a scale of 10-100 angstroms. These results suggest that an interpenetrating polymer network (IPN) morphology may exist at the interphase formed between these two types of resin and wood. In the case of PF, molecular size of the resin monomers influences the scale of interactions between the cured network and wood. PF containing mainly monomers and dimers interacted on a smaller scale than PF containing a greater proportion of higher molecular weight oligomers. Cure temperature was also shown to affect the scale of PF interactions with wood. PF resins cured at low temperatures interacted on a more intimate level than when cured at high temperatures. This can be explained based upon competing rates of resin diffusion into the wood cell wall and bulk resin polymerization. Polymeric isocyanate, which possessed a relatively low molecular weight, was found to interact with wood on a scale of 10-20 angstroms only after sufficient time had elapsed between application of resin and hot pressing. This time dependence is a result of the absence of any solvent (i.e. water) which decreases the propensity of the liquid resin to diffuse into the wood cell wall.

7.5 References

1. Frink, J.W. and H.I. Sachs. 1981. In Urethane Chemistry and Applications. K.N. Edwards ed. ACS Symposium Series 172, American Chemical Society, Washington, D.C. 285

2. Johns, W.E. 1989. In Wood Adhesives Chemsitry and Technology. A. Pizzi ed. Marcel Dekker, New York, 75.

3. Hawke, R.N., B.C.H. Sun and M.R. Gale. 1992. Forest Products Journal. 42 (11/12), 61.

4. Marcinko, J.J. 1996. Proceedings of the Third Pacific Rim Bio-Based Composite Symposium. Hiromu Kajita and Kunio Tsunoda eds. Kyoto, Japan.

5. Charles E. Frazier, Robert G. Schmidt and Jianwen Ni. Proceedings of the Third Pacific Rim Bio-Based Composites Symposium. Hiromu Kajita and Kunio Tsunoda eds. Kyoto, Japan. December 1996.

6. Marra, A.A. 1992. Technology of Wood Bonding: Principles In Practice. New York: Van Nostrand Reinhold

7. Wendler, S.L. and C.E. Frazier. 1996. Int. J. Adhesion and Adhesives. 16, 179-186.

8. Mantanis, G.I., R.A. Young and R.M. Rowell. 1994. Holzforschung. 48 (6), 481-491

9. Takegoshi, K. 1995. Annual Reports on NMR Spectroscopy. 30, 98-130.

10. Fyfe, C.A. 1980. Solid State NMR for Chemists. Guelph University Press. Guelph, Canada.

11. Gobbi, G.C., R. Silvestri, T.P. Russell, J.R. Lyerla and W.W, Fleming. 1987. J. of Polym. Sci. Part C. Polym Letters. 25, 61-65.

12. Parmer, J.F., L.C. Dickinson, J.C.W. Chien and R.S. Porter. 1987. Macromolecules. 20, 2308-2310.

13. Guo, M and H.G. Zachmann. 1993. Polymer. 34 (12), 2503-2507.

14. Zhang, X., A. Nathansohn and A. Eisenberg. 1990. Macromolecules. 23, 412-416.

15. Roland, C.M., J.B. Miller and K.J. McGrath. 1993. Macromolecules. 26, 4967-4969.

16. Nathansohn, A., M. Lacasse, D. Banu and D. Feldman. 1985. J. Appl. Poly. Sci. 19, 899.

Chapter 8

Fracture Toughness Testing of Bonded Wood Assemblies

8.1 Introduction

In order to correctly design adhesively bonded wood composite products for end-use applications, estimates of their mechanical performance must be obtained. Traditionally, these types of products are evaluated by some form of shear testing. Common tests include compression shear (ASTM D 905), for the evaluation of laminated lumber products and tensile shear (ASTM D 805-72) for the evaluation of laminated veneer products (1). Although the use of these tests is widespread, it is recognized that they suffer drawbacks which limit their capability to accurately estimate in-situ performance and durability (2). These include the development of complex stress states, measurement of an average not critical failure strength and the use of wood failure as an estimate of adhesive performance (2). For a detailed description of the limitations of these tests, the reader is referred to Chapter 2 – Literature Review.

While fracture toughness testing has already been introduced in Chapter 2, it is useful to re-state some of the key points of the background theory and treatment. Fracture testing is based on concepts of fracture mechanics which originated with the work of Griffith (3). The underlying assumption of this approach is that the materials under evaluation behave in a linear elastic fashion (i.e. no permanent deformation). The most common property determined from fracture testing is the strain energy release rate (G_c). This is a measure of the energy required to create two new surfaces through fracture of the adhesive bond (4).

When a crack extends through the adhesive layer of two adhesively bonded beams, as shown in Figure 8.1, it is assumed that no change in total energy of the system occurs (assumption of linear elasticity).

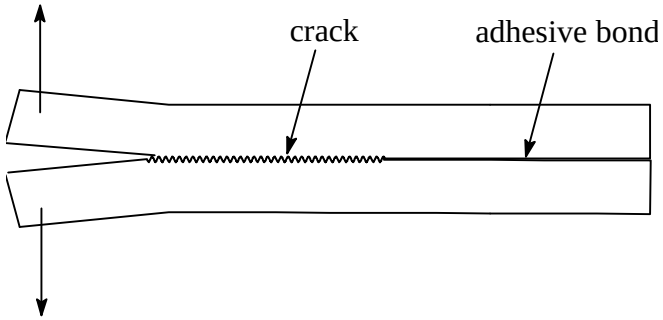

Figure 8.1: Crack extension through an adhesive layer during cleavage testing

The total energy of the system is represented by (4):

$$dE = dD + dS = 0 \tag{8.1}$$

where E is the total energy of the system, D is the potential energy of deformation and S is the surface energy. The strain energy release rate (G), or rate of change in potential energy with crack length is defined as (4):

$$G = \frac{-dD}{bda} \tag{8.2}$$

where b is the width of the specimen and da is the crack extension. The potential energy of deformation (D) is represented by (4):

$$D = U - P\Delta \tag{8.3}$$

where U is the strain energy, P is the applied load and Δ is the displacement. For a linear elastic material (4):

$$U = 1/2P\Delta \tag{8.4}$$

and the strain energy release rate becomes (4):

$$G_{Ic} = \frac{P_c^{\ 2}}{2b}\frac{dC}{da} \tag{8.5}$$

where G_{Ic} is the crack initiation energy, P_c is the critical load at crack initiation, b is the width of the specimen and dC/da is the change in compliance of the beams with crack length. The subscript I denotes opening mode fracture. This approach to the calculation of G is often referred to as the direct compliance method (5). This approach is most often taken when using a contoured double cantilevered beam (CDCB) geometry. The reason for this is that the contours can be designed so that dC/da is constant. This removes the need to monitor crack length during testing. Unfortunately, the calibrations required to use this geometry, are very time consuming.

Strain energy release rates can also be calculated using the simple beam theory approach which models the adherends as beams on elastic foundations. In this approach, G is represented by (5):

$$G = \frac{12P^2a^2}{b^2h^3E} \tag{8.6}$$

where h is the height of the specimen and E is the modulus. The modulus may be calculated by (5):

$$E = \frac{8Pa^3}{bh^3d} \tag{8.7}$$

where d is the beam displacement.

It has been found that in cases where the adherends possess low ratios of plane shear to axial modulus, the application of simple beam theory is inappropriate. In these cases, flexure of the adherends causes shear forces to develop at small crack lengths. This effect reduces the measured crack length by some value below what it would be in the absence of shear effects. In order to correct for the effects of shear, Williams (6) has

derived a shear correction factor χ, which allows the correction of measured crack lengths. The shear correction factor can be calculated from the experimental relationship between compliance and crack length (5):

$$C^{1/3} = \left(\frac{8}{Bh^3 E} \right)(a + ch) \tag{8.8}$$

Since crack length is used in simple beam theory for the calculation of both modulus and strain energy release rate, both must be corrected. The corrected modulus is represented by (5):

$$E_c = \frac{8P(a + ch)^3}{bh^3 d} \tag{8.9}$$

and the corrected strain energy release rate is represented by (5):

$$G = \frac{12P^2(a + ch)^2}{b^2 h^3 E_c} \tag{8.10}$$

Calculation of G by this approach is referred to as the shear corrected beam theory approach. Use of the beam theory approach (corrected or uncorrected) to the calculation of G is most often used when a simple cantilevered beam (DCB) geometry is used.

Arrest loads (P_a), which are the loads maintained by the specimen after the crack arrests, can be used to calculate G_a, which is the amount of energy stored in a specimen upon fracture. Both G_a and G_c can be used to calculate I, the brittleness index (7):

$$I = \frac{G_c - G_a}{G_c} \tag{8.11}$$

While fracture toughness testing has been applied to the evaluation of wood-adhesive systems, the dominant method has involved the use of the CDCB geometry (2,8,9). The use of DCB specimen geometry and the application of simple beam theory has only been recently applied to the study of wood-adhesive systems (10,11). The validity of this approach remains unclear. Any permanent deformation in the adherends (i.e. plastic loss) renders the use of linear elastic beam theory invalid. In addition, since wood possesses low plane shear strength, the application of beam theory necessarily requires a shear correction. While beam theory has been applied to fracture tests of bonded wood assemblies, no use of shear correction has been reported in the literature.

In the previous chapter, a new theory of the mechanism by which some adhesives may form bonds with wood has been introduced. In summary, evidence has been found that under certain conditions, both phenol-formaldehyde and polymeric isocyanate adhesives have the capability to molecularly diffuse into the wood cell wall where subsequent polymerization creates an interpenetrating polymer network (IPN) morphology. For a more detailed discussion, the reader is referred to Chapter 7. This

type of interphase morphology at the bondline may have profound implications on the mechanical performance and durability of such bonds. No literature exists which relates mechanical performance to this type of adhesive mechanism.

This study has three main objectives. First, to evaluate a new DCB test geometry and method of crack measurement for the calculation of fracture energies to test the validity of the use of linear elastic fracture mechanics principles. Second, to compare values of fracture energies calculated by direct compliance, uncorrected beam theory and shear corrected beam theory methods. Third, to gain insight into the influence of molecular phenomena on macroscopic performance and durability of wood-adhesive bonds.

8.2 Experimental

8.2.1 Materials

All chemicals were used as received. Phenol (99 %) was purchased from Fischer Scientific. Paraformaldehyde (95 %) was purchased from Aldrich Chemicals. Air dried yellow poplar (*Liriodendron tulipifera*) sapwood lumber, free of knots, was utilized throughout. Initial board dimensions were 51 mm (2") in thickness, 200-250 mm (8-10") in width and 3.7 – 4.6 m (12-15 ') in length. Polymeric diphenylmethane diisocyanate adhesive (pMDI - Rubinate M) was obtained from ICI Polyurethanes.

8.2.2 Methods

Resin Synthesis

Phenol formaldehyde (PF) resin was synthesized with a P : F : Na molar ratio of 1 : 2 : 0.2. Two different resins were synthesized, based on reaction time. Resin was synthesized in 1 L batches. 250 g (2.656 mols) of phenol and 167.8 g of paraformaldehyde (5.313 mols) were combined in a 2 L reaction flask. 439 g of distilled water and 42.5 g (0.5313 mols Na) of NaOH was then added. Target resin solids was 50 %. The flask was heated and allowed to reflux for either 20 (product designated PF-low) or 45 minutes (product designated PF-high). After the desired reaction time had elapsed, the reaction was quenched by immersion of the reaction flask in a cold water/acetone bath. A third resin (designated PF-mix) was made by preparing 500g of a 1 : 1 mixture of the 20 minute cook (PF-low) and 45 minute cook (PF-high) resins.

Resin characterization

PF and pMDI resins were derivatized for molecular weight determination. PF resin was acetylated in a 1 : 1 molar mixture of pyridine : acetic anhydride at room temperature for 72 hours. The reaction mixture was then added to a 250 mL separatory funnel. 20 mL distilled water was added to decompose excess acetic anhydride followed by 20 mL of saturated NaCl solution. 25 mL of chloroform was added. After vigorous shaking, the organic layer was collected. The aqueous layer was washed twice with 25 mL chloroform, which was also collected. The organic phases was dried with anhydrous sodium sulfate and then filtered. The chloroform was removed by rotational evaporation.

The product was an oil with the odor of pyridine. The pyridine was removed by addition of 200 mL of toluene and rotational evaporation.

pMDI resin was reacted with diethylamine in chloroform at room temperature for 30 minutes. Residual diethylamine and chloroform were removed by rotational evaporation.

Molecular weights were determined using gel permeation chromatography. Detection was accomplished with a Viscotek viscometer (Model 100) and a Waters differential refractometer (Model 410). Waters ultrastyrogel columns were used. Three columns used in sequence with pore sizes of 10^3, 10^4 and 10^6 angstroms respectively. Samples were run at 40 ^oC in tetrahydrofuran.

Viscosities of the resins were measured with a Brookfield Viscometer (Model DV-I). Isocyanate content of the pMDI, obtained by the manufacturer was 31 %.

Billet Manufacture

The yellow poplar lumber was cut into 250 mm lengths and edged on the tangential faces. Widths of the pieces were 200 mm. The pieces were sliced on a band saw at 5 ^{o} angle with respect to the grain, into 15 mm thick billets. A diagram illustrating this procedure is shown in Figure 8.2. The billets were then planed to a thickness of 10 mm. The final dimensions of the billets were 10 mm (thickness) x 250 mm (length) x 200 mm (width). They were placed in an environmental chamber at 20 ^oC (± 1 ^oC) and 65 % relative humidity (± 1 %). They were allowed to equilibrate to a moisture content of 14 % (± 0.5 % - oven dry wood basis), which required approximately 72 hours.

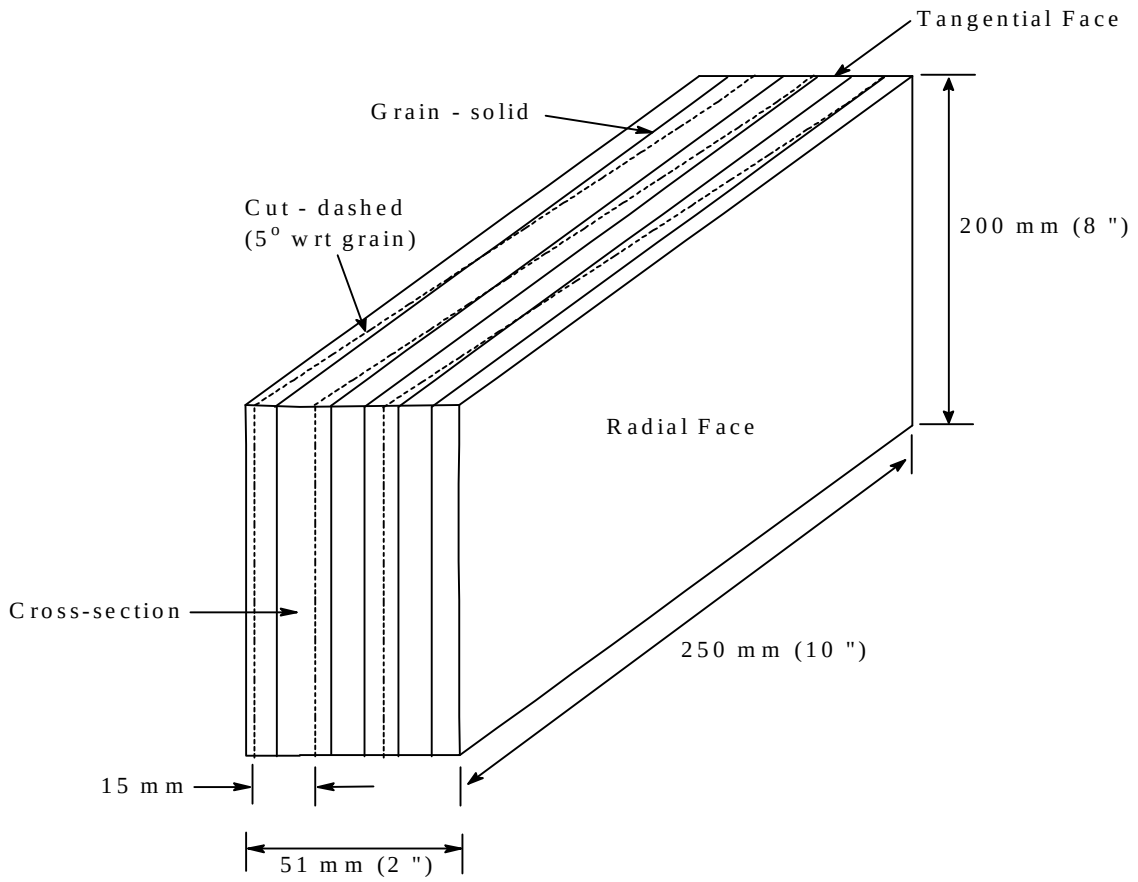

Figure 8.2: Preparation of Billets

Specimen Preparation

Billets with matching grain angle were paired so that the grains converged at the bondline. The bonding surfaces were lightly hand sanded prior to bonding. Sanding consisted of 3-4 light strokes of the bonding faces along the grain with 220 grit sandpaper immediately prior to application of resin. Dust was removed from the bonding surfaces by wiping them with a clean paper towel. 116 g/m^2 of resin solids (3 - 4 % oven-dry wood basis) was applied to each surface. A wire-wound metering bar (No. 8 – R-K Printcoat Industries) was used to apply the adhesives to ensure uniform coverage. The assemblies were placed between steel caul plates and pressed at 2.76 MPa (400 psi) for 20 minutes at either 135 or 175 ^{o}C.

Assemblies bonded with the three PF resins were pressed within 5 minutes of the sequential application of resin to the bonding faces. Assemblies, which were bonded with pMDI and cured at 135 ^{o}C, were also pressed within 5 minutes of the application of resin.. For pMDI-bonded composites cured at 175 ^{o}C, the resin was applied in two different ways. One series was made by hot-pressing within 5 minutes after the application of resin. Samples produced in this fashion were designated pMDI-0. A second series was prepared by applying 58 g/m^2 resin solids (1.5-2 % resin, oven dry wood basis) to each bonding face and allowing them to sit for 24 hours in open

atmosphere, after which time an additional 58 g/m^2 of resin was applied to each bonding face and they were pressed. Sample produced in this fashion were designated pMDI-0/24. Resin application for these specimens was accomplished using a wire-wound metering bar (No. 3 – R-K Printcoat Industries).

Two bonded assemblies were prepared for each resin cured at 135 ^{o}C. Four bonded assemblies were prepared for each resin cured at 175 ^{o}C. For the samples cured at 175^{o}C, two assemblies were tested with no pretreatment and two assemblies were subjected to simulated weathering prior to testing.

Immediately after hot-pressing, all bonded assemblies were allowed to cool at 20 ^{o}C (± 1 ^{o}C) and 65 % relative humidity (± 1 %) for 1 hour. 29 mm (¾ ") thick oriented strand board (OSB) was bonded to both sides of the assemblies using 5 minute epoxy. After the backings were adhered to the bonded assemblies, they were pressed at 0.03 MPa (5 psi) for 1 hour to allow full strength development of the epoxy. Samples were then cut to final dimensions (19 mm width, 49 mm depth and 203 mm length) and placed in the environmental chamber for 24 hours, after which time they were tested. Four specimens were cut from the center of each bonded assembly, yielding eight specimens per treatment. The periphery of the bonded assemblies was discarded. Precracks were sawn 40 mm into the bondline using a band saw and holes were drilled using a drill press for the test apparatus. Cure bondline thicknesses were in the range of 80-120 μm, as determined by measurements with optical light microscopy. The final specimen geometry is shown in Figure 8.3.

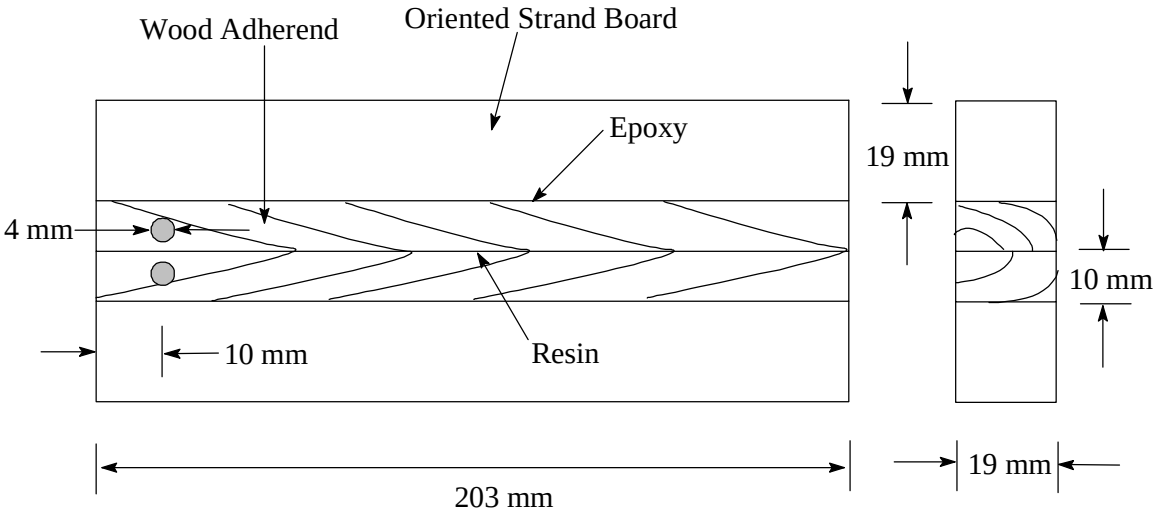

Figure 8.3: Fracture Toughness Specimen Geometry

Simulated Weathering of Bonded Assemblies

Two bonded assemblies for each resin cured at 175 ^{o}C were weathered prior to testing. Simulated weathering consisted of immersion in water under low vacuum (~ 50 kPa) for 24 hours at room temperature followed by oven drying at 103 ^{o}C (± 2 ^{o}C) at atmospheric pressure for 24 hours. This cycle was repeated once. After weathering, the bonded assemblies were placed in an environmental chamber for 72 hours. Application of backing and cutting of specimens was then performed as described above.

Testing

Opening mode cleavage testing was performed using a Materials Test System (MTS - 810). Sample loads and displacements were recorded using a PC data acquisition system. A 454 kg (1000 lb) load cell was utilized at 20 % of its full scale. Maximum displacement of the crosshead was 12.7 mm (0.5 "). Loading and unloading rates were 2 mm/minute. One end of the specimen was placed in the test apparatus while the other was supported by an elastic cord to prevent moment development during the test. A CCD camera connected to a VCR, video monitor and time-date generator, was mounted on a moveable stage to monitor the crack propagation during testing. Prior to testing, Wite-Out^{TM} was applied as a thin film to the bondline to aid in crack measurement. A scale was also placed on the specimen to allow crack measurement to be made directly from the video monitor as the test was progressing.

In a typical run, the sample was loaded until crack initiation. At this point the displacement was held constant until the crack arrested. The load was then released from the sample. This procedure was repeated until sample failure, which gave approximately 4 – 8 data points per sample with which to calculate G.

Calculation of G

Opening mode crack initiation and arrest energies (G_{Ic} and G_{Ia}) were calculated by three different methods: the direct compliance method, uncorrected beam theory and shear corrected beam theory (5). G values determined from the direct compliance method were calculated using equation 8.5. Compliance values were calculated from the linear portions of the load-displacement curves and the crack lengths were monitored by video camera. Compliance as a function of crack length was fitted to a second order polynomial equation. This equation was then integrated to determine dC/da for each crack length. For uncorrected beam theory calculations, moduli were calculated using equation 8.7 and G was determined from equation 8.6. For corrected beam theory calculations, shear correction factors (χ) were determined using equation 8.8. This was accomplished by performing a least squares regression of $C^{1/3}$ vs. crack length as per reference 5. The intercept of the regression line was divided by the slope and the height of the specimen to yield χ. The corrected moduli (E_c) were calculated using equation 8.9 and G was determined using equation 8.10.

Since the initial pre-crack possessed a blunt tip, not indicative of a true crack, the first data point from each specimen was not used in the calculation of G. Brittleness indices (I) were calculated using equation 11 for values of corresponding G_{Ic} and G_{Ia} determined from the direct compliance method.

Values of G_c at a given crack length were calculated using the crack length at which the loading cycle began (i.e. the crack length from the previous loading cycle). Values of G_a at a given crack length were calculated using the crack length at which arrest occurred (i.e. the crack length when the current loading cycle ended). Mean values of G_c were compared using Tukey's multiple comparison test at an alpha level of 0.05, modified to account for unequal sample sizes (12).

8.3 Results and Discussion

Characterization data for the resins used in this study are shown in Table 8.1. It is shown that the viscosity and molecular weight of the PF adhesives increased substantially from a cook time of 20 minutes (PF-low) to 45 minutes (PF-high). Molecular weight of the pMDI adhesive is shown to be considerably less than either PF-low or PF-high.

Table 8.1 : Viscosities and Weight Average Molecular Weights for Resins Used

	PF-low	PF-high	PF-mix	PMDI
Viscosity (mPa.s)	45.4	23040	325	1500
M_n (g/mol)	740	2700	--	300
M_w (g/mol)	1610	18300	--	460

A typical load-displacement profile obtained during testing is shown in Figure 8.4. It is shown that the load-displacement curves returned to zero displacement without the development of any significant compression loads. It is also shown that subsequent loading curves reach the maximum values of load established during the previous loading cycle. These facts indicate that no energy loss occurred due to plastic deformation of the adherends (13). It should be noted that this behavior was observed for all specimens tested in this study. Therefore, the samples are behaving in a linear elastic fashion and theoretically, the application of linear elastic fracture mechanics (LEFM) for determining fracture energies is valid for these systems.

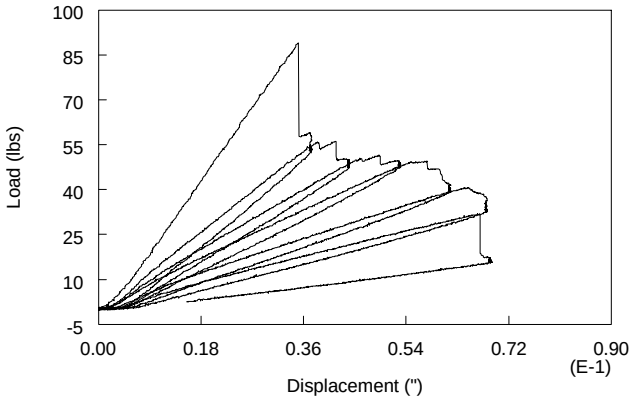

Figure 8.4: Typical load-displacement curve
Specimen was cured with PF-low at 175 ^{o}C , tested with no pretreatment.

Evaluation of Different Methods of Calculating Fracture Energies

Figure 8.5 shows a typical compliance vs. crack length relationship used to determine dC/da for a series of specimens cured under the same conditions with the same adhesive. The curve fits to second order polynomial equations show high correlation coefficients ($R^2 > 0.95$) with low variability in the data.

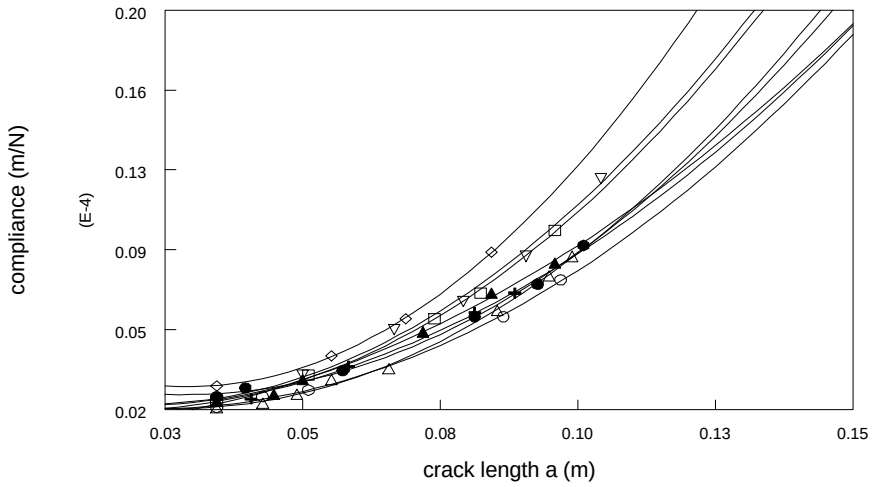

Figure 8.5: Compliance versus crack length used to calculate dC/da Specimens were cured with PF-low at 175 ^{o}C, tested without weathering

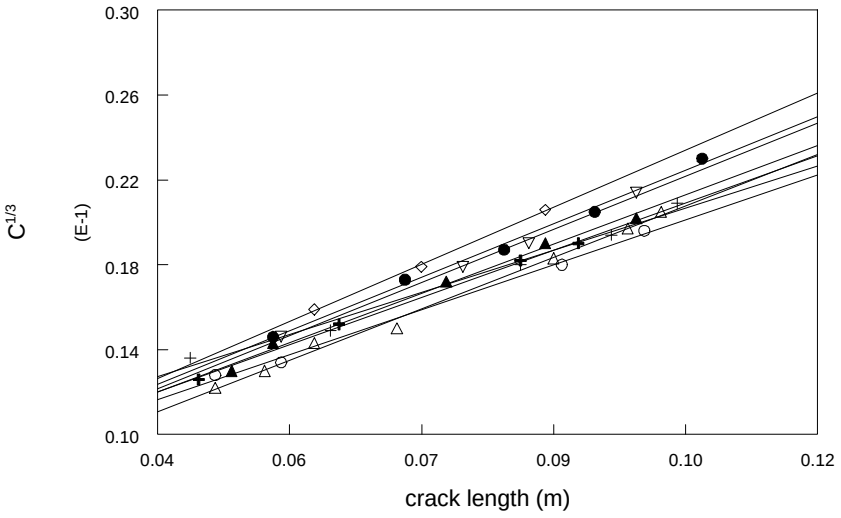

Figure 8.6: $C^{1/3}$ versus crack length used to calculate χ.
Specimens were cured with PF-low at 175 ^{o}C , tested without weathering

Figure 8.6 shows a typical plot of the cube root of compliance as a function of crack length used to calculate the shear correction factor χ, for a series of specimens cured under the same conditions with the same adhesive.

The need to apply χ to simple beam theory calculations of fracture energy (G) for DCB specimens arises as the result of linear elastic flexure in adherends with low shear strength. As mentioned, wood possesses a low plane shear strength. This results in end rotation of the specimens and causes the deflection of the beams to be dominated by shear forces at small crack lengths. This effect requires a correction of the measured crack length, by the amount χh. It has been found that the effect of χ on the calculation of G is minimal in cases where h << a (i.e. low values of χ are determined). For the geometry used in this study however, this condition is not met and therefore χ is expected to have a significant influence on the calculated value of G.

Values of χ, calculated for each type of specimen tested in this study, are shown in Table 8.2. Calculated χ values range from 1.0 to 3.0. This is in agreement with published values of χ for orthotropic materials (~ 2.5) (6). Large values of χ (i.e. > 1) are associated with assemblies prone to microcracking of the adherends (6). Microcracking of wood has been shown to occur around crack tips in a variety of wood-adhesive fracture specimens (7).

Table 8.2: Average shear correction factors (χ), standard deviation in parenthesis. Number of observations = 4-6 for each treatment.

Cure Temp (^{o} C)	PF-low	PF-high	PF-mix	pMDI-0	PMDI-0-24
135	2.0 (0.6)	1.5 (0.3)	1.6 (0.3)	1.4 (0.6)	--
175	1.6 (0.4)	1.5 (0.6)	1.6 (0.4)	1.0 (0.4)	2.5 (0.4)
Weathered	2.1 (0.6)	1.9 (0.6)	2.4 (0.5)	2.4 (0.5)	3.0 (0.6)

The shear correction term is used to correct calculated moduli. The effect of χ on the moduli is shown in Figure 8.7 for all specimens tested in this study. Uncorrected moduli fall into a tight grouping, increasing as a function of crack length. This apparent increase in modulus is the result of shear forces dominating deflection at small crack lengths. This indicates that a correction for this effect must be made in order to appropriately use beam theory for the calculation of G for these systems. When this correction is applied, the modulus is shown to increase substantially. High variability in the values of corrected modulus is evident. This is a result of the sensitivity of the corrected modulus to the shear correction factor.

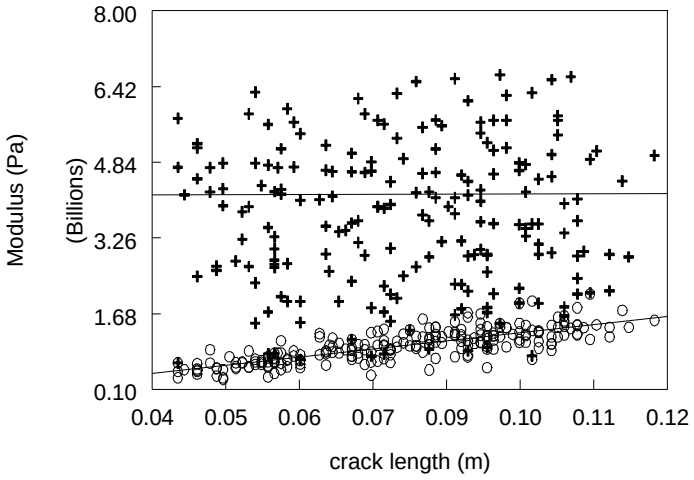

Figure 8.7: Effect of χ on modulus calculated from beam theory. ❍ - uncorrected modulus, ✙ - corrected modulus

A typical plot of G_c as a function of crack length, calculated by compliance, uncorrected beam and shear corrected beam theory is shown in Figure 8.8. For all

specimens tested it was found that calculation of G_c by the compliance method yields constant values as a function of crack length. It is shown that G_c, calculated from uncorrected beam theory methods, decreases significantly as a function of crack length, eventually reaching values calculated from the compliance method at large crack lengths. This is due to the aforementioned shear deflection, which dominates at small crack lengths

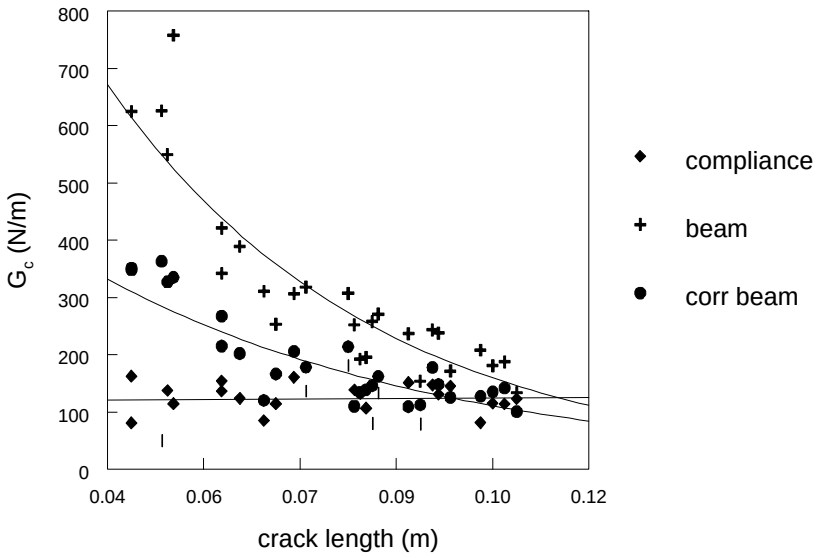

Figure 8.8: G_{Ic} calculated from direct compliance, beam and corrected beam theories. Specimens were not weathered, cured with PF-high at 175 ^{o}C.

but become insignificant at large crack lengths. At long cracks lengths therefore, beam theory calculations should match direct compliance calculations which is what is observed.

It is shown that although the values of G_{Ic} calculated from corrected beam theory are in better agreement with those of the compliance method, a decrease in G_{Ic} is still noted as a function of crack length. Theoretically, shear effects should be removed by the application of χ and the results of corrected beam theory calculations should agree with results obtained from compliance method calculations for all crack lengths. Figure 8 shows G_{Ic} for all specimens tested from corrected beam theory calculations plotted as a function of G_{Ic} calculated from the compliance method. It can be seen that, on average, corrected beam theory overestimates G_{Ic}.

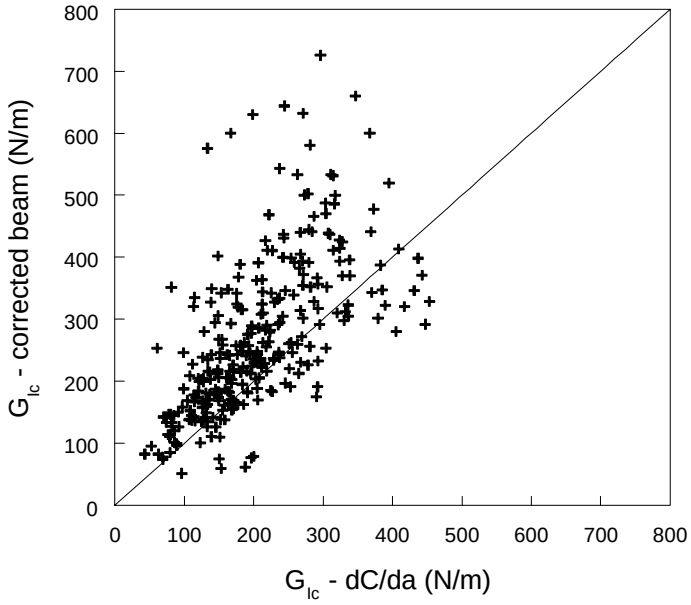

Figure 8.9: G_{Ic} from corrected beam theory versus G_{Ic} from direct compliance

There are several possible reasons for the disparity between direct compliance and corrected beam theory calculations. The shear correction factor χ, was successfully developed for isotropic and orthotropic materials to correct the measured crack length. The bonded assembly used in this study is anisotropic due to the nature of the wood adherends. The anisotropy at the bondline of a bonded wood assembly will be highly dependent on the microstructure, which will affect the density and therefore modulus. It has been found that the location and type of fracture that occurs in wood (or in the case of laminate fracture, the wood-adhesive interphase) is dependent on the type of cells present, the direction and type of load, the grain angle and weathering effects (7). All of these factors can vary with position at the bondline. The derivation of χ for orthotropic materials assumes that the modulus of the adherends is constant throughout the bondline (6). In the case of wood however, morphological and density variations along the beam will result in variations in modulus (7). This implies that the assumptions underlying shear corrected (and uncorrected) beam theory are invalid when dealing with bonded wood assemblies.

There are four main reasons for the application of the correction to the measured crack length . These are: shear forces in the adherends (6), displacement and rotation of the crack root (6), the formation of a damage zone in front of the growing crack (i.e. microcracking) and the formation of non-linear crack fronts (14). The theoretical treatment of χ for orthotropic materials only takes into account shear forces and crack root distortions (6). Specimens tested in this study yielded constant values of G with

crack length, as calculated from the direct compliance method. This indicates that the effects of damage zones ahead of the crack front and non-linear crack fronts play insignificant roles in the correction of the measured crack length. This means that although χ can theoretically account for the remainder of the factors influencing crack length, the heterogeneity at the wood-adhesive bondline, make its use inappropriate for the systems tested in this study.

Effects of Temperature and Accelerated Weathering on the Fracture Toughness of PF and pMDI Bonded Wood

Crack initiation and arrest energies determined from direct compliance method calculations as well as brittleness indices are shown in Table 8.3 and 8.4 for PF and pMDI bonded specimens. Table 8.5 shows values of G_c for all specimens, ranked in order of increasing G_c, with their groupings obtained from Tukey's multiple comparison test. Published values of G_c for a variety of wood-adhesive systems have been shown to fall in the range of 100 – 300 N/m (7), which are in good agreement with the results of Tables 8.3 –8.5.

Table 8.3: Crack initiation (G_{Ic})and arrest (G_{Ia}) energies in N/m for PF samples. Also shown are Brittleness Indices (I). Standard Deviations are shown in parenthesis.

	PF-low			PF-high			PF-mix		
Cure Temp (^{o}C)	**G_{Ic}**	**G_{Ia}**	**I**	**G_{Ic}**	**G_{Ia}**	**I**	**G_{Ic}**	**G_{Ia}**	**I**
135	156 (47)	149 (51)	0.04	202 (48)	193 (50)	0.04	186 (107)	163 (95)	0.12
175	118 (24)	107 (29)	0.10	143 (26)	143 (29)	0	161 (36)	154 (32)	0.04
Weathered	304 (67)	304 (89)	0	240 (47)	200 (82)	0.17	300 (67)	298 (68)	0.01

Table 8.4: Crack initiation (G_{Ic})and arrest (G_{Ia}) energies in N/m for pMDI samples. Also shown are Brittleness Indices (I). Standard Deviations are shown in parenthesis.

	PMDI-0			PMDI-0-24		
Cure Temp (^{o} C)	**G_{Ic}**	**G_{Ia}**	**I**	**G_{Ic}**	**G_{Ia}**	**I**
135	210 (35)	201 (32)	0.04	--	--	--
175	288 (46)	272 (40)	0.06	186 (58)	179 (74)	0.04
Aged	167 (51)	167 (33)	0	103 (50)	91 (67)	0.12

Brittleness indices (I) are shown to range from 0 – 0.17. The closer the value of I is to 1, the more brittle the material. I values of 0 indicate ductile behavior.

Table 8.5: Groupings of G_{Ic} obtained from Tukey's multiple comparison test. α = 0.05. The specimens are ranked in order of increasing G_{Ic} . W denotes samples exposed to accelerated weathering. N = number of observations.

Specimen	Cure Temp (^{o}C)	Grouping								N
PMDI-0-24 (W)	175	A								14
PF-low	175	A	B							25
PF-high	175	A	B	C						16
PF-low	135		B	C	D					20
PF-mix	175			C	D	E				16
PMDI–0 (W)	175			C	D	E	F			20
PF-mix	135			C	D	E	F			35
PMDI-0-24	175				D	E	F			13
PF-high	135					E	F	G		36
PMDI-0	135						F	G		21
PF-high (W)	175							G		12
PMDI-0	175								H	22
PF-mix (W)	175								H	18
PF-low (W)	175								H	23

It is shown that for specimens bonded with PF-high, crack initiation energy (G_c) decreased with increased cure temperature. Specimens bonded with PF-low and PF-mix showed no significant difference in G_c between the two cure temperatures. PMDI-O specimens cured at 175 ^{o}C show higher G_c values than those cured at 135 ^{o}C. Smaller values of G_c mean increased brittleness while larger values of G_c mean increased toughness.

Non-weathered pMDI-0 samples were shown to be tougher than all non-weathered PF samples cured at 175 ^{o}C. At 135 ^{o}C, pMDI-0 was tougher than PF-low and PF-mix samples but not significantly different from PF-high samples. This finding most likely reflects the differences in cure behavior between the two types of resin. The PF utilized in this study was comprised of 50 % solvent (i.e. water). The water will initially penetrate into the surface layers of the wood when the resin is applied. It is subsequently vaporized during cure. It has been found that the use of water-based resins results in considerable stresses being developed during cure as a result of shrinkage and swelling of the wood surface layers. These stresses have been known to cause brittleness and delamination of the cured bondline (7). pMDI contains no solvent when applied. Therefore cure stresses, caused by solvent interaction with wood, will be absent in the pMDI-0 specimens. This may explain their increased toughness over PF bonded specimens.

The effect of applying the pMDI in two stages showed to significantly reduce the fracture toughness. Weathered specimens showed the lowest values of Gc obtained in this study. Recall, that these specimens were prepared by applying 1.5 – 2% resin (oven dry wood basis) initially and an additional 1.5 – 2 % after twenty-four hours. pMDI initially applied would react with water present in the wood and the open atmosphere to form a polyurea network. This may act to deactivate the bonding surface and form a weak boundary layer within the adhesive when the remainder of the resin is applied and cured.

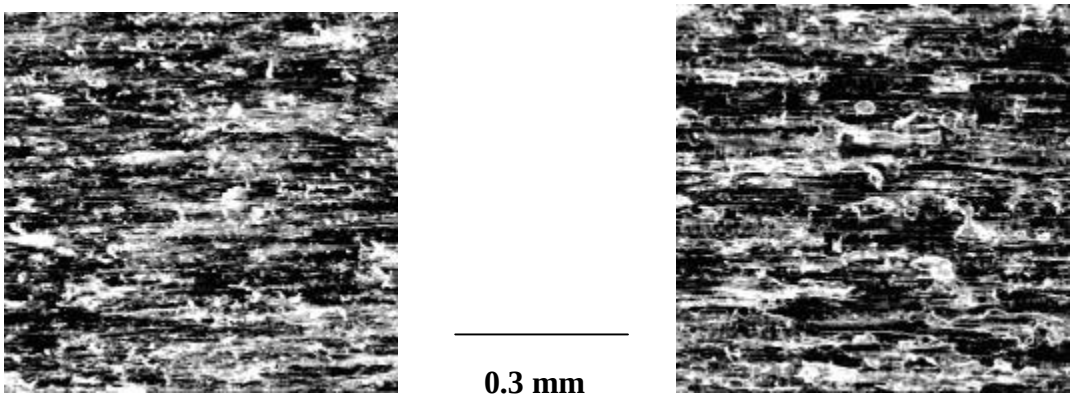

Figure 8.10: Photomicrographs showing pMDI-0 (left) and pMDI-0-24 cured after two stage application of resin (right). Magnification = 75 X.

Figure 8.10 compares fracture surfaces of pMDI-0 and pMDI-0-24 samples. All specimens were cured at 175 ^{o}C. pMDI-0-24 samples show greater evidence of adhesive tearing. This indicates that a greater portion of crack propagation has occurred within the adhesive as opposed to the wood-adhesive interface or interphase. It has been hypothesized that a weak boundary layer has been formed when the resin was applied in two stages. This would act to decrease the resistance of the bondline to crack propagation and lead to decreased fracture toughness.

Weathering resulted in a significant increase in the fracture toughness of all PF bonded samples compared with un-treated specimens. Photomicrographs of the fracture surfaces of un-treated and weathered PF samples are shown in Figures 8.11-8.13. It can be seen that the amount of fiber pull-out and the roughness of the fracture surface increased significantly as a result of weathering. It has been found that cure shrinkage

stresses occuring after hotpressing can cause microcracks in the adhesive layer and damage the wood interphase (15).

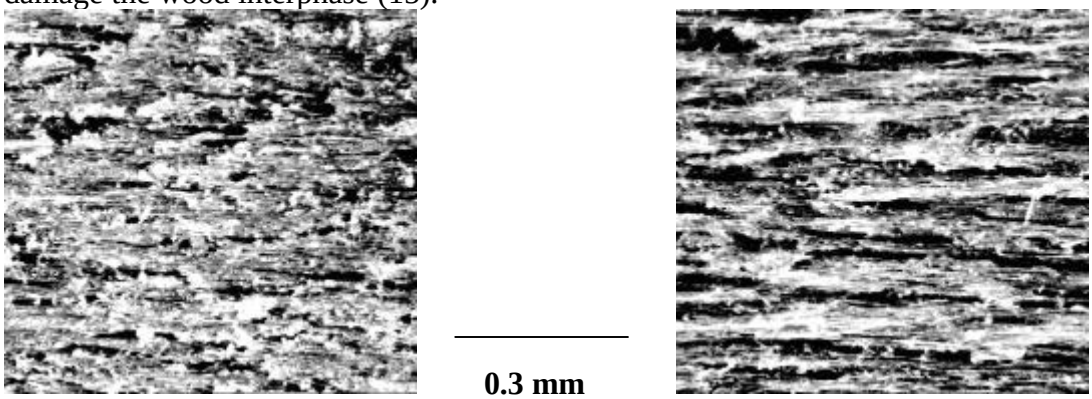

Figure 8.11: Photomicrographs showing PF-low un-treated (left) and PF-low weathered (right). Magnification = 60 X

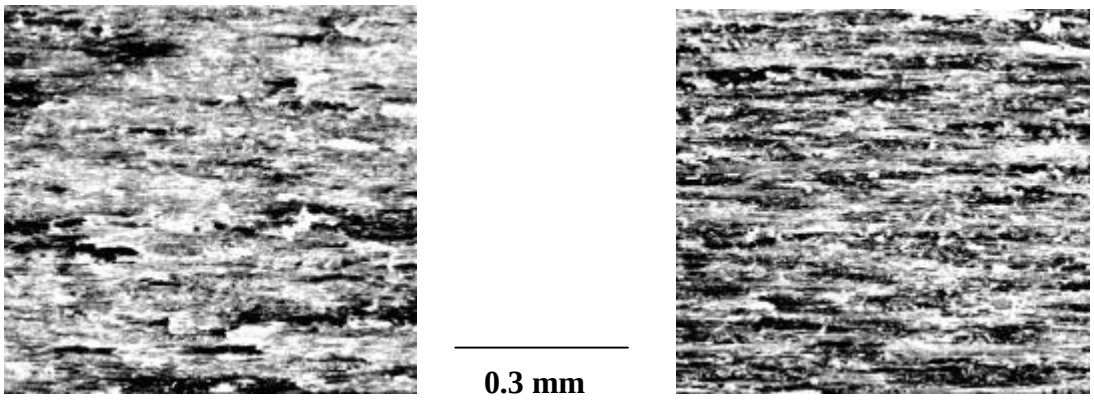

Figure 8.12: Photomicrographs showing PF-high un-treated (left) and PF-high weathered (right). Magnification = 75 X

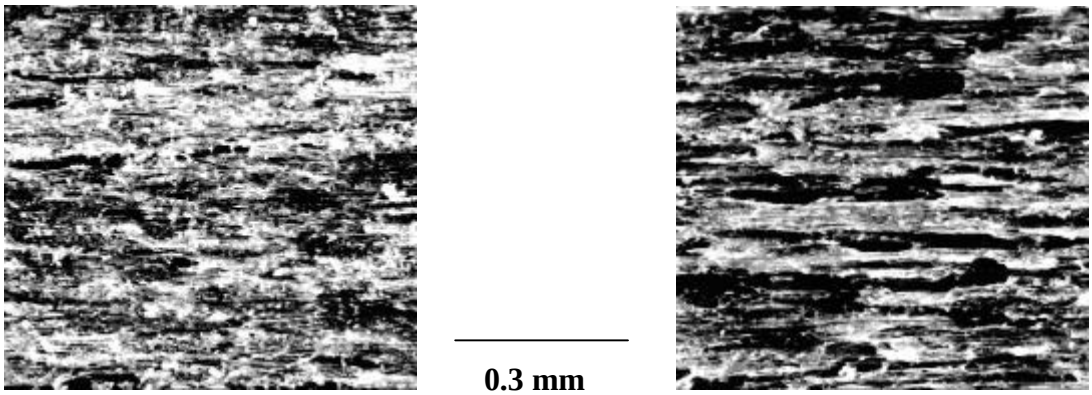

Figure 8.13: Photomicrographs showing PF-mix un-treated (left) and PF-mix weathered (right). Magnification = 75 X

During the cyclic ageing process, the wood cells at the interphase were subjected to the greatest stresses during the wetting and drying cycles due to the restriction caused by the adhesive. Macroscopic adhesive penetration into the adherend lumens was noted for all PF specimens tested in this study. If these cells are sufficiently weakened prior to or during weathering, the growing crack front will not be restricted to the two-dimensional interface during the test but may propagate within the three-dimensional interphase (15). Crack propagation in this interphase has been termed shallow wood failure (7). The increased roughness of the weathered specimens' fracture surfaces indicates that greater amounts of shallow wood failure occurred in the aged specimens. Fracture toughness measured at the interphase will have contributions from both the bulk wood and adhesive. Wood is generally known to possess greater fracture toughness than typical thermosetting resins, in the range of 50 – 1000 N/m (7). The increased fracture toughness of aged specimens therefore, reflects the contribution of the shallow wood failure.

It is interesting to note that weathered samples bonded with PF-low and PF-mix possessed enhanced toughness when compared to weathered samples bonded with PF-high. Recall that PF-low was purely low molecular weight material and PF-mix was comprised of 50% low molecular weight material. In the previous chapter it had been shown that low molecular weight PF has the capability to diffuse into the wood cell wall and upon cure, may form an interpenetrating network with the wood polymers. Molecular penetration occurs when the adhesive prepolymers diffuse into the cell wall, as opposed to simply the cell lumens. If molecular interpenetration has occurred for samples bonded with PF-low and PF-mix, it would act to increase the resistance to swelling and shrinkage of the wood adherends during weathering. Therefore, stresses would be increased at the bondline, increasing the amount of damage to the surface layers. This would mean a greater contribution to the observed value of G would be from the surface layers of the adherends, resulting in an enhanced toughness. The fact that weathered PF-low and PF-mix bonded specimens display increased fracture toughness (G_c and I) over weathered PF-high bonded specimens therefore may point to molecular interpenetration of the resin into the wood cell wall.

The effects of weathering on the pMDI bonded samples resulted in significant decreases in fracture energy. This is opposite to the trend shown for the PF bonded specimens. This finding illustrates an important point. In order to correctly design adhesive systems for specific applications, a knowledge of the durability of the system is essential. pMDI bonded specimens showed increased fracture toughness over PF bonded composites, when tested with no weathering. The results of weathering however indicate that the PF bonded composites possess a greater durability.

8.4 Conclusions

A new test geometry for the measurement of wood-adhesive fracture energies was evaluated. It was found that the application of oriented strand board backings to the adherends resulted in linear elastic behavior. Application of beam theory and shear corrected beam theory for the calculation of fracture energies is invalid for this system. Uncorrected beam theory clearly shows the presence of shear stress development. The shear correction factor χ, theoretically accounted for all factors influencing the measured crack length. Its derivation based on assumptions of uniform moduli of the adherends

made it unsutiable for application to the systems tested in this study. Fracture energies calculated from direct compliance measurements did not suffer from the theoretical drawbacks of the beam theory approaches and yielded reproducible results. Isocyanate bonded specimens were shown to be tougher than PF specimens when untreated. PF bonded specimens however, demonstrated enhanced durability over isocyanate bonded specimens. Results from weathering studies showed that PF resins containing low molecular weight fractions possessed enhanced durability. This could represent evidence of an IPN morphology at the molecular interphase between wood and phenol-formaldehyde.

8.5 References

1. Marra, A.A. Technology of Wood Bonding: Principles in Practice. 1992. Van Nostrand Reinhold, New York.

2. Ebewele, R., B. River and J. Koutsky. 1979. Wood and Fiber 11 (3), 197-213.

3. Griffith, A.A. 1920. Phil. Trans. Roy. Soc. Lond., 221, 163.

4. Liechti, K. Fracture Testing and Failure Analysis. 1990. Engineered Materials Handbook – Adhesives and Sealants – Section 5 – Testing and Analysis. H. Brinson, technical chairman. ASM International.

5. Blackman, B., J.P. Dear, A.J. Kinloch and S. Osiyemi. 1991. Journal of Materials Science Letters, 10. 253-256.

6. Williams, J.G. 1989. Composites Science and Technology, 21. 367-376.

7. River, B.H. 1994. In Handbook of adhesive technology. A. Pizzi and K.L. Mittal eds. Marcel Dekker, New York. Chapter 9.

8. Scott, C.T., B.H. River and J.A. Koutsky. 1992. Journal of Testing and Evaluation, 20 (4). 259-264

9. River, B.H. and E.A. Okkonen. 1993. Journal of Testing and Evaluation, 21 (1). 21-28.

10. Lim, W.W., Y. Hatano and H. Mizumachi. 1994. Journal of Applied Polymer Science, 53, 967-973.

11. Lim, W.W. and H. Mizumachi. 1997. Journal of Applied Polymer Science, 63, 835-841.

12. Ott, L. Introduction to Statistical Methods and Data Analysis. Academic Press, New York.

13. Hashemi, S., A.J. Kinloch and J.G. Williams. 1990. Proc. R. Soc. Lond. A, 427. 173-199.

14. Dillard, David A. personal communication.

15. Ebewele, R.O., B.H. River and J.A. Koutsky. 1982. Journal of Adhesion, 14. 189-217.

Chapter 9

Conclusions

Three new techniques have been successfully developed which will permit an improved understanding of several aspects of the adhesion of wood. A great deal of valuable information can be obtained thorough the use of ^{13}C CP/MAS NMR and Fracture Testing.

The utility of ^{13}C CP/MAS NMR for the characterization of cured phenol-formaldehyde resin has been demonstrated. Relative degrees of conversion can be evaluated by monitoring the integrals of methylene and hydroxymethyl carbon signals. Proton longitudinal relaxation in the rotating frame ($^{H}T_{1\rho}$) probes molecular motions which correlate with cure temperature, glass transition temperature and crosslink density of neat cured phenol-formaldehyde. Although contributions from non-motional effects (i.e. spin diffusion) are present, they do not obscure this relationship. It was shown that the sensitivity of this technique can be increased by diluting the spin system with deuterium. This provides a method of determining relative degrees of network mobility within cured PF.

The utility of ^{13}C CP/MAS NMR for elucidating molecular structure and dynamics of phenol-formaldehyde at the bondline of laboratory prepared wood-flake composites has been demonstrated. The use of ^{13}C labeling of PF allows qualitative estimates of relative degrees of resin conversion to be made from the corrected ratios of methylene to hydroxymethyl signals. Proton rotating frame spin lattice relaxation times ($^{H}T_{1\rho}$) can be used to assess relative degrees of adhesive network mobility, although the presence of spin diffusion can obscure motional contributions. Results from $^{H}T_{1\rho}$ measurements indicate that the protons of the hydroxymethyl carbons are in a significantly different motional environment than those of the methylene carbons. This may indicate preferential association of the hydroxymethyl groups with the wood substrate. Variable temperature $^{H}T_{1\rho}$ experiments can offer insight into changes in the distribution of molecular motions for both adhesive and wood components.

^{13}C CP/MAS NMR can be applied as a technique to determine differential degrees of PF resin cure within a wood based composite panel. The use of ^{13}C labeled PF allows the relative state of resin cure to be monitored by measurement of the resin methylene and hydroxymethyl carbons. It was shown that samples cured at the face of panels had higher degrees of resin conversion than those cured at the core. The use of ^{13}C labeled and 50% deuterium enriched PF allows fine structural differences in the cured resin to be assessed. It was shown that samples cured at the face of panels had a greater proportion of ortho-ortho resin methylene ratios. Proton rotating frame spin-lattice relaxations are relatively insensitive to changes in resin network motions. They do reveal however, the important and complicated role moisture plays during cure of phenol formaldehyde.

A technique has been established for the in-house synthesis of labeled formaldehyde for the synthesis of labeled, formaldehyde-based wood adhesives. Reduction of carbon dioxide in the presence of lithium aluminum hydride resulted in good yields of formaldehyde however the product was in very dilute solution which proved problematic to convert into a useable form. Oxidation of methanol resulted in lower yields than the reduction of carbon dioxide however the product was in the form of paraformaldehyde

which is easily converted into a useable form. For this reason, oxidation of methanol is favored over carbon dioxide reduction for the production of formaldehyde for use in synthesizing formaldehyde-based wood adhesives. Using this technique, paraformaldehyde-^{13}C-d_2 was produced in appreciable yields by the oxidation of methanol-^{13}C-d_4.

The use of deuterium labeling of resin and NMR relaxation experiments allowed the evaluation of relative degrees of molecular interaction between PF and pMDI resins with wood. Results from cross polarization and proton spin-lattice longitudinal relaxation studies indicate that both cured phenol formaldehyde and polymeric isocyanate possess the capability of interacting with wood on a scale of 10-100 angstroms. These results suggest that an interpenetrating polymer network (IPN) morphology may exist at the interphase formed between these two types of resin and wood. In the case of PF, molecular size of the resin monomers influences the scale of interactions between the cured network and wood. PF containing mainly monomers and dimers interacted on a smaller scale than PF containing a greater proportion of higher molecular weight oligomers. Cure temperature was also shown to affect the scale of PF interactions with wood. PF resins cured at low temperatures interacted on a more intimate level than when cured at high temperatures. This can be explained based upon competing rates of resin diffusion into the wood cell wall and bulk resin polymerization. Polymeric isocyanate, which possessed a relatively low molecular weight, was found to interact with wood on a scale of 10-20 angstroms only after sufficient time had elapsed between application of resin and hot pressing. This time dependence is a result of the absence of any solvent (i.e. water) which decreases the propensity of the liquid resin to diffuse into the wood cell wall.

A new test geometry for the measurement of wood-adhesive fracture energies was evaluated. It was found that the application of oriented strand board backings to the adherends resulted in linear elastic behavior. Application of beam theory and shear corrected beam theory for the calculation of fracture energies is invalid for this system. Uncorrected beam theory clearly shows the presence of shear stress development. The shear correction factor χ, theoretically accounted for all factors influencing the measured crack length. Its derivation based on assumptions of uniform moduli of the adherends made it unsutiable for application to the systems tested in this study. Fracture energies calculated from direct compliance measurements did not suffer from the theoretical drawbacks of the beam theory approaches and yielded reproducible results. Isocyanate bonded specimens were shown to be tougher than PF specimens when untreated. PF bonded specimens however, demonstrated enhanced durability over isocyanate bonded specimens. Results from weathering studies showed that PF resins containing low molecular weight fractions possessed enhanced durability. This could represent evidence of an IPN morphology at the molecular interphase between wood and phenol-formaldehyde.

VITAE

Robert George Schmidt Jr. was born to parents Wendy and Robert Sr. on September 2, 1971 in East York, Ontario, Canada. He attended De La Salle College "Oaklands" where he graduated as an Ontario Scholar in 1989. He studied at the University of Toronto and obtained a B.Sc.F in Wood Products Science with first-class honours in 1993. He subsequently enrolled in the doctoral program in the Department of Wood Science and Forest Products at Virginia Polytechnic and State University. During that time he was a Graduate Fellow of the Center for Adhesive and Sealant Science. He completed his dissertation in January of 1998.